Peer-to-peer urban channel characterization for military UHF band

Qian, Xing

2015

Qian, X. (2015). Peer-to-peer urban channel characterization for military UHF band. Master's thesis, Nanyang Technological University, Singapore.

https://hdl.handle.net/10356/65528

https://doi.org/10.32657/10356/65528

PEER-TO-PEER URBAN CHANNEL CHARACTERIZAITON FOR MILITARY UHF BAND QIAN XING 2015

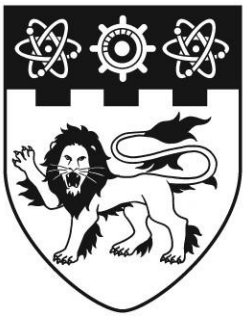

NANYANG TECHNOLOGICAL UNIVERSITY

PEER-TO-PEER URBAN CHANNEL CHARACTERIZAITON FOR MILITARY UHF BAND

QIAN XING

SCHOOL OF ELECTRICAL AND ELECTRONIC ENGINEERING

2015

PEER-TO-PEER URBAN CHANNEL CHARACTERIZAITON FOR MILITARY UHF BAND

QIAN XING

QIAN XING

School of Electrical and Electronic Engineering

A thesis submitted to the Nanyang Technological University in partial fulfillment of the requirement for the degree of Master of Engineering

2015

Acknowledgements

I would like to express my heartfelt thanks to my families, friends and people involved for their helps and supports during the course of Master study in Nanyang Technological University.

First and foremost, I would like to thank my supervisor, Associate Prof. Lee Yee Hui, who has kindly tolerated my innumerable questions and confusions. Without her patient guidance and constructive suggestions, the fruition of this work would have been impossible.

I would like to thank my fellow lab mates and research fellows for their generosity in sharing information and advices. Special thanks are devoted to Dr. Mao Xiaohong, for her continuous assistance and teaching during this study. Her active involvement in this project has been of great constructiveness. My gratitude also extend to the DRTech who fully sponsored my research fellowship.

Finally, a most humble word of thanks goes to my families for their relentless supports and encouragement, I owe them so much if not everything that I have achieved.

Table of Contents

Summary

The thesis presents the peer-to-peer wireless channel characterization study for two urban environment settings in military UHF band based upon measurement campaigns conducted in two distinctive places in Singapore which feature urban high rise indoor-to-indoor and outdoor-to-indoor channel propagation. The Military UHF frequencies were the selected frequencies ranging from 250 to 470 MHz. To date, few publications have been done to characterize the propagation features of low-rise and high-rise urban channels in the frequency band. There have been even fewer could be found on the characterization of the wireless channels in terms of distribution modeling of the multipath components and delay dispersions. Our measurements employed a separate transmitter and a receiver, from which both path loss and delay dispersion characteristics were analyzed for link distances of up to 2.8 km from the measurements of two kinds: one by fixing both transmitter and receiver in the indoor environment, the alternative by fixing only the receiver in the indoor environment and moving the transmitter along the designated routes. As a result, log-distance path loss models and link availability are described; power delay profile decay rate and delay dispersion characteristics are presented. 3-D ray tracing simulations are performed to explain propagation mechanisms. These results serve as useful immediate references for implementation of reliable and robust wireless communication systems in similar environments under warfare condition.

List of Figures

List of Tables

Chapter 1

Introduction

Wireless communication technology permeates in every facet of urban life. The surging amounts of bring your own devices (BYOD) have driven the fast development of new wireless technology that provides faster data access and ample channel bandwidth, due to its nature of greater flexibility, mobility and cost efficiency to adapt to the pace of global urbanization. However, there present a number of hurdles to establish reliable wireless communication system, because when wireless signals travel the path from a transmitter to a receiver in the form of electromagnetic waves, they will go through reflections, diffractions and get scattered, absorbed by buildings, foliage, moving vehicles pedestrians and earth. They could also be attenuated by weather and atmospheric interferences such as rain [1], ducting effect [7], lateral waves effects [8] and cloud. While all of aforementioned comprise the propagation environment that characterizes wireless channel, the intangible wireless channel presents amorphous nature. To realize a more robust communication system with high performance and reliability which is especially crucial for military tactical applications, wireless engineer has to understand thoroughly the idiosyncrasies of wireless channel. Therefore, the characterization of the wireless channel is the vital first step to warrant the optimal design of any wireless communication system for achieving good link performance given channel distortions [2].

The idea of wireless channel characterization can be chased back to 1920's when researchers studied ionosphere attenuation effect upon the wireless signals in which

concept of wide sense stationary uncorrelated scattering channels (WSSUS) and swept-frequency channel sounding were introduced and are still utilized in a lot of research works today [3]. Ever since then, several milestones have been made over the scores. In 1972, Cox [4] introduced spread spectrum cross-correlation for measuring the magnitude of the channel impulse response (CIR) through power delay profile that provides routine standard to characterize the wideband channel delay dispersion. Digital cellular channel characterization such as [5] became a great hot hit later in 80s, 90s due to the soaring demands of wireless technology from private consumers of mobile and personal communication devices.

The objective of channel characterization is to deepen our understandings how certain wireless channel impairs and distorts signals in order to help in devising, testing and achieving wireless communication systems with high link- and system-performance in complex environments and circumstances. With that knowledge, new ways of distortion mitigation and necessary measures to prevention over degradation of wireless signals would be possible. In [2], channel modeling was recognized as the most important and essential activities in all existing research activities upon mobile radio.

Wireless channels have been characterized for disparate environments by various systems and in multiple frequency bands. There are a large body of literature that characterize the different kinds of indoor environments including line-of-sight (LOS) and non-line-of-sight (NLOS) links in residential [9], office [10], library [11], factory [12] and railway station [13]. The outdoor propagation models are also of great interest to many researchers. The outdoor channels are well examined that covers a wide variety of environments such as dense urban district [14], sea [15] and forest [16]. The outdoor-to-indoor channels have also appeared in a number of

recent publications [17] [18], but this area has far less published works than the previous two kinds of channels. Furthermore, no standardized model of this type of channel yet is generally recognized. Therefore, the propagation characterizations of outdoor-to-indoor link and indoor-to-indoor link in complex environment are the general research topics of the interest. The research work is performed to investigate military UHF band (250 - 470MHz) propagation channel characteristics in urban environments.

1.1 Motivation

With the fast development of global urbanization, seamless connected communication experience has become one of the core pillars for the future smart city, which drives the fast advancement in wireless technology that requires faster data rate, wider bandwidth and exceptional quality of service. Especially in future warfare, excellent voice and video communication over the air in the extremely cluttered metropolitan city are indispensable from the military tactical perspectives. Imagine a war bursts out in the city, soldiers have to be able to communicate directly with each other to inform their whereabouts when they are spread over different locations of the battlefield, which features ground based peer-to-peer communication. On the other hand, they need to report status quo to commanders who are located in a command center at elevated height or a temporary underground fort which forms outdoor-to-indoor propagation links. Indoor-to-indoor communication also has to be provided for reliable communication between military officers. All these crucial details, which are vital to whether one could stand a better chance to win the war, must be warranted by reliable battlefield communication network systems. However, In order to devise such systems for urban warfare

communications, determine rational selection of signaling parameters (transmitting power, carrier bandwidth, symbol rate) and come up with the remedy to counteract the channel distortion (equalization), key channel characteristics include path loss exponent, time dispersion, coherence bandwidth, temporal correlation have to be well informed [19]. Although there is a large body of literature to characterize the urban channel, most of recent studies align their research interests with the most recent commercial wireless application and focus of measurements are taken place on propagation centered on range from 700MHz to 2100MHz, which provides band coverage of long term evolution (LTE) standard and personal communication service (PCS) band. In recent years, however, as world's urbanization expands, there emerges soaring interests in studying the urban propagation since there are great demands for communications, connectivity and bandwidth for future warfare [20]. However, many existing literatures on urban channel are difficult to cope with military tactical applications. In [21], Hampton illustrated the difficulty by tabulating 12 existing famous urban path loss models and elaborated their limitations to be applied in military purpose including famous Okumura model [22], Hata Model [23] and COST 231 Model [24]. The constraints include antenna height, link distance and operational frequencies. Hampton filled up the gap by performing the path loss modeling over the ground based outdoor communication over frequency range of 225 to 450MHz that encompasses interested frequency bands of our work. Limited research works have been done to characterize the indoor-to-indoor and outdoor-to-indoor urban propagation links in pertaining military UHF band as featured in our study. In this regard, a comprehensive measurements and modeling of urban channel characterization in the military UHF band from both large scale and small scale perspective need to be performed, since

the data and models are currently not widely available for the unique channel condition at the given frequency bands.

1.2 Objective

The focus of this thesis is to characterize and model the peer-to-peer urban wireless channel in the military UHF band in Singapore. This is achieved by performing a series of channel measurements over a wide range of in two typical urban environments in Singapore, namely the high rise complex that encompasses office environment, underground tunnels and shopping malls, and hotel located in the endsville shopping boulevard in Singapore. To fulfill the objectives, the focus of this thesis is as follows:

- A comprehensive literature review of the wireless channel characterization and modeling, especially in typical high rise urban environment, is performed. This exercise helps to review the key concepts to understand methodology mentioned in the research work and better understand the drive behind projects conducted. It also facilitates the further exploration of the related research topic by providing an overview of progress made in the specific field.
- Theoretical verifications of the propagation mechanisms in the measured urban settings were performed and illustrated. Both LOS links presented on the same level, NLOS links in inter-level as well as the long range outdoor-to-indoor links have been theoretically testified by 3-D ray tracing simulation. Main propagation mechanisms are identified in different type of propagation links. The statistical model that best describes the signal variation is also examined and presented for both

environments.

- Large scale channel characterization of the shopping district outdoor-to-indoor links is studied. Path-loss models are obtained based upon collected narrowband data at different measured frequencies within military UHF band. Further comparison between empirical results and simulation results is performed to verify the correctness of the results.
- Small scale channel characterization parameters of two urban environments are evaluated and modeled. Parameters such as distribution of the number of multipath components, delays of multipath components models and time dispersion characteristics. Suitable stochastic distribution models are proposed.

The outcome of the master study has generated some contributions and developments over the existing research works, and is outlined in the next section.

1.3 Major Contribution of the Thesis

In this thesis, urban channel characterization and modeling in the typical metropolitan city environments at selected frequencies in military UHF band were performed. The followings are the major contributions of the research work:

1. Path-loss model in an urban shopping district channel is studied and verified. The classic log-distance model is chosen as the model to fit the measurement results in this thesis. Thus, the path loss exponents are determined for each experiment route at each frequency. The residual path loss modeling is also performed and we propose new path loss models and interpretations based on above two combinations. The model shows high

degree of expression of the measured data.

2. The complex 3-D models for ray-tracing simulation that reproduces the major high rise settings in the Singapore endsville shopping district-Orchard area and a high rise complex building model with detailed interior structure, which are used to verify outdoor-to-indoor propagation mechanism and indoor propagation. From the meticulous 3-D models, we present a closely matched simulation results in comparison to measured results. We also verify dominating propagation mechanisms for the specific link or the overall channel environment based on the simulation results.
3. The statistical distributions of the number of multipath components under the complex urban environments are studied. The determination of multipath components is based on the constant false alarm rate (CFAR) threshold algorithm that was previously used in radar application. The distribution of the number of multipath is found to be best fitted with lognormal distribution across all tested frequencies based on Kolmogorov-Smirnov (KS) goodness of fit method. The model parameters $\boldsymbol{\mu}$, $\boldsymbol{\sigma}$ are listed out across all the tested frequencies for later comparison analysis.
4. Multipath decay rate modeling of the urban channel in military UHF band is also part of the study. From multipath cluster identification based on power delay profile obtained from post processing, we find that the outdoor-to-indoor channel power delay profiles are best modeled b negative exponential model, while in enclosed indoor environment, linear models applies. From determined model, decay factors are compared across frequencies.

5. Time dispersion are characterized from 90% of the CDF, the small scale channel variability is thus determined with coefficient of variation, recommendation is given for the usable system bandwidth based on the parameter determined. Moreover, investigation of distance dependency of root mean square delay spread (RMS-DS) is studied, we proposed a linear relationship between logarithmic RMS-DS value with distance with little varied gradient value across all selected frequencies in outdoor-to-indoor links around Orchard area in military UHF band. This could serve as a reliable reference for future channel coherence bandwidth estimation in the similar urban settings.

In summary, the work presented here is to fill the vacuum by presenting channel measurement and modeling results - including propagation mechanisms, path loss modeling (large-scale channel characteristics), distribution of the number of multipath components, delays of multipath components models and time dispersion characteristics – for indoor-to-indoor and outdoor-to-indoor peer-to-peer urban channel in military UHF band (250-470MHz). The data and models are currently not widely available for the unique channel condition at the given frequency bands and serves as a good guideline for military communication engineers that permits immediate channel parameter predictions based on measured channel parameters and facilitates more efficient network implementation and coverage

1.4 Organization of the Thesis

The remainder of the thesis is organized as follows. Chapter 2 is the literature review chapter. It provides elaboration on some key concepts on radio wave

propagation that are relevant to the research work and performed comprehensive summaries on the current literature on the channel characterization and modeling in urban channels in the dense high rise districts. The review lastly covered the introduction of other commercial radio propagation simulators.

In Chapter 3, both narrowband and wideband channel sounders are illustrated. The comparison of our deployed system with VNA based systems has been reviewed briefly. In addition, the 3-D ray tracing simulator used in the project is introduced briefly.

Chapter 4 describes the narrowband path loss modeling in outdoor-to-indoor urban propagation links in the endsville Singapore district-Orchard Road. The results are analyzed both empirically and theoretically. The classical log-distance model is used to fit the measured data in order to gain more insights of the channels path loss behavior. To verify the result, the simulation model of the district is also constructed in ray tracing simulator according to the actually urban settings. A closely matched simulated result is obtained to help us to investigate more on the signal variations. Meanwhile, we propose path loss models based upon log-distance model with new interpretations. From the 3D ray tracing simulation, we also study more on propagation mechanisms

In Chapter 5, small scale urban channel characteristics are investigated. It covers in details on the number of multipath components and its modeling, delays of multipath components models and time dispersion characteristics of the multipath for the outdoor-to-indoor urban links. The further investigation upon distance and path loss dependency of time dispersion is also performed.

In Chapter 6, wideband channel characterization is studied in indoor links measured in high-rise complex buildings. It covers the details on the number of

multipath components, decay rate of multipath components and time dispersion characteristics of the multipath for the indoor links. Furthermore, 3D-ray tracing simulation is performed to study the both indoor LOS and NLOS links. Combining the empirical and simulated results, we explain the propagation mechanisms in two types of the link scenarios.

Finally, thesis is concluded in Chapter 7, both conclusion and future work recommendation are covered in the chapter.

Chapter 2

Literature Review

In the last Chapter, we have explained the significant importance of channel modeling to the communication system design and RF planning and briefly retrospect the historical milestones of the wireless channel characterization. In this chapter, we summarize the fundamental approaches to characterize wireless channels and propagation phenomena. The detailed reviews of current literatures in urban channel modeling from larger scale path loss modeling to small scale multipath fading re also presented in the chapter. Lastly, the reviews on the two popular existing commercial radio propagation simulators are performed for a comparison with the software used in the research project.

2.1 Radio Propagation Fundamentals

Wireless networks have been an omnipresent metropolitan infrastructure. From transmitting source to receiving devices, information propagates in form of electromagnetic wave and travels through the radio propagation channel. In the process, wireless signals will be attenuated through reflections, diffractions, scattering and absorption due to the presence of buildings, foliage, mountains moving vehicles and people and so many different obstructions. Signal would experience greater distortion and attenuation in real wireless channel than travelling in the free space. Besides, signal may be scattered during the propagation, this leads signal to take multiple paths from the transmitter to the receiver and at different

delays. Thus, wireless channel has very amorphous nature compared to the wired communication [2]. In order to perform robust wireless communication system design and have good mitigation measures to the impairment of the wireless signals, we have to model the channel that captures the essential characterization and knowledge of how the channel twists and distorts the signals during the propagation.

Channel model is a statistical model that builds upon the empirical data collected from measurements taken from particular propagation environment for certain frequency band. However, it only reflects partial truths about the communication channels with a simplified mathematical model and would be impossible to offer full coverage of channel variations, especially in complex environments. We would focus some key aspects of wireless channels, namely, distance dependent path loss, large-scale shadowing models and small-scale fading models. The distance dependency of path loss serves as good reference for wireless communication system coverage area estimation and planning, which is mainly affected by terrain and environment. Large-scale shadowing introduces the extra variation of path loss for propagation links with similar link distance, which results from obstacles like buildings, mountains and foliage. Small-scale fading is the fading emerged within half to few wavelength distances over short duration of microseconds or nanoseconds which is caused by mobile obstructions and multipath [36]. The large-scale fading can be statistically modeled around the median received power as shown in Figure 1. The mean received power strength decreases as link distance increases.

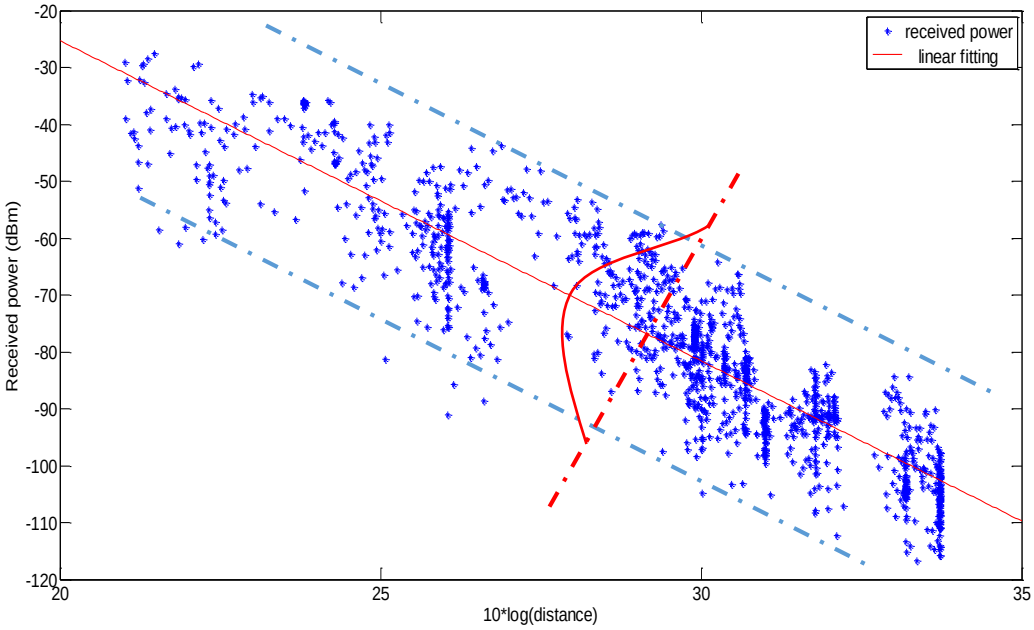

Figure 1. Example of received power plot versus log-distance and large-scale fading

Before going into detailed introduction of three aspects of wireless channel, we first classify channel environment. By classification of ITU-R M.1225 [37], propagation environments are categorized in three types, namely, picocell, microcell and macrocell. Picocell is usually the indoor environment with link distance of less than 100 meters. Microcell extends to outdoor with both transmitter and receiver placed under rooftop height within the same street canyon with the link distance up to 1km. In microcell setting, the possibility of line of sight (LOS) links is often considered. Macrocell refers to the outdoor environment with link distance larger than 1km, the base station is usually elevated, and remote system is placed at height that is much lower than local rooftop level. Macrocell links are generally Non-line-of-sight (NLOS) links.

2.1.1 Path Loss

Path loss is the qualitative signal power dissipation measure caused by the wireless channel when signal travels through wireless channels. The path loss is usually considered distance dependent. With the increase of transmitter and receiver separation, path loss increases. The path loss is the common basic measure of channel quality. We will cover three basic models for path loss.

A. Free Space Path Loss model

The model applies in the ideal free space propagation which assumes absolute unobstructed line-of-sight static link without multipath components. The model provides theoretical estimation of path loss between transmitter and receiver as a function of separation distance *d*. The equation can be expressed in decibels (dB) by assuming antenna gain of 0dB [38].

$$L_{FSL}(dB) = -27.56 + 20 * \log(f / f_0) + 20 * \log(d / d_0) \quad (2.1)$$

Where f is transmitting signal frequency in MHz, d is the transmitter and receiver separation in meter. f_0 = 1MHz, d_0 = 1m.

From (2.1), free space model assumes a pass loss exponent of 2. In real world wireless channels, the free space propagation model is not pragmatic, because the presence of single LOS link is de facto impossible.

B. Ray Tracing Path Loss Model

Ray tracing use geometric approach to predict the propagation paths that wireless radio signals traverse from transmitter to receiver. The ray tracing model is site specific and requires detailed information about the experiment environments in order to generate convincing model. In the model, signal in form of electromagnetic wave is modeled as many ray tubes. The travelling of signal is considered as

propagation of electrical field. Ray tracing method is widely used in simulation software such as “Wireless Insite” used in our study. In this section, we review on the most fundamental and well-known two-ray (ground reflection) model.

For most of propagation links, there should be at least two paths for signal to travel from transmitter to receiver: LOS link and ground bounce off path. Thus, the two-ray path loss model which considers both paths is found to be more feasible in the situation the radio systems operate at relative short range ground based link distance (less than a few tens of kilometers) with relatively homogeneous environments [35] [38] [39]. Typical example would be wireless channel over sea between vessels, in [40] [41], two-ray model illustrated good match to the measurement results for land to sea link at 5 GHz.

The Two-ray model is based on assumption of flat earth model and perfect plane ground. The received signal is the vector summation of the direct LOS ray and the ground bounce-off indirect ray. Figure 2 shows the simple geometry of the two-ray path loss model.

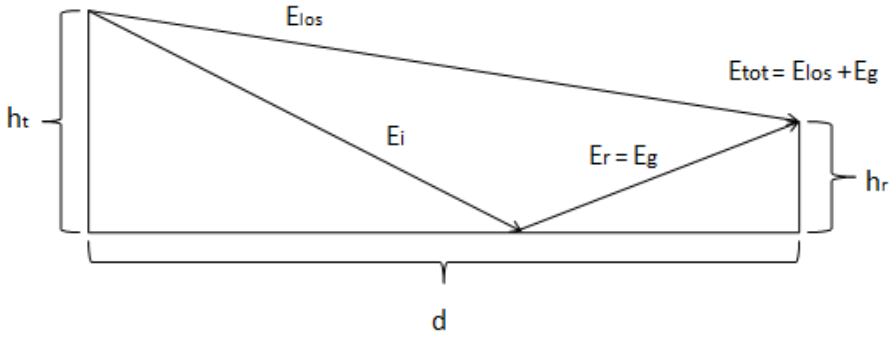

Figure 2 Two-ray Model Geometry

The two ray models can be simplified after cutoff distance ($d > 4h_t h_r/\lambda$) with power decay in $1/d^4$. If the plat earth assumption is valid, we can use (2.2) to estimate the

path loss

$$L(dB) = 40\log(d) - (20\log(h_t) + 20\log(h_r)) \quad (2.2)$$

Beyond the two-ray models, we can have model with as many rays as we need [38], such as six-ray and ten-ray model. While ray tracing models consider reflection of ray from all kinds of surfaces and terrain, there presents other factors like diffraction, penetration and even wall gap which forms corridor for ray to travel elsewhere and introduces additional path loss [42]. In complex and non-homogeneous environments, deterministic ray tracing models are rarely used, because high-resolution environment description is not usually readily available and cost of modeling is the other concern.

C. Log-distance Path Loss Model

In order to adapt to different channel environment settings, a large body of derived new model based on classic empirical model has been developed, the most widely used models include IEEE 802.16(SUI) [46], Hata [23] and COST-231 model [44]. These models take basic form of the classic log-distance path loss model [38] is used. The model that aims to calculate the path loss exponent *n* from linear regression upon measured data with least square error method (LSE), is expressed as follow:

$$L(d) = 10*\mathrm{n}\log_{10}(d) + L_0 \quad (2.3)$$

where *d* is the separation distance between the transmitter and the receiver, and intercept L_0 is the reference path loss at calibration distance d_0. The primary focus of the one-slope model is the path loss exponent *n* which indicates the shift of path loss against logarithmic link distance value.

2.1.2 Large-Scale Shadowing

Shadowing is the fading over a large scale to describe the variation around the local median received power over a distance of 10λ [36]. The effect of shadowing can be reflected from Figure 1, measured path loss varies for locations with the same or similar transmitter and receiver separation. The large-scale variations are caused by shadowing of obstacles like buildings, turning corners. Large-scale shadowing is usually modeled with log-normal distribution in urban or suburban environments [47] [48], and thus it follows the Gaussian Normal distribution when measured in decibels (dB). In practice, the shadowing effect is considered together with path loss by adding additional zero-mean Gaussian random variable behind the classic path loss model with a standard deviation of σ, and express as (2.4)

$$L(d) = 10*\text{n}\log_{10}(d / d_0) + L_0 + X_\sigma \tag{2.4}$$

where X_σ is the additional shadowing term that follows Gaussian Random distribution. The model has been extensively applied to various environments (urban, suburban or rural). Seidel [49] performed his measurement in suburban area of Stuttgart at 900MHz and obtained the path loss exponent of 2.8 with shadowing variation of 9.6dB. Porter [50] also reported *n* value of 3.2 and σ value of 9.5 dB in urban channel at frequency of 3.7GHz. Range of 7dB-11dB for shadowing standard deviation σ has been reported in many research works.

2.1.3 Small-Scale Multipath Fading

In the previous section, ray tracing model has introduced the concept of ray, knowing that a signal will not only have one path to receiver when it is transmitted out. During the propagation, the signal travels in the form of electromagnetic wave and interacts with many scatterers. The scatterers will scatter and redirect a part of

signal power that produces more signal replicas to traverse in different paths and eventually arrive at receiver at different amplitude, phases and delays. We called the phenomena Multipath. In the urban communication environment as shown in Figure 3, scatterers might be a large metal shingles or building walls, or it might be building edges that cause the diffraction of the propagating radio waves. Thus the final received signal replicas encompass components that travel different paths with different distance and thus arrive in time delays. The constructive or destructive interference of the multipath components will lead to fluctuation of the received signal and produce nulls and peaks. We call the phenomena multipath fading. Studying small scale multipath fading is instrumental to avoid inter-symbol interference (ISI), symbol errors and achieve better data rates in wideband communication systems. Thus, it is necessary to quantify the aspect of the channel with appropriate measures which is covered in the following.

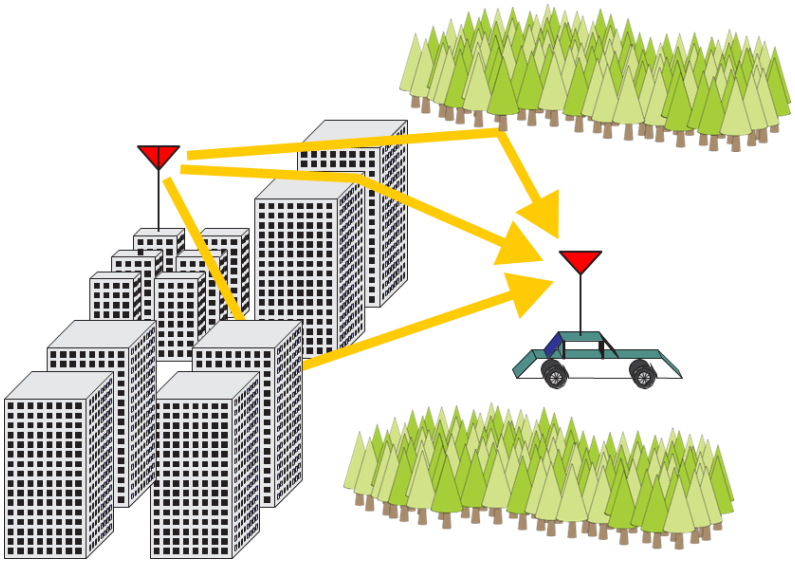

Figure 3 multipath phenomena caused by scatters such as building walls, foliage

A. Channel Impulse Response

In time domain, the multipath components reach the receiver with different amplitude and delays. The characteristics of multipath fading can be well represented by channel impulse response (CIR) $h(\tau)$ as shown in Figure 4. The each bin presented in Figure 4 is considered a discrete multipath component. Mathematically, the baseband (complex low-pass filtered. The CIRs, as denoted in $h(\tau, t_i)$, is defined as equation (2.5)

$$h(\tau, t_i) = \sum_{k=1}^{N} a_{ki} \, \mathrm{e}^{j\varphi_i} \, \delta(\tau - \tau_{ki}) \tag{2.5}$$

where i indexes the i^{th} power delay profile (PDP), N is the number of multipath components (MPC) in the i^{th} PDP, α_{ki}, τ_{ki} and φ_{ki} represent amplitude, delay and phase of the k^{th} MPC, and δ is the delta function.

The instantaneous power delay profile, defines envelope of the received power is expressed as (2.6), the channel response is usually represented by mean PDP through averaging several instantaneous power delay profiles in time domain in order to better represent the small-scale characteristics of channel.

$$P_i(\tau) = \sum_{k=1}^{N} \left| a_{ki} \right|^2 \delta(\tau - \tau_{ki}) \tag{2.6}$$

Power delay profile is a plot of relative received power against excess delay with respect to a reference time delay. In order to facilitate the small scale multipath fading analysis, every power delay profile obtained after post processing in our study has normalized noise floor of -20dBm and set the reference first peak power components to zero delay. Figure 5 shows a typical power delay profile plot from the Orchard road trial, determined from a number of closely sampled instantaneous

profiles.

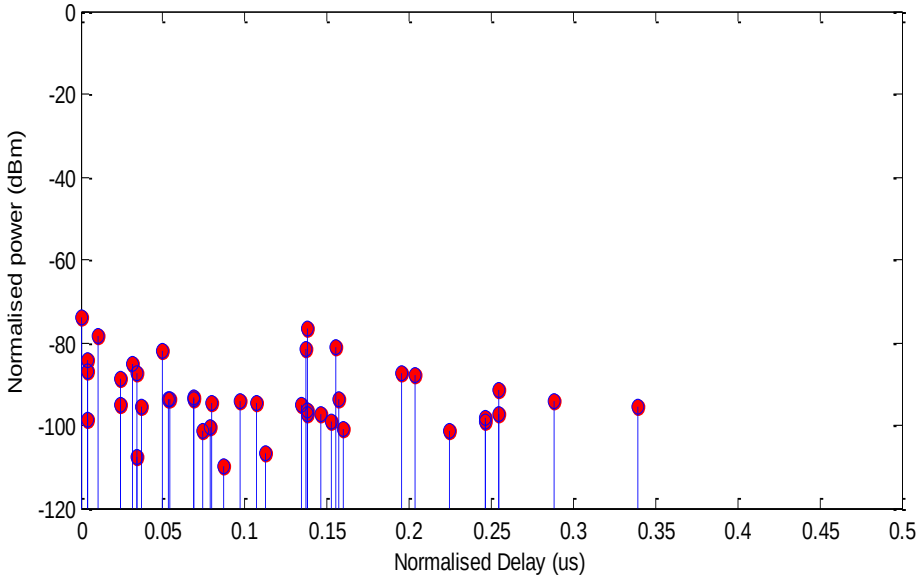

Figure 4 Tapped delay line model of multipath components

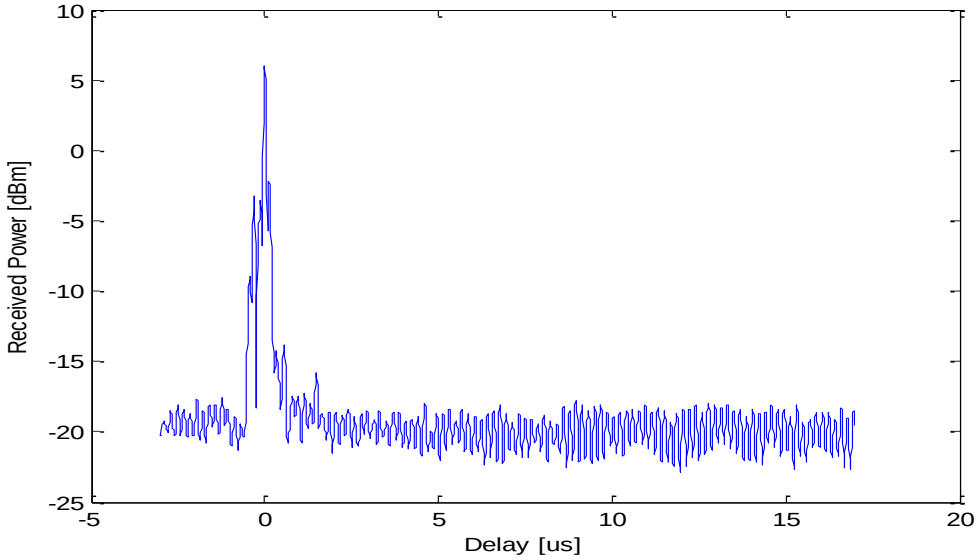

Figure 5 Typical Example of Power Delay Profile from shopping district experiment

From the power delay profile, several key parameters to characterize the wideband channel can be evaluated. The time domain multipath parameters include mean excess delay, RMS delay spread and excess delay spread. The frequency domain parameter refers to coherence bandwidth. All of them are introduced in the

following.

B. Time Domain Multipath Parameters

Time domain multipath parameters include mean excess delay, root mean square delay spread and excess delay spread. For wideband multipath channels, mean excess delay and RMS delay spread are the most common measures of the channel delay dispersion [36]. The excessive delay is defined as the first moment of power delay profile and expressed as:

$$\bar{\tau} = \frac{\sum_{k=1}^{N} \tau_k a_k^2}{\sum_{k=1}^{N} a_k^2} \tag{2.7}$$

RMS delay spread is defined as the square root of the second central moment of the PDP and given by:

$$\tau_{rms} = \sqrt{\overline{\tau^2} - (\bar{\tau})^2} \tag{2.8}$$

where

$$\overline{\tau^2} = \frac{\sum_{k=1}^{N} \tau_k{}^2 a_k^2}{\sum_{k=1}^{N} a_k^2} \tag{2.9}$$

where a_k and τ_k are the signal strength and propagation delay of the k^{th} multipath component. Note that the delays are measured against first detected signal arrival time. Prior to determining the delay spread, a proper threshold algorithm associated with noise floor value has to be determined so that legitimate multipath components could be determined apart from noise component for RMS delay spread calculation. The other term maximum excess delay (*Ix* dB) of the power delay profile is defined to be the delay duration which multipath energy falls to the X dB below the peak received power strength.

C. Frequency Domain Multipath Parameters

The Frequency Domain Multipath parameter, Coherence bandwidth is inversely proportional to RMS delay spread. In the range of coherence bandwidth, the channel is considered “flat”, in other words, spectral components are expected to pass channel linearly with equal gain [38]. The coherent bandwidth as the bandwidth over which frequency correlation coefficient is above 90%, the approximate expression is given as:

$$B_c \approx \frac{1}{50\sigma_\tau} \tag{2.10}$$

Coherence bandwidth for frequency correlation coefficient above 0.5 can be estimated from equation (2.11)

$$B_c \approx \frac{1}{5\sigma_\tau} \tag{2.11}$$

If the modulation technique is given, the maximum achievable data rate without applying equalizer can be estimated. For example, if QPSK is used, the maximum bit rate is equal to the double value of the coherence bandwidth.

Additionally, coherence bandwidth value is associated with frequency selective fading of channel. If bandwidth of transmitted signal (symbol rate) is much larger than the coherence bandwidth of value, the time delayed replicas of on symbol might be received within the time slot allocated for the next symbol, thus the received signal will be distorted and lead to inter-symbol interference (ISI) and eventually cause poor link performance. One of solution to mitigate the issue is to use multi-fingered rake receivers with time diversity

2.2 Urban Channel Modeling

In this section, existing literature on urban channel modeling and characterization are described in details. The observations and findings are from either theoretical or experimental studies over the past few decades.

2.2.1 Path Loss Modeling in Urban Environment

Over the past 60 years, extensive efforts have been made to predict the value or distribution of path loss in urban area via proper modeling and characterization. There are more than 50 proposed path loss models as claimed in [51]. In this part of literature review, we review path loss models of the past literature works performed in urban channel from two broad approaches, namely, measurement based path loss modeling and propagation analytics based modeling

A. Measurement based path loss modeling

In the early attempt of urban channel path loss modeling, the most popular models is the Okumura Model and Hata Model proposed in 1968 and 1980 [23] [52]. The extensive measurement campaigns took place in Tokyo, Japan at several frequencies within the frequency range from 150-1920 MHz. Okumura is suitable to the scale of macro cell with radii from 1km to 100km with confined base antenna height range of 30-200m and receiver height 1-10m. Note that Okumura Model took into extra propagation parameters such as terrain irregularity, environment types (urban suburban or rural) and is expressed as:

$$L_{median}(dB) = L_F + A_{m.u}(f,d) - G(h_t) - G(h_r) - G_{Area} \tag{2.12}$$

where L_{median} is the median value of the propagation path loss, L_F is the free-space propagation loss as introduced in the previous section. $A_{m.u}$ is the median attenuation

in the medium relative to free space in the urban area, $G(h_t)$ and $G(h_r)$ are the height gain factor of the Base station and mobile antennas, G_{Area} is the correction factor based on the actual measurements.

The Hata model is the formula based Okumura model based on the graphics provided by Okumura. The Urban areas path loss prediction is based on:

$$L(urban)(dB) = 69.55 + 26.16\log f_c - 13.82\log h_{te} - a(h_{re}) + \log d(44.9 - 6.55\log h_{te}) \quad (2.13)$$

where f_c is the frequency in MHz which is valid in range from 150 MHz to 1500MHz. $a(h_{re})$ is the correction factor for the effective height of the receiver antenna of the mobile unit, which is the function of the size of the coverage area details can be found in [55]. The model has been widely applied in path loss prediction in Japan urban area and is well recognized in the path loss prediction in urban macro-cell environments with good accuracy.

Based upon Hata model, many extension and corrections have been done to its usage in urban environment. COST-231Extension [53] to Hata model has been done to expand the usable frequency to 2000MHz. The correction for urban environment follows the equation below:

$$L(urban)(dB) = 49.3 + 33.9\log f_c - 13.82\log h_{te} - a(h_{re}) + \log d(44.9 - 6.55\log h_{te}) \quad (2.14)$$

where $a(h_{re})$ is the correction factor for the effective height of the receiver antenna of the mobile unit.

The other extensions include Hata-Davidson [57], ECC-33 model [56] and ITU-R/CCIR modification [57].

In the Hata models and its extensions, diffraction from buildings edges is not considered. In 1991, Saunders and Bonar [58] proposed the Flat-edge model which added the knife-edge diffraction loss in the path loss computation due to the multiple regularly spaced buildings, the model idealizes the situation that between

the transmitter and receiver, there are n evenly spaced obstructions with constant spacing of s and height h_o with receiver height less than h_o, the total path loss equals the sum of loss due to Fresnel obstruction by the obstacles, the free space path loss and the total diffraction loss caused by the final obstruction. Based on approximate fit in [53] the additional diffraction loss is estimated with following equation:

$$l_{diffraction} = -(3.29 + 9.9\log(\phi\sqrt{\frac{s\pi}{\lambda}}) - (0.77 + 0.26\log(n))) \quad (2.15)$$

when n<100, and $\phi\sqrt{\frac{s\pi}{\lambda}}$ <1

Based on the flat edge model, COST231/Walfisch-Ikegami, which incorporates the Walfisch-Bertoni model [59] and Ikegami model [60] was proposed based on the UHF band measurement in urban environments. The model considered path loss in dB as the summation of three terms, namely, the free space path loss, diffraction loss due to the building rooftop to street level and multi-screen diffraction loss due to the taller buildings in the path of transmitter and receiver link. This can be illustrated with following:

$$L = L_0 + L_{rts} + L_{msd} \ , \quad (2.16)$$

where L_0 is the free space path loss that follows equation (2.1)

$$L_{rts} = -16.9 - 10\log w + 10\log f + 20\log(h_{roof} - h_{mobile}) + L_{ori} \ , \quad (2.17)$$

where L_{ori} is the Loss term related to the angle of incidence of the received signal relative to the direction of the street. Final loss term L_{msd} is expressed as:

$$L_{msd} = -18\log(1 + h_{base} - h_{roof}) + k_a + k_d\log d + k_f\log f - 9\log b \quad (2.18)$$

The k_a, k_d, are coefficients based on the based height and rooftop height comparison. k_f is the coefficient depends on the size and type of coverage areas (metropolitan or medium size city and rural).

The above models stand alone and provide path loss prediction along a single path and coefficient of correction is made based on the multiple measurements. Parameters like link distance, operating frequency and antenna height are considered. Some models contain parameters that are exclusive to the model and selection of different modes for computation based on different situations specified. Those deterministic models which may perform relative accurate prediction in one environment will not make it a good model in all others. Thus, there are some supplementary models to make further refined corrections to the existing models by considering additional loss factors such as ducting effects in sea to land communication [61] [62], foliage obstructions [63] [64], terrain roughness [65] and antenna directionality [67]. In the typical Urban Environment, building is probably the other main factor to cause the signal attenuation. De Jong et al. in [66] proposed the supplementary model on building-transmission to model the signal loss caused by wall penetrations. De Jong et al. performed the measurement of transmission loss for a set of 22 buildings at a frequency of 1.9 GHz. They found a loss rate in the range of 1.4 to 3.8 dB/m and mean value of 2.1dB/m. and compared the result with the COST 231 which alleged typical building penetration loss is around 0.3 to 0.6dB/m. De Jong claimed their gradient value take into account for all losses that include interior interface, exterior walls and the free surrounding space of the buildings.

Some other models introduce random variables to better describe the path loss model with the additional fading in the radio channel which includes both large scale fading and small scale fading (scattering and multipath). They collected the residual errors data between measurement data and deterministic model and fit the residual errors with stochastic distribution model. The conventional model of

shadowing has been covered in the previous section and written in equation (2.4). The model is usual named as "lognormal shadowing" model, where path loss exponent *n* and Gaussian random deviation σ are fitted with the empirical data. The model is mainly for large scale effects modeling and combined with path loss modeling. The typical example is the Barclay-Okumura model [53], which remodeled the Okumura data in the urban area and proposed the new model expressed as:

$$PL = -52\log(d) + 20\log_{10}(f) + 32.5 + N(0, 0.65\log_{10}(f)^2 - 1.3\log_{10}(f) + 5.2) \quad (2.19)$$

Some path loss models attempt to capture both large scale effects and small scale fading to better express the time-varying features of wireless channel. The Herring [68] conducted a series of channel measurement trial in Cambridge, Massachusetts to measure wide range of links range from few tens meters to several thousand meters at 2.4GHz and transmitted 20MHz bandwidth signal. Two separated models are proposed, one for ground-to-ground, the other for air-to-ground. The air to ground is modeled by two components: signal travels over the air follows the free space path loss model and path loss caused by low level scatters that follows the log-normal distribution with mean of 30dB and 8.3 dB standard deviation. The model is written as:

$$PL = 20\log_{10} d + N(30, 8.3) \quad (2.20)$$

where *d* is the transmitter and receiver separation, *N*(30, 8.3) is the Gaussian random component that models the fading caused by low level scatters (buildings and trees).

The Ground to ground model proposed associates the path loss exponent values with two stochastic models and expressed as:

$$n = U(2,5) + N(0, 0.22) \quad (2.21)$$

The path loss exponent expression is then combined with excess path loss based

on the classic empirical model and written in the form of (2.22).

$$PL = 10n\log_{10}(d) + N(40, 5.5) \tag{2.22}$$

For the path loss modeling in military tactical UHF frequency band (250-450 MHz), very limited works [69] [71] [72] [73] are presented. Hampton et al. [69] was one of the prominent examples that conducted a series of narrowband measurement campaign for path loss modeling in downtown Philadelphia at 225-470MHz, straight and L-shape routes were studied. Hampton claimed that LOS link was accurately modeled by the two-ray model. The L-shape links path loss was modeled with LOS component, a step-down loss of 6.3dB caused by building edges and corner and NLOS segment with a steeper fall off rate than LOS components. The path loss was inspired by the two slope model proposed in [70], which calculated two path loss exponents for the segment before the 'Fresnel breakpoint' and after break point, the prior segment is usually estimate around value of 2 due to the LOS conditions and post segment path loss exponent value is between range of 2 to 7.

Even with presence of overwhelming pool of path loss models, the classical empirical path loss model could be the first model to start in order to obtain first hand characterization of the channel the particular researcher is exploring. Like many other researchers, they collected data from environments to develop new models through corrections upon the existing models and evaluate the proposed models based on comparative study with other few competing models. Since data from a specific model are not usually available, in order to find out the model translation performance, one should apply a large body of models over a common empirical dataset from diverse environments and varied landscapes.

B. Propagation Analytics based modeling

Propagation analytics based modeling is the modeling method based on the propagation characteristics of electromagnetic waves which is the form that wireless signal travels in space. In these models, signal propagation is computed deterministically by solving Maxwell's equations. The models rely little on the measurements, but on the available data describing the details of the environment and obstacles. In urban channel modeling, two types of propagation analytics based models are commonly utilized: Ray-Tracing Technique and Waveguide Model, we will review the Ray tracing model in more details and cover Waveguide model in brevity.

The Ray tracing models are developed based on Geometrical Opics (GO) theory, which assumes the radiation of the energy of the signal can be modeled as tiny small tubes or rays. In free space, the rays travel in straight line and may get redirected when interacting with environment and obstacles through reflection, refraction and diffraction which is based on geometrical theory of diffraction (GTD), uniform GTD (UTD) [74]. With consideration of three types of rays, models are able to maintain the good field continuities. The path loss calculation is done through summing up all the loss along many distinct paths more than just LOS links. The normal input data of ray tracing models include vector dimension data of buildings in 2-D or 3-D, interfering structures, material properties and terrain information for urban channels. In the early stage of ray tracing modeling, researchers focused on construction of two-dimensional models. In 2D models, all rays are launched in a plane along different directions. The angle resolution of the rays are the determine factor of computation time. Some 2-D ray racing applications in urban settings can be found in [75], [77]-[79], [77] modeled the LOS links in urban microcell with 2D 6 rays tracing models, [78] proposed a 2-D ray tracing model for urban

microcellular environments with non-uniform buildings and arbitrary layouts which furthered the efforts made in [79] whose model built upon uniformly spaced building and street layout. The earliest 2-D ray tracing model that factored in diffraction is reported in [75]. The buildings in the urban microcell environments, which are much higher than the base station antenna and receiving antenna, were modeled as the vertical knife edges and ignore the over-rooftop diffraction and ground reflection since author found out no rays that reach the receiver consists of ground reflection interaction existed in NLOS links and ground reflections is very insignificant in LOS link in terms of affection to the overall link performance.

For 2-D ray tracing technique, important parameters include building location vector, building wall complex permittivity, antenna location vector and radiation pattern at the operating frequency. The 2-D ray tracing model are considered appropriate and accurate model in the urban Canyon condition which describes the ground based peer-to-peer wireless communication in high rise urban environments whose building rooftop is much higher than antennas [76].

The more recent research works focused on 3-D ray tracing models as computation power has become less of an issue. Over 2-D ray tracing models, 3-D ray tracing requires more environment details thereof the additional dimensions. The transmitter and receiver are modeled as a point source in a 3D space, so antenna pattern has to encompass the azimuth and elevation beam width and both the elevation angle and azimuth angle have to be accounted to predict the propagation path. However, the computation procedures behind 2-D ray tracing and 3-D ray tracing are similar. To obtain better performance, 3-D ray tracing would normally determine the limited number of the dominant ray path to estimate the path loss. However, the deployment of diffraction model makes it extremely time consuming

since diffraction caused by impingement of signal on the building edge would lead to generation of the whole family of new rays. However, to achieve the balance between accuracy and the complexity, only the limited number of refraction could be considered in the any given path, normal value is set below 2.

The 3-D ray tracing modeling examples are presented in many recent literatures. In [80], authors proposed a 3-D ray tracing model that combines with COST-231 for LOS links in urban area and indoor links for radio network planning. A larger amount of preprocessing was done to mitigate the modeling complexity. In [81], Liang et. al. tried to account more diffractions in the 3D ray tracing model they proposed through developing vertical plan launch (VPL) method which was able to approximate the diffractions from horizontal edges and limit the diffracted rays to lie in either the plane of incidence or in the plane of reflection.

Many hybrid modeling strategies also emerged to improve the efficiency of 3D ray tracing. In [82], hybridization of Finite-Difference Time-Domain (FDTD) method is used for modeling of indoor radio-wave propagation. FDTD is used because FDTD is better than ray chasing model in the prediction of propagation characteristics in structure defined with complex material properties. The other hybrid attempts in [83] combined the ray tracing with periodic moment method (PMM) for indoor propagation study for periodical structures in buildings. The collective data on reflection coefficient, grating transmissions were obtained by PMM and further input to ray tracing model to find the reflected and grating rays that intrude in one of the periodic structure. Contiguous trace of the ray needed to be done to find the final received power at the receiving end. In addition, more comprehensive coverage of various ray tracing methods and optimizations can be found in [84].

Overall, the ray tracing model achieved the good accuracy in radio propagation prediction of large buildings which encompasses multiple walls in between transmitters and receivers. Still, ray tracing model's accuracy is closely correlated to the data describing the empirical environment, which is seldom available and subject to change regularly, the cost of collecting and updating the data would also be tremendous. Although some researchers [76] [86] have shown that the accurate results can be achieved with mediocre degree of environment details, the link between input details and result accuracy is still unjustifiable. On the other hand, the ray tracing model is notorious for its tedious analysis duration. In a nutshell, ray tracing model is promising by delivering a high prediction performance of radio propagation channel characterization with the premise of high fidelity of environment data as input. Further efforts are necessary in order to achieve better efficiency.

The waveguide model is developed for metropolitan areas which have dense high rise and both base station and mobile unit are under rooftop. In the case, the streets function as the lossy wave guide [87] [88]. In [87], the mapping of field in street waveguide structure was performed, the street is modeled as multislit waveguide and the stilts are assumed to follow poison distribution. Actual attenuation measured in urban 1-2km LOS links in UHF frequency band showed good match with proposed theoretical path loss prediction method. Path loss study of waveguide like structures are performed further in [89]-[91] for LOS corridor links in commercial buildings and office buildings, the path loss was found to decay slower than free space path loss model and thus author attributed the main reasons to the analog waveguide effects.

2.2.2 Small scale multipath fading in urban channel

The small-scale multipath fading is usually characterized by the channel impulse response (CIR) and delay dispersion of the channel. Extensive research works have been done in urban environments. Early in 1975, Cox et al. [92] conducted a series of multipath measurement in New York at 910MHz, they model the power delay profile with exponential models with negative slope and found value of mean delay spread that account for 90^{th} percentile of cumulative distributions approximates 400ns. Cox [4] is also the first researcher who introduced spread spectrum cross-correlation for measuring the magnitude of the CIR through power delay profile that provides routine standard to characterize the wideband channel delay dispersion. In [5], Sousa et al. proposed a new improved constant false alarm rate (CFAR) threshold algorithm to treat multiple power delay profiles obtained from the measurements conducted in Toronto area to justify the multipath from noise components, the CFAR was originated from Radar application to find the probability that noise surpasses the threshold in any given sample data. The new threshold algorithm combines the original CFAR method and Markov chain that was used to describe the sequential processing of multiple PDPs. The Sousa deployed the spread spectrum sliding correlator system to measure delay spread at 910 MHz and yields the RMS delay spread value up to 3μs and excess delay spread up to 5μs in urban cell measurements. The algorithm is also deployed in our analysis later. Besides, authors also investigated the effect of directive antenna with 60 degree beam width. They claimed an average 60% of reduction of delay dispersion of measured channels. The delay spread values were overall smaller compared to the [94] measured in US due to the flatness of Toronto area and experiments were conducted in real existing cell thus smaller shadowing effects. [94] Reported the measurements conducted in four US cities: Washington, Greenbelt, Oakland, and San Francisco, the average

delay spread value up to 6μs, which is considered significantly larger than most of measurement results in other literature. In [95] [96], measurements in Philadelphia, Pennsylvania, Denver, Colorado were conducted in both urban high rise and normal urban environments. The measured delay spread values were much smaller than what was reported in [94] and reported delay spread in urban high rise are very similar as shown in Table I

Table I: Delay spread measurement in [95] [96]

Environment	90 % RMS DS	50 % RMS DS	10 % RMS DS
Urban [95]	0.06μs	0.14μs	0.41μs
Urban High-Rise [95]	0.2μs	0.65μs	1.2μs
Urban High-Rise [96]	0.3μs	0.7μs	1.2μs

More recently, Matolak et al. [14] conducted a series of peer-to-peer ground based urban channel characterization experiment with VNA based system in Denver financial district with focus of public safety frequency bands in 700MHz and 4900MHz. The LOS PDP is modeled with negative exponential models and the number of MPC components is found to follow uniform distribution with proper weighting method applied. Since the experiments were conducted in short range (less than 100m), the 90 percentile values of root mean square delay spread (RMS-DS) is found to range from 100ns for LOS at 700MH to the 170ns for NLOS at 4900MHz. the author further characterized the delay dispersion through maximum excess delay at 25 dB, mean value is found to range from 384ns for LOS at 700MHz to the 791ns for NLOS at 4900MHz.

For urban macro-cell, COST 259 macro model [98] cited the work done by Greenstein et al [48] to explain the RMS DS characterization in general typical urban

(GTU) and general bad urban (GBU), Greenstein measured the delay spread data from the city of Stockholm, Sweden and fitted those data to lognormal, Nakagami, Rayleigh, Rice Suzuki, and Weibull distributions with Kolmogorov-Smirnov goodness-of-fit to find the most suitable distribution. Greenstein claimed that the lognormal distribution best represented the RMS delay spread from all measured locations and recommended the median RMS delay spread value of 400ns for the GTU and 1μs for GBU. It is worth to note that Greenstein further investigated the correlation between delay spread, distance and path loss with assumption of lognormal distribution of delay spread for particular distance range, and an equation between median delay spread value and distance in urban areas was given by (2.23):

$$\tau_{med} = 0.76Td_{\max}^{0.5} \tag{2.23}$$

where T is the distance range of interest, d_{max} is the maximum radius of the measurement areas.

Interestingly, Greenstein furthered his effort of relating RMS delay spread to distance by using the data set from Devasirvatham [100] who failed to do so. Instead of correlating to the distance directly, Greenstein related RMS delay spread value to received power, and found power factor in 2.23 changes from 0.5 to 0.48.

2.3 Review of RF propagation Simulators

In this study, commercial RF propagation software based on ray tracing model is used. The RF propagation simulators offer virtual platform for network service providers to predict service coverage, build high fidelity of electromagnetic environment and offers cost-effective solution to simulate repeatable experiments in the environment models devised by the users to save the upfront investment cost in real field trial deployment. On the other hand, software provides high scalability

regarding the size of simulated environments and the number of deployed hardwares in the system. However, the general pitfall of wireless existing simulators is tedious computation duration especially for large propagation environment or complicated network topologies. For example, the computation of diffraction mode requires enormous time as mentioned in the ray tracing model review in the section 2.2. In this section, we would introduce two popular commercial wireless propagation simulators (highlighted in yellow in Table III). Remcom Wireless Insite will be introduced in the Chapter 3. Furthermore, we will also tabulate out the most of available RF propagation simulators for inquisitive readers to further explore the available choices.

The Winprop [102] is the wave propagation and radio network planning tool developed by AWE communication [101]. It is the one of the most well rounded wave propagation and network planning tools available in the market because of a body of modules included for different intendance. The WinProp has six modules available for propagation scenarios: PRO-R for Rural area; PRO-U for Urban areas, PRO-C for Hybrid Urban & Indoor scenarios, PRO-I for Indoor & Campus, PRO-T for Tunnels & Stadiums and PRO-V for Time variant objects. PRO-U and PRO-C are suitable for our studies.

PRO-U assumes dominating mode of reflection and diffraction of the buildings for EM wave propagation in urban scenarios. It supports the Hata, COST 231 Walfish-Ikegami Model, Urban Dominant Path Model and 3D Ray Tracing Model.
PRO-C is a slightly more complex engine that allows the transition between urban and indoor propagation. The hybridization of urban model and indoor propagation models works cohesively in the engine with adapted resolutions as shown in figure 6. Thus for outdoor propagation it follows the same models as PRO-U but

additional fidelity is added to account for signal propagation in indoor environment which considers the signal penetration through the wall.

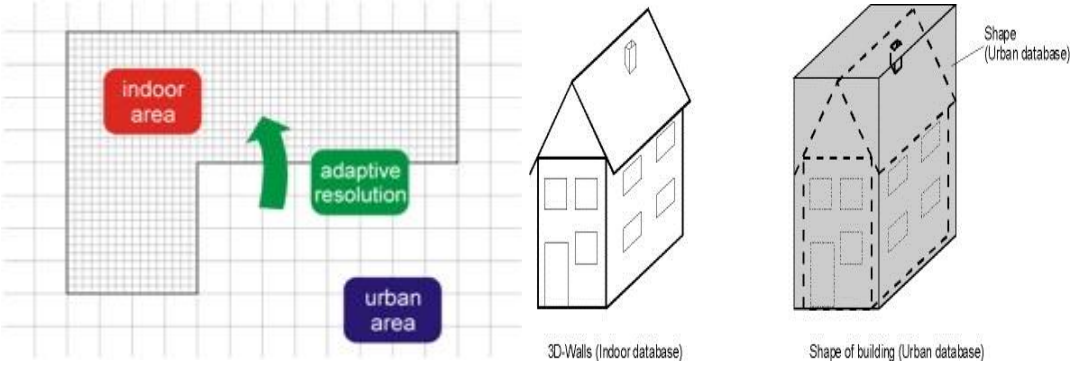

Figure 6 Adaptive resolutions for different scenarios © AWE

Urban Dominant Path model is based on wave guiding models due to the multiple reflections in the urban street canyons, the wave guiding effect is computed at each at each point in the prediction model. The 3D urban intelligent ray tracing is the ray tracing engine for urban scenario. The engine approaches computation of ray path through intensive preprocessing of the building data and accelerate the computation process based upon three assumptions:

- Dominating rays deliver the majority of energy
- The visibility relation between walls and edges does not depend on the position of the base station antenna
- Similar rays reach for neighbouring receiver pixels

One downside about the PRO-U compared to the simulator we used is the maximum number of reflection can only be set to 6 as listed and maximum 2 diffractions are allowed as shown in the following table:

Table II: Path Class in PRO-U 3D ray tracing Engine © AWE

Path Class	Description
1	Direct path
2	Single reflection
3	Double reflection
4	Single diffraction
5	Triple reflection
6	One reflection + one diffraction
7	Double diffraction
8	Two reflections + one diffraction
9	Four reflections
10	Five reflections
11	Six reflections

Due to the reason of very limited number of reflections and diffractions, the ray may or may not reach the prediction point, the remaining job of path loss prediction need post-processing with COST 231 Walfisch-Ikegami Model. The credibility of hybrid method is difficult to assess when prediction points are not reached sometimes, the lack of sound representation of the propagation paths is the other problem to illustrating the results. Thus WinProp is suitable choice for our experiments.

The EDX SignalPro is the RF planning software designed by EDX wireless that provides the advanced network design abilities in frequency range of 30MHz to 100GHz for various kinds of RF planning. The most unique feature of SignalPro includes seamless integration with Google Earth Plug-in by importing KML file as shown in Figure 7.

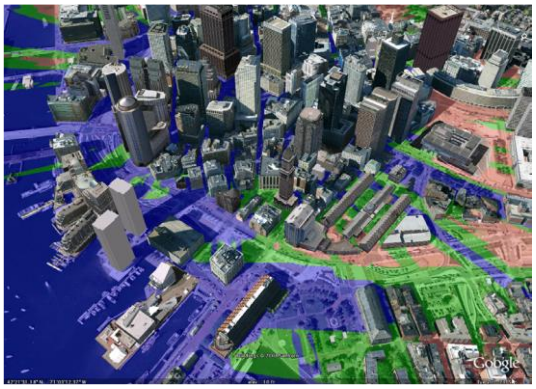

Figure 7 Google Earth Plug-in Integration Feature © EDX

The tool offers peer-to-peer and peer-to-multipoint path analysis by considering the rain fade outages, link availability and fade margin and allows foliage, building and terrain and many other elements to be built in models and provides real time link analysis with the interactive display. It supports 2D or 3D route study. The software contains advanced propagation module which include 2D and 3D ray tracing. It is able to generate simulation results like path loss, field strength, received power, shadowing, BER, link availability, Delay spread, Channel capacity and so on. Moreover, it encompasses the interactive interface to show real time waveform of the received signals for user to visualize the dynamic nature of the distortions more intuitively as shown in Figure 8.

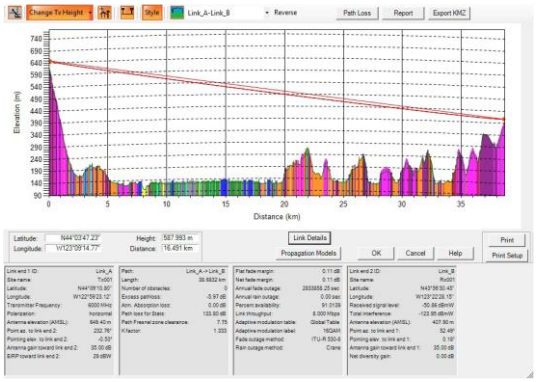

Figure 8 Peer-to-Peer Path Study © EDX

The software provides great convenience for urban channel simulation since the integration of Google Earth plugin and Bing Maps. This made the originally scarce

city landscaping data easily accessible from credible sources. Due to availability of the software, we are not able to judge whether it is more suitable software for our studies. However, the Google earth plugin is the enchanting asset that our simulator is lacking.

Table III lists many major commercial radio propagation tools and associated links to the details introduction for inquisitive reader to further explored the desired options. Broadly speaking, 3-D ray tracing make use of ray tracing engine to predict possible reflection, transmission and diffraction during the propagation of ray in the 3-D environment. User can either build 3D models from a clean slate or import the data source that is within the software capacity. The option has made RF propagation software popular since it is more site specific and heuristic than empirical models that were determined elsewhere and were normally confined in certain frequency range and parameters such as antenna height and environment types.

The selection of RF propagation simulators depends on preference of the network designer and library supports that include all necessary modeling components or the intended models, the fidelity of the available data and corresponding software support capacity. During the actual simulation, the proper parameter settings, boundary scale, model selection and computation duration have to be pondered on in order to obtained legitimate simulated results.

Table III: Lists of Available Commercial Radio EM propagation Tools

Tool	Company	Website
Wireless InSite	**Remcom, Inc,**	http://www.remcom.com/wireless-insite
Athena	**Wave Concepts**	http://www.waveconceptsintl.com/
CellOpt	**Actix**	http://www.actix.com/main.html
EDX SignalPro	**EDX Wireless**	http://www.edx.com/
ENTERPRISE Suite	**ENTERPRISE Suite**	http://www.aircominternational.com/
LANPlanner	**Motorola, Inc.**	http://www.motorola.com
Mentum Planet	**Mentum Planet**	http://www.mentum.com
Pathloss	**Contract Telecommunication Engineering**	http://www.pathloss.com/
PlotPath	**V-Soft Communications LLC**	http://www.vsoft.com/
Profiler-eQ	**Equilateral Technologies**	http://www.equilateral.com/
RFCAD	**Sitesafe**	http://www.rfcad.com/
RPS	**Radioplan GmbH**	http://www.radioplan.com
Volcano	**SIRADEL**	http://www.siradel.com
Wavesight	**Wavecall**	http://www.wavecall.com
WinProp	**AWE Communications**	http://www.awe-communications.com/

2.4 Conclusion

This chapter performed the detailed review to the topics that are related to channel modeling and characterization in urban environments. The chapter starts with introduction of fundamentals in radio propagation that help to understand basic approaches to characterize wireless channels and propagation phenomena. The chapter proceeds with detailed review of literature on urban channel modeling from two aspects: large-scale path loss modeling and small-scale multipath fading. In large scale path modeling, both empirical based path loss models and propagation analytics model are reviewed. In small-scale multipath fading review, several

measurements results of delay dispersion in European and American cities are covered, novel attempts to characterize time dispersion of urban channels are presented. Lastly, the chapter briefly reviewed two existing popular commercial radio propagation software and their suitability to our studies.

Although the urban channel is well studied with presence of numerical literature in indoor, outdoor, microcell and macro-cell condition, most of recent studies align their research interests with the most recent commercial wireless application and focus of measurements are taken place on propagation centered on range from 700MHz to 2100MHz, which provides band coverage of LTE standard and PCS band. The urban channel characterization in military UHF band is lacking. Thus, the research work which investigates channel characterization in military UHF band in Singapore fills the vacuum. We will cover them in details in the following chapters.

Chapter 3

Channel Sounder Systems & Simulator

In the last chapter, we reviewed on the past literature and research works of urban channel characterization and modeling in related type of links and relevant frequency range of interest. There have been sizable evidential proofs that channel sounding techniques provided reliable data and models for channel parameter estimation for the pertaining environments. In our research work, specially devised channel sounder system has been used to perform the sustainable and reliable channel data collections over the long haul measurement campaign in past two years. The details of the system setup used in the measurement campaign will be elaborated with the explanation of the working mechanisms beneath the systems and sample data sample will also be displayed to facilitate the deeper understanding. On the other hand, the ray tracing simulator used to restore the empirical channel setting and verify propagation mechanism will be covered in the chapter.

3.1 Channel Sounder Systems

Our measurement campaigns are carried out in two kinds, namely, narrowband measurements and wideband measurements which examine the large scale channel characteristics and small scale channel characteristics respectively. Channel Souder is the instrument that captures the response of a wireless channel.

3.1.1 Narrowband Channel Sounder

Narrowband channel sounder has the simplest form among all types of channel

sounders. The source end transmits single frequency signal and receiver end recorded received signal strength. One of downside of single carrier measurements infinite temporal resolutions, so the replicas of signal arrive with different delays are not distinguished. In order to address the problem, we usually use average received power strength from data collected from temporal sampling.

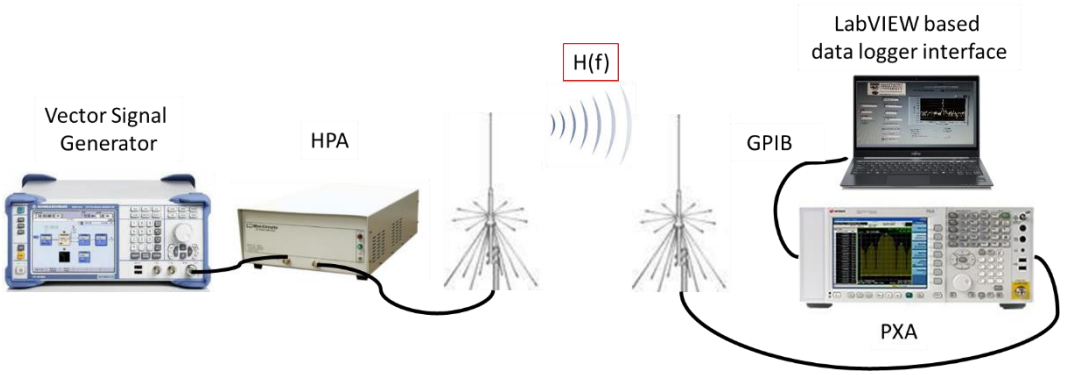

Figure 9 Narrowband Channel Sounder

Figure 9 shows the block diagram of the narrowband sounder deployed in our channel measurements. Vector signal generator is the source that transmits a single frequency signal, a high power amplifier with a gain of 30dB is used to ensure the signal reception and a human height (1.7m) Omni-directional vertical polarized discone antenna constitutes the transmitting end. At the receiver, the discorn antenna with the same specifications is used to receive the signal. The experimental data is captured by the spectrum analyzer (Agilent PXA) and are passed to a Laptop via a General Purpose Interface Bus (GPIB), the peak signal strength is logged at every one second interval to address aforementioned replicas problem by a data logger using the in-house LabVIEW program.

For outdoor-to-indoor link measurement, transmitting antenna is fixed on a small van as shown in Figure 10. GPS data is logged continuously throughout the measurement process to obtain altitude, longitude, and latitude stamped with satellite time, at data logger end, the time has to be synchronized with the satellite

time prior to the experiment so that all the data recorded are time stamped with the GPS time in order to synchronize the data collected at the receiver with the location to estimate slant link distance and map them accurately.

Figure 10 Transmitting antenna setup

3.1.2 Wideband Channel Sounder

The aforementioned narrowband sounding technique has limitations in terms of distinguishing the signal replicas that arrive at different delays, which make it impossible to measure the other important aspects of channel characterization, small-scale fading effects. Wideband channel sounding is designed to resolve the issue. Swept-frequency approach based on vector network analyzer is commonly used in wideband channel sounding. It sweeps a single frequency across a frequency band in quickly contiguous manners and compares the amplitude/phase of the received signal with the transmitted signal. Complex channel frequency response is gauged by applying inverse Fourier transform to the directly measured complex frequency channel response. This approach has been widely used for short range indoor link such as in [26] [27] [28], it has also been deployed in outdoor links in [14] with measurement links distance up to 100 meters. While VNA based channel

sounder offers many advantages such as easy implementation, high delay, spatial resolution, and high resolution of angle of arrival (AOA) [27]. They are limited by slow frequency sweeping rate, channel has to be ensured to be static over the frequency sweep time. On the other hand, measurement distance is the other hurdle, not only the feasibility of the system will be constrained by the availability of length of cable since both transmitter and receiver have to be connected to the two ports on the VNA, the synchronization between transmitter and receiver accounting for the amplitude and phase change introduced by the long range connection. In our measurement campaigns, the link distance is up to 3 km. VNA based system would be inappropriate for our measurement. Therefore, we will introduce the other suitable wideband channel sounder that used in our measurement campaign, namely, spread spectrum correlator.

This practical method is first used by Cox [4] in 1972 to measure the outdoor suburban environment at 910 MHz. The sliding correlator channel sounder is the time domain channel sounding technique. It transmits a direct sequence spread spectrum (DSSS) signal, which uses BPSK to modulate an RF carrier with maximal-length pseudo-random noise sequence, which is also called m-sequence. At the receiver end, the sliding correlator is to produce a time-dilated PN autocorrelation, while in the real case, the sliding correlator involves two similar signals whereby one is slightly delayed in time compared to the other, this makes filtering the subsequent essential stage to obtain a ‘clean’ time-dilated autocorrelation. We then obtain the channel impulse response at the output of the dispreading process. One of the biggest advantages over VNA based system is elimination of m sequence synchronization through the sliding correlator, besides, it requires lower transmitting power due to the inherent “process gain” from spreading

power spectrum of unwanted noise. Another advantage is the good immunity to the passband noise [30] and thus all of above offer very good potential for long range link measurements.

Figure 11 shows the block diagram of the spread spectrum sliding correlator channel sounder used in our study. In our measurement 8901-bit PN sequence is preloaded in the vector signal generator, a selected single carrier signal in military UHF band of interest will be spread over the m sequence and amplified by the 30dB high power amplifier. It is subsequently transmitted in chip rate of 10Mysms/s with temporal resolution of 100ns, which indicates a minimum range resolution of 30 meters. At the receiver end, signal is received and down converted by the Agilent PXA and sampled by NI data logger with 100MSamples/s sampling rate and is GPS time labeled like narrowband measurements. The following table summarizes the parameters settings of the wideband system,

Table IV : Parameter Settings for Spread Spectrum Sliding Correlator Channel Sounder

Centre frequency	250 MHz - 370MHz
Modulation	BPSK
PN length	8091-bits
Transmitting power	20dBm
PN Chip rate	10Msymbols/s

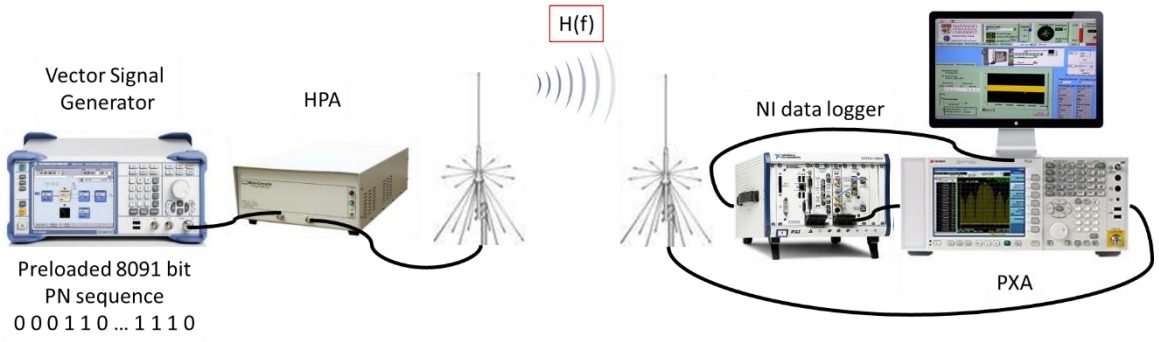

Figure 11 Wideband Channel Sounder

The collected data is then despreaded with the source PN sequence in Matlab to obtain the channel impulse response (CIR). The obtained CIR fidelity is controlled by system capacities which are determined by only three parameters: PN length L, PN chip rate f_c and slide factor γ. Several key system capacities in time-invariant wireless channel measurement are introduced below.

1. **Processing Gain**

   Process gain is the ratio of post process signal to noise ratio (*SNR*) to the original *SNR*. In DSSS system [31], high process gain weakens the power spectrum density (PSD) of undesired noise. When baseband wave multiplies with the receiver PN will spread the noise power spectral density across a bandwidth of f_{chip} (chip rate of PN sequence at sliding correlation process) and filtered. The processing gain is thus expressed as (3.1):

$$G_p = 10\log_{10}(L)(dB) \tag{3.1}$$

2. **Dynamic Range**

   The dynamic range is defined as the difference in signal strength between possible largest and smallest received path components in the output power delay profile (PDP). The upper bound of realized dynamic range that a DSSS system can provide, $D_{R,\,ceil}$ is approximated as (3.2) in

$$D_{R,ceil} = 20\log_{10}(L)(dB) \quad (3.2)$$

3. **Time Resolution**

   The time resolution indicates how the system is able to resolve the delay of the multipath component. For sliding correlator channel sounder, the upper bound of time resolution is defined as (3.3)

$$T_{res} = 1/f_c \quad (3.3)$$

4. **Maximum Resolvable Path Length**

   Maximum resolvable path length is defined as product of one period of the transmitted PN sequence and signal propagation velocity in free space (speed of light). The max resolvable path length is expressed as (3.4)

$$d_{\max} = c\frac{L}{f_c} \quad (3.4)$$

From above, our system capacities could be estimated. The wideband channel sounder introduced in figure 3 has estimated process gain of 78.2 dB, provides maximum dynamic range of 39 dB, temporal resolution of 100ns and maximum resolvable path length of 242 km. These should provide the ample capacity for our measurement campaigns.

3.1.3 GPS System

Figure 12 shows the GPS system and antenna deployed in our study. It is the XL-GPS system from Symmetricom. The GPS is able to synchronize to the Coordinated Universal Time (UTC) and provides better than 30 ns RMS accuracy to UTC after connected with sufficient satellites and feed the time information and Geographical coordinate data (latitude, longitude, and elevation) in to data logger and stamp every

collected data files. The XL-GPS integration with the system is shown in Figure 13 with highlighted read cables.

Figure 12 Symmetricom XL-GPS

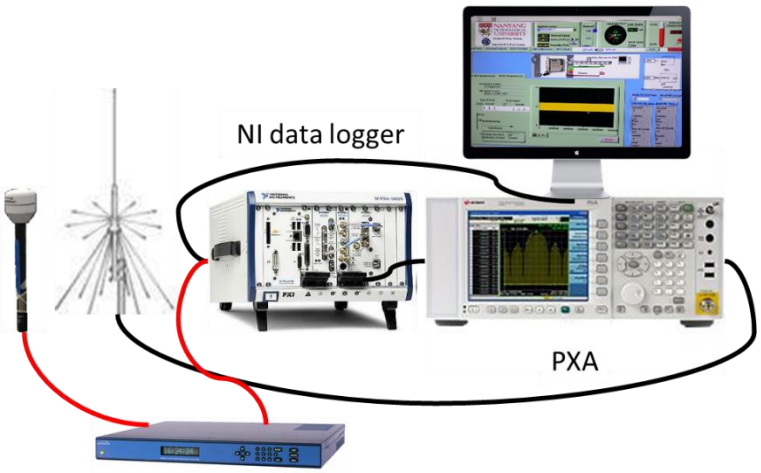

Figure 13 XL GPS Integration with Receiver

3.2 Simulator

The 3D ray tracing simulations is performed in this work with the commercial 3D ray-tracing simulator "Wireless Insite [32]" to investigate and rationalize most possible propagation mechanisms in the measured channel links.

The simulator allows the user to build a virtual building or terrain environment with the inbuilt editing tools, or to load the environment settings from file formats such as DXF, DETD, and USGS.

The Full 3-D propagation model used in the simulations in this work is a ray tracing model based on the Uniform Theory of Diffraction (UTD). Ray-tracing algorithms are combined with UTD to find the propagation paths to each receiver

point. The shooting bouncing ray algorithm [34] is used to form the propagation links from the transmitter to the receiver points which shoots rays from the transmitters and propagating them through the designed environmental model. Geometrical Theory of Diffraction (GTD) is the procedure used to identify diffracting edges.

The shooting ray will interact with environment features which includes reflection; diffraction off of an edge and/or penetrations through a wall. The effects of each interaction along each ray's path to the receiver are displayed in the simulation results and the received signal level is evaluated based on the different propagation mechanisms. At each receiver location, rays are combined and evaluated to determine signal characteristics such as path loss, delay, delay spread, direction of arrival, and impulse response. The simulation setup parameters include the transmitter power, maximum number of reflection, transmission, diffraction and the output path. After simulation, users can also view the specific ray paths and combinations of ray paths for each transmitter/receiver pair and the amplitudes associated with the paths.

The simulation results based on actual measurement compared are covered in later Chapters. However, it is noteworthy that the results serve as only qualitative illustration of the propagation phenomena observed from the measurement results but provide little in qualitative reference. Because the 3-D models constructed in simulation is the only simplified version of the actual sounding environment during measurement.

3.3 Conclusion

In summary, brief introductions on the channel sounding systems and ray-tracing simulator are covered in the chapter. Both narrowband and wideband system setup are shown and explained. The narrowband sounding system is straight forward but limited in large scale channel characterization measurement. Spread spectrum sliding correlator channel sounder is selected as the appropriate wideband sounding system over frequency-swept VNA based system due to the nature of measurement campaign and system limitations stated. The devised system capability is assessed with several key parameters. The used GPS tracking system is also briefly touched. Finally, 3-D ray tracing simulator which is used to validate the propagation mechanisms based on the measurement results is introduced in this chapter.

Chapter 4

Urban Shopping District Path loss Modeling

Large-scale path loss characterization is investigated around dense urban environment in Singapore in the presence of dominating non-line-of-sight (NLOS) links scenarios at military UHF band for selected frequencies (250-370MHz). Measurements deployed the narrowband sound system described in the chapter 3 are conducted at the Singapore endsville shopping district-orchard road. The objective of the measurement is to characterize the outdoor-to-indoor link path loss performance. The results are then modeled with classic empirical log-distance model with least minimum square error linear regression. Furthermore, the 3-D ray tracing simulation is carried out to verify the experiment data collected in narrowband measurements. The further investigation of propagation mechanism is performed, finally, the link availability of outdoor-to-indoor links are analyzed along the two routes. The results and discussions are elaborated in the following sections.

4.1 Measurement campaign

(a) (b)

Figure 14 (a) Antenna position within the hotel room. (b) Surrounding buildings.

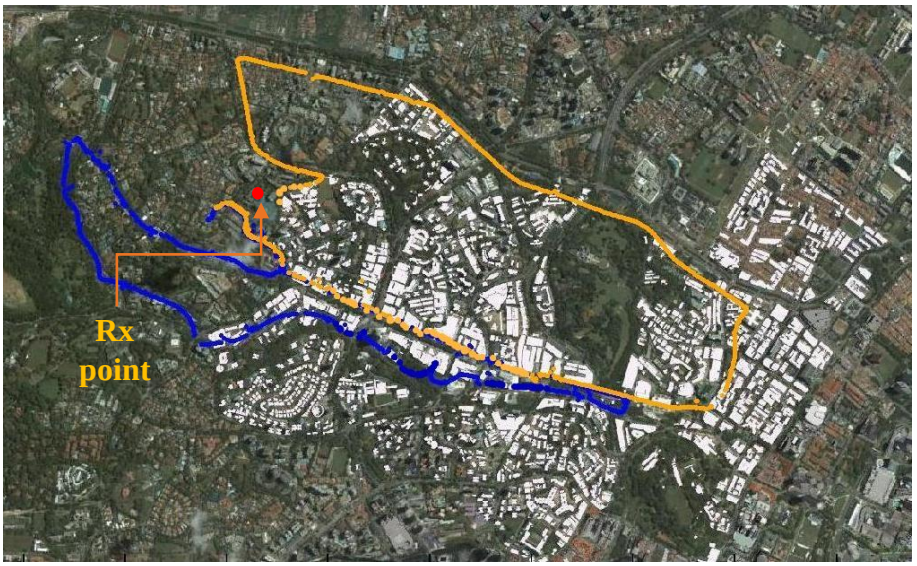

Figure 15 Measurement Route

The measurements were conducted around the area of central shopping district - Orchard road in Singapore on March 6th and 7th, 2013. In the outdoor-to-indoor measurement campaign, the outdoor environment features sizable amount of dense high rise buildings, shopping malls and hotels as shown in Figure 14(a). The

receiver antenna was placed indoor in a hotel guest room environment as shown in Figure 14(b). The receiver antenna was placed at approximate elevation of 60m above street level (level height of 58m and antenna height of 1.7m). Receiving antenna was placed near French window in order to suffer from less propagation loss and better signal reception.

The ground based transmitting antenna with pedestrian height was installed in a moving van and travelled along two preplanned routes at speed up to 30 km/h as illustrated from Figure 15. Based upon the GPS data collected during the measurement, we computed that the link slant distance of links varies from 300m to 2300m for route 1 and 300m to 2800m to route 2. The most of links presented are considered Non Line of Sight (NLOS) links due to the indoor location of receiving antenna.

The measurement deployed Agilent PXA spectrum analyzer to capture the experiment data which contains information of channel transfer function H (f). The data was stored for post processing. The two identical vertically polarized omni-directional discone antennas are used at transmitter and receiver sites. Figure 11 illustrates the spread channel sounding setup. Both antennas are mounted on tripods for the convenience of standing and moving. Both antennas have standing height of 1.7m and 2.4dBi gain and VSWR of 1.5.

For narrowband channel sounding, a single frequency signal is transmitted from the transmitter. We performed measurements in four selected frequencies in UHF band, which are 250MHz, 320MHz, 350MHz and 370MHz. Constant transmitting power of 20dBm is used to ensure consistency of collected data across different frequencies.

4.2 Measurement results

4.2.1. Interference Level Measurements

Figure 16 shows the average interference level obtained from 1000 copies of continuous noise floor measurements in the Hotel guest room. From Figure 16, four clusters of significant signal transmission are observed over the frequency band of interest ranging from 220 to 500 MHz. Among these clusters, the 4th cluster transmitting at above 410 MHz is large one containing interferences at different frequency band. Based on IDA spectrum allocation chart [103] listed in Table V, the source for all the four clusters of interference can be identified. Frequencies (250 MHz, 320 MHz, 350 MHz, and 370 MHz) are carefully selected to avoid those interferences. The noise floor of the selected frequencies in the measurement for four frequencies has mean value of -111dBm

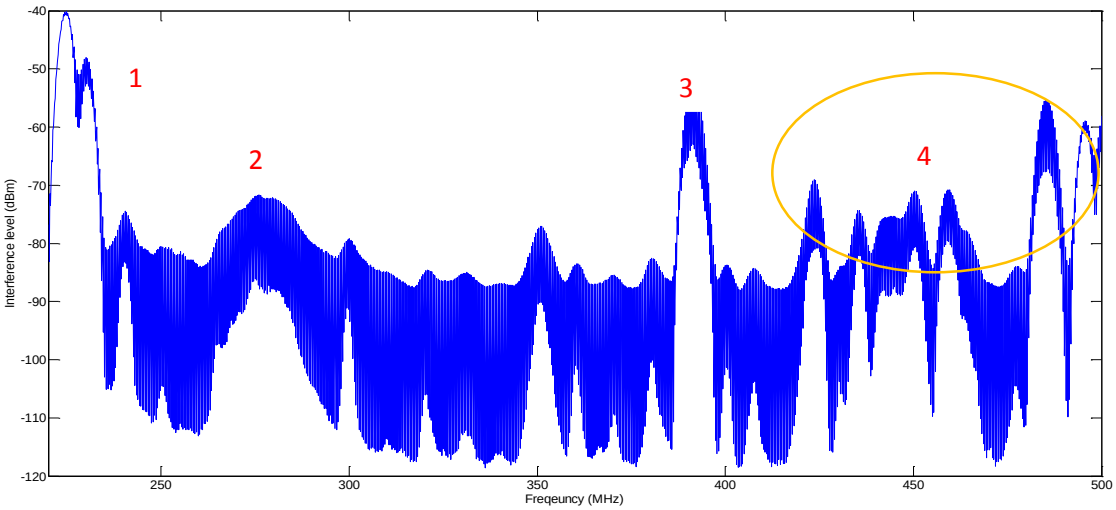

Figure 16 Average Interference Level over the band of interest in the Hotel Guest Room

Table V: Spectrum Allocation from IDA [103]

Frequency Range	Existing Service	Corresponding Cluster in Figure 16
174-230 MHz	Digital Broadcasting Services	1
279-280 MHz	1-way/2-way Paging Services	2
380-400 MHz	Trunked Radio Services	3
410-430 MHz	Digital Trunk Radio Systems	4
430-470 MHz	Mobile Services	4
470-494 MHz	Low power Land Mobile Services	4
494 -790 MHz	Analogue/Digital Broadcasting Services	4

4.2.2. Route Study along the Orchard Area

Path losses are measured under narrowband setup which transmits a single frequency continuous wave (CW) signal from the mobile transmitter to indoor receiver. We recorded the peak received power levels through LabVIEW programme via PXA within span of 0.01MHz centered in one selected UHF frequency each time. Due to big coverage of devised routes, the received power levels of approximate 1500 transmitter-receiver location pairs along each route were recorded. Each data was assigned with corresponding GPS geo location data for link distance estimation.

Figure 17 shows a plot of received power at 320 MHz for two preplanned routes in Orchard area. Geographical map is snapped from Google Earth 2013, in which white clusters are the 3-D models of significant buildings with the measurement area. Based upon which, 3-D ray tracing model was constructed in simulator to verify the general trend pattern of path loss and will be covered in details later. The received power is depicted in the corresponding location along the route by scatter plot, where strength of power is indicated by the color bar. Red color indicates strong signal strength up to -27dBm and blue indicates weak signal strength down to -118dBm. The mean received power collected from route 1 (-79.3dBm) is 8.2 dB higher than

route 2 (-88.1dBm). Similar deduction can also be obtained from observation of Figure 17, with the identical power scale, route 2 exhibited longer blue segment concentrated around the right side of the route in Figure 17(b) compared to route 1. The main reason is that route 2 encircles the much denser high-rise cluster which is highlighted within the yellow circle.

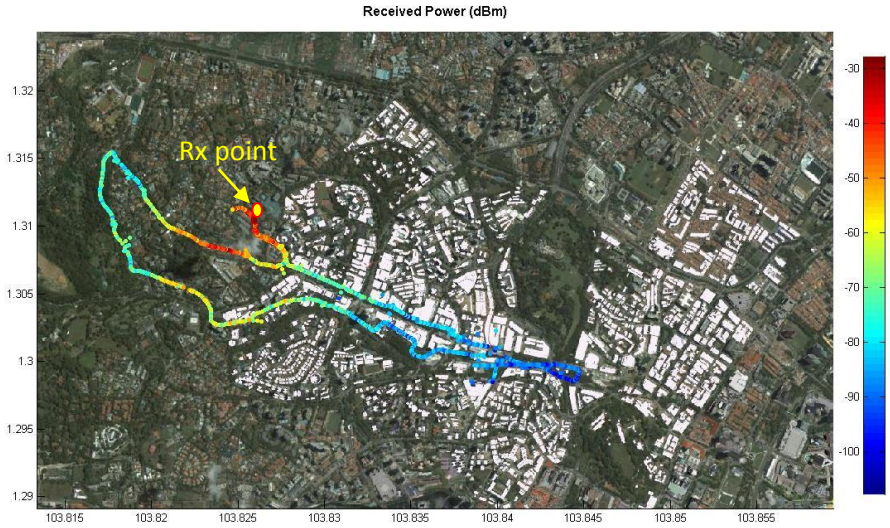

(a)

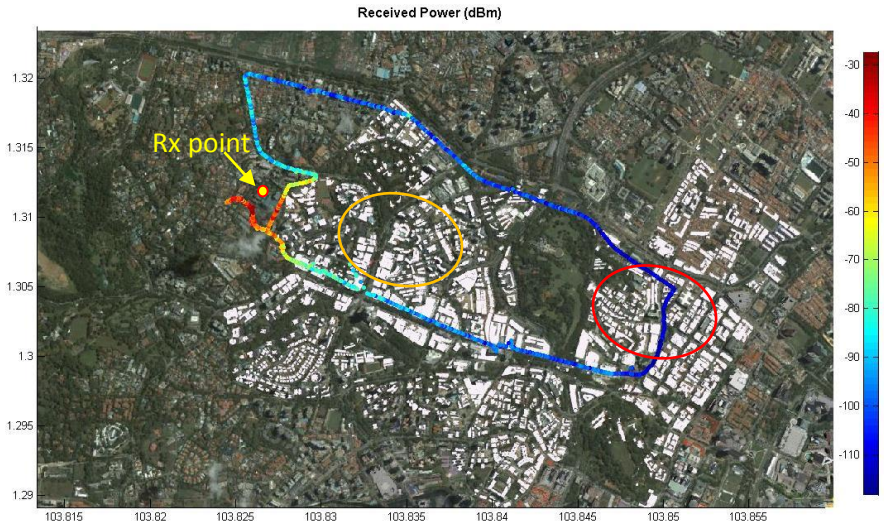

(b)

Figure 17 Empirical received power strength for 320MHz Geographical Map plot (a) Route 1. (b) Route 2

Transmitted signal will have to take longer path through a number of diffractions

and reflections instead of propagating through the dense clusters via a number of transmissions through building's brick walls (at least two layers of brick walls transmission are required for one buildings) and attenuate the signal for a great magnitude and fall to noise floor level before it reaches the receiver. A simulated propagation link with the longest distance from full 3-D ray tracing simulator is shown in Figure 18, where 5 most significant multipath components (blue path) with smallest path loss are illustrated, it has been known that the received signal for a transmitter receiver pair consists of vector summation of multiple signal replicas which is referred to as multipath. In urban outdoor propagation the dominant propagation is reflections and transmissions assumed by many ray tracing models. From Figure 18, we clearly see that signal has to travel more extra length than the slant distance of the links, which leads to the deep fade area highlighted in red circle of Figure 17(b).

Figure 18 Visualization for multi-path components propagation paths with the longest link distance

The other possible reason that Route 1 has general better received power level is likely due to that more test points along route 1 experience OLOS whose dominant propagation links transmit through French window directly to outdoor environment without complicated indoor propagation mechanism or transmitting out from indoor

space through transmission of concrete wall. Dielectric material skin depth as defined in (4.1) provides valid theoretical reasoning by defining the propagation distance in certain dielectric material whose strength experience decay of e^{-1} (0.37) of its value at the surface of the dielectric for a plane wave incident on the surface.

$$\frac{1}{k''} \cong \frac{2}{\sigma}\sqrt{\varepsilon_r' / \mu_0} \tag{4.1}$$

Where k'' is the imaginary part of propagation constant, ε'_r is the real part of relative permittivity. Normal value of ε' for concrete is about 4.5 [104] which introduces significantly the same percentage of penetration loss than glass material with relative permittivity of 6.5 for shorter propagation distance within dielectric material. In addition, concrete wall of the hotel is thicker than the windows glass for the tested hotel room. In [105], Valcarce modeled the additional indoor path loss from the scenario of UHF band outdoor-to-indoor transmission by factoring the number of walls next to outdoor environment and signal frequency, in which, path loss caused by concrete walls increases linearly with the number of walls which signal travelled through with a gradient value of 5.8.

4.2.3. 3-D Ray Tracing Simulation

In this work, 3-D modeling of the Orchard area has been created in this project to compare the measured path loss results and investigate propagation mechanisms. Figure 19 shows the simulation scenario 3D Urban Model of experiment district and aerial photo for the part of the area. All the available building data is collected and rebuilt into Wireless Insite Full 3-D city model [32]. The constructed Full 3-D model is based upon the existing 3-D building dimension from Google Earth (© 2013 Google, Map Data). The material of all buildings is modeled as concrete (relative permittivity is set to 4.5) [104]. Only one side of the hotel's surrounding

faces are defined as glass to correspond to the French window side of the building as shown in Figure 14(a).

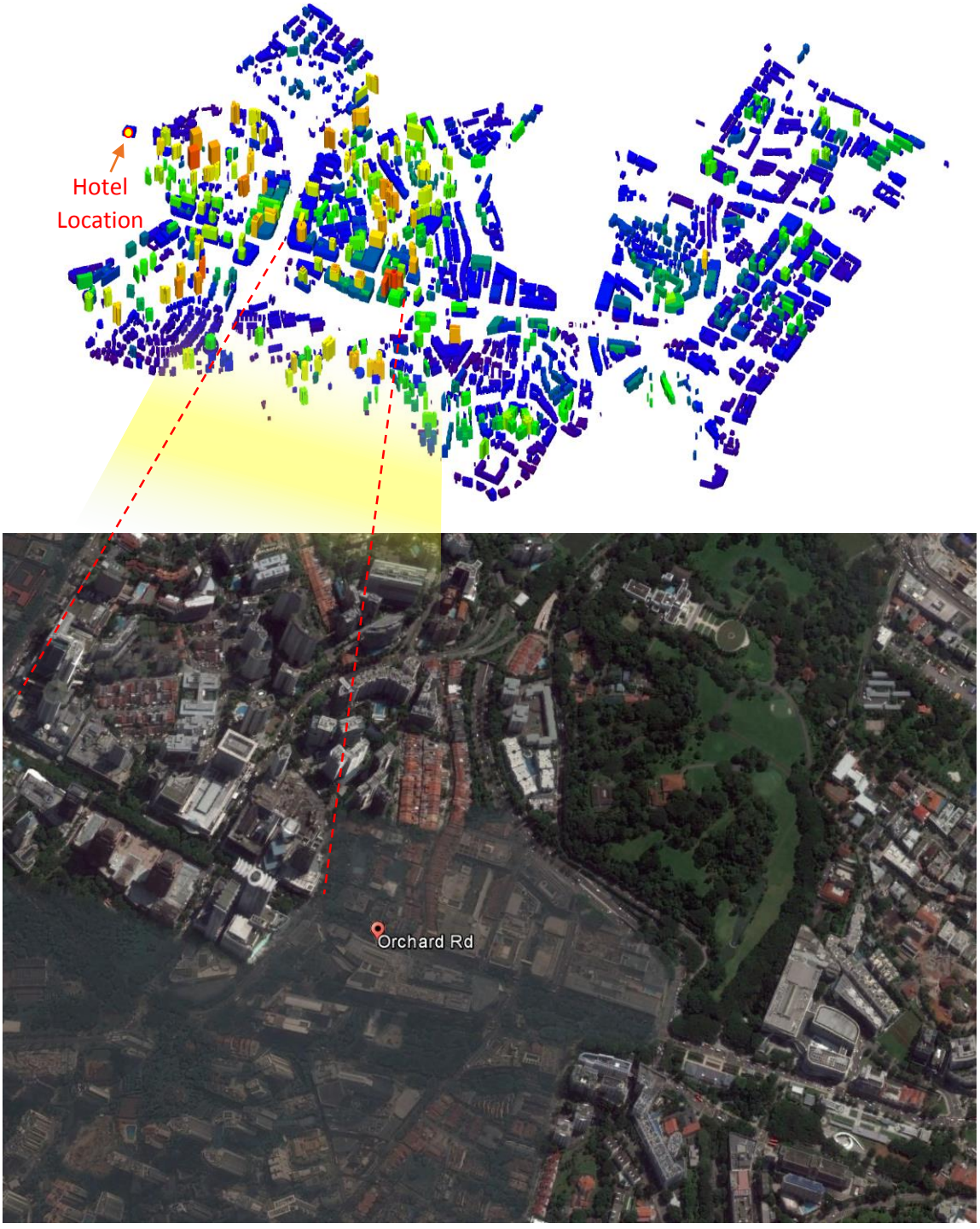

Figure 19 3D Urban Model based on KML data from Google Earth & Aerial view photo of Orchard Area (©2013 Google, Map Data)

Vertically polarized omni-directional dipoles with VSWR of 1.5 are set as the transmitting and receiving antennas. The maximum number of reflection is set to 26 and the maximum transmission is set to 4 and maximum number of diffractions is set to 4 to maxi out the computation complexity in the big urban model. Each transmitter and receiver pair is set to generate maximum 25 rays or multipath to describe ray propagation conditions for the specific link.

In the simulation, Route study mode is applied with single antenna place in the hotel building at the elevation of 60m and all other antennas are placed at 1.7 m height at even space to plot the two predefined routes in our actual experiment. Figure 20 shows the simulated route details in 2D view (one can refer to Figure 15 which plots the route information on actual satellite photo). Each route contains the number of receivers to match the actual collected data points in order to perform comparative study between simulation and empirical results.

Figure 20 Simulated Route 1 and Route 2 in the 3-D Urban Model

Table VI summarizes the simulation scenario information:

Table VI: Summary of 3-D simulation setup

3-D City Model	2887 Buildings & 115606 Faces
Topography Difference	298m
Transmitter Route 1	1.7m 2.4dBi @ 320MHz 1437 in total
Transmitter Route 2	1.7m 2.4dBi @ 320MHz 1406 in total
Receiver Height	60m 2.4dBi @ 320MHz
Full 3D Simulation Settings	SBR Ray tracing method (26 Reflections, 4Transmissions & 4Diffractions)

Figure 21 shows the received power results from both measurement data collected from Orchard area and simulated results for two experiment routes respectively. The correlation coefficient between two groups of data is evaluated, the correlation values are found to be 0.66 and 0.85 for route 1 and route 2 respectively. The correlation values indicate that the simulation has described the real situation at a good level. From route 1 figure, the mean difference between predicted received power and measured values is 11.59 dB, median value 11.37 dB, which means prediction discrepancy are small. On the other hand, Route 2 prediction discrepancy has mean value of 9.55 dB and median value of 7.53 dB. It can be seen that the predicted path loss was mostly within 10 dB of the measured values for route 2. The few data points with the considerable divergence could be due to the objects in the real world that were not modeled in the urban 3-D model.

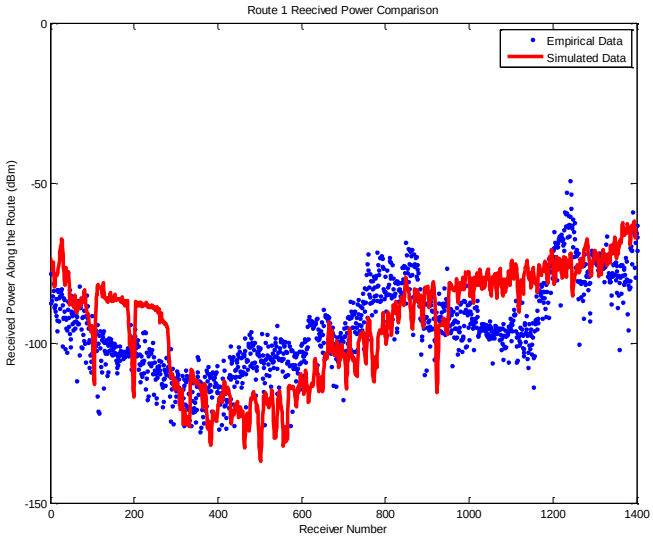

(a)

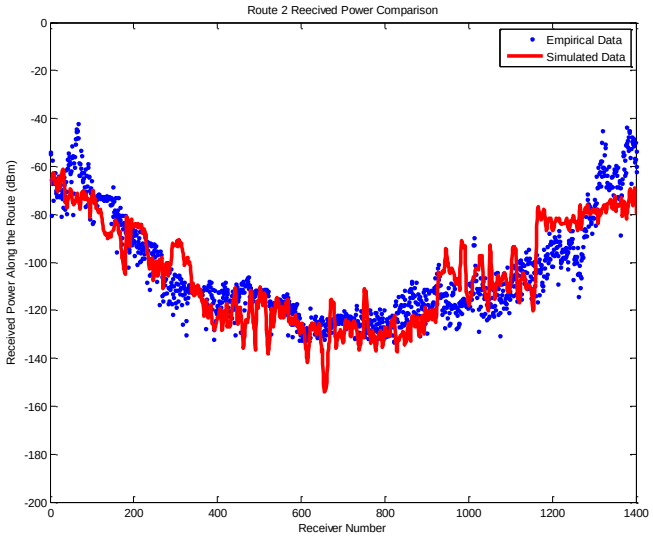

(**b**)

Figure 21 Received power against receiver number comparison (a) Route 1 (b) Route 2

4.3 Path Loss Modeling

4.3.1. Path loss modeling with classical empirical model

The measured path losses of two routes are modeled with the linear regression in classical empirical log-distance model from as:

$$L(d) = L_0 + 10\text{n}\log_{10}(d) + X_\sigma \qquad (4.2)$$

where n is the path-loss exponent, L_0 is the fixed loss component and the X_σ is zero mean Gaussian distributed random variable representing the shadowing component around the mean path loss with standard deviation σ (in dB). n, L_0 and σ are obtained from the measured data sets using minimum mean square error (MMSE) curve fitting techniques.

Figure 22 displays both the scatter plot of link length versus power received (dBm) and MMSE curve fittings for both measured data and predicted data for route 1 and route 2 at the frequency of 320MHz. Figure 15 displays the aerial view of the measured links. Where blue route represents route 1, brown route represents route 2. The receiver location is indicated by a red dot which sits 60 meters high from street level. A large variance was spotted in the relation between received power and link distance.

Form Figure 22, closely matched path loss trends are presented between both routes' measured data and ray tracing data. For route 1, measured path loss exponent is found to be about 4.944dB/decade with σ_{1_exp} to be 7.3 dB while simulated result is 4.935 dB/decade with σ_{1_sim} to be 8.4 dB. Similarly, for route 2, the measured path loss exponent is found to be 4.8dB/decade with σ_{2_exp} to be 8.7 dB while simulated result is 4.9dB/decade with σ_{2_sim} to be 8.6 dB. Based on both data correlation analysis and path loss data fitting results, our 3-D simulation model inherits the essential characteristics of the experiment urban channel environment. We thus can investigate more into the details of propagation mechanisms.

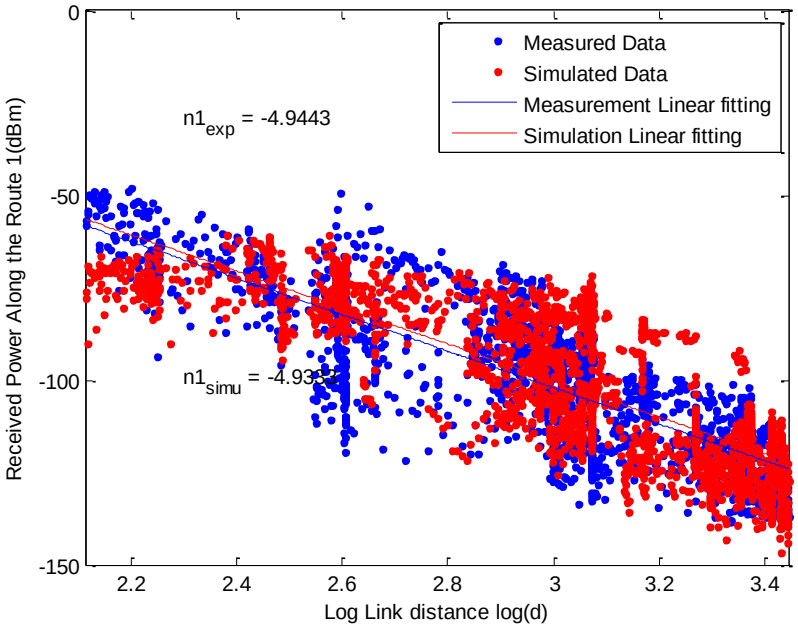

(a)

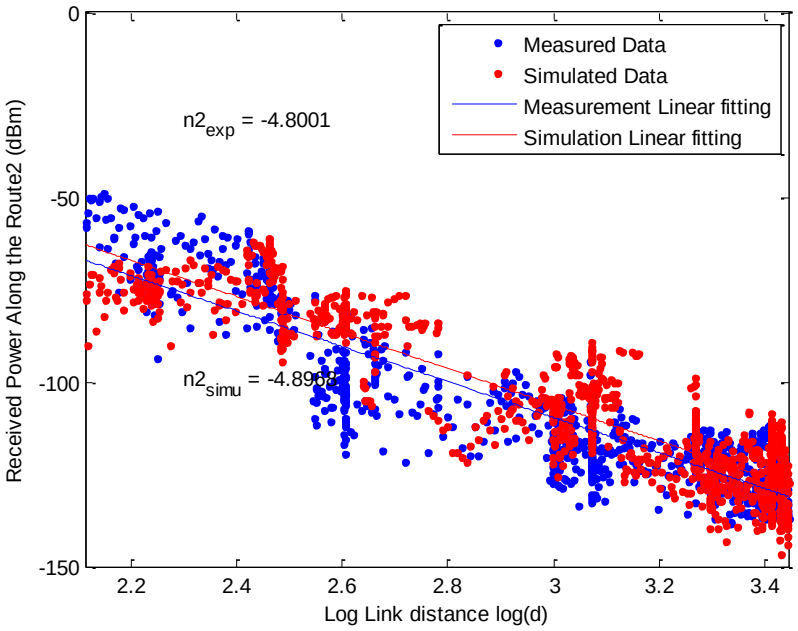

(b)

Figure 22 Measured and simulated received power of outdoor-to-indoor links obtained at 320MHz. (a) Datasets of Route 1 (b) Datasets of Route 2

Ray tracing model suggested that there were three main reasons to cause the large path loss exponent and big variance. Firstly, combination of indoor propagation segment, the inhomogeneous neighborhoods and high density of high rise buildings constitutes highly cluttered and complex channel environments that lead to the fast

decay of approximate 5dB/decade. The outrageous decay rate is commonly seen in indoor and enclosed environment like small room (5.18dB/decade) and testing lab (4.7dB/decade) as presented by L ähteenam äki [107] and path loss range from 3.7 to 4.5 is founded in heavily clogged NLOS links in [108]. Secondly, the path loss can be affected by passing through the narrow gap between two buildings walls 'tunnel' and streets which are analogous to the lossy waveguide as shown in Figure 23, the overall inhomogeneous long distance route can thus be partitioned into small yet homogenous components in terms of the gap proportion to overall street segment length on both sides. As suggested in [68], the gap widths/street length fit with path-loss exponent with only 0.27 RMS residual errors which implies very accurate predictive linear relationship which features gradient value of 3.2. Therefore, links with similar distance but different gap proportion along the street segments lead to big variance of path loss. The additional waveguide modeling of urban channel propagation could be found in [87] [88]. Thirdly, mixed loss arises from additional corner loss and some other shingles and window curtain walls which might introduce additional loss if they deflect incident rays to unintended directions.

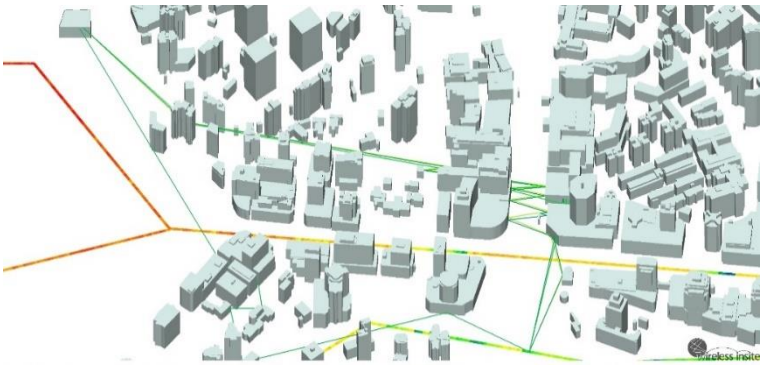

Figure 23 Visualization of analogous lossy waveguides formed by the gaps between building walls.

From above discussions, we consider path loss model in this typical channel environment consists of two regions. The clogged high rise buildings and indoor environment contributes to the high path loss decay and forms the first region.

Ground node end corner loss and shadow fading form the second region which includes all large-scale uncontrolled phenomena during the propagation caused by scatters and loss caused by random materials and geographical difference that contributes to corner loss. The residual losses from region 2 are usually described in statistically distribution. In the case of 320MHz we presented, we can then compute the loss of the second region by subtracting $10\log_{10}$ $[G_tG_rG_a/d^n)]$ from existing observed loss, where antenna gain G_t, G_r are 2.4dBi for each end and amplifier delivers additional 19dB gain denoted by G_a. We fit the received power samples to three distribution recommended for large-scale fading through maximum-likehood algorithm [33], the probability density plot of residual path loss contributed by the second region from both routes are thus depicted in Figure 24. As expected, we found that the Gaussian distribution N (μ, σ^2) in dB (lognormal distribution in normal unit) fits the best compared with Weibull distribution and Rayleigh distribution. The variance of the distribution arises from the foliage, low-rise buildings and shingles near the ground and apparently high variance would requires high link capacity which is commonly implemented in metropolitan district.

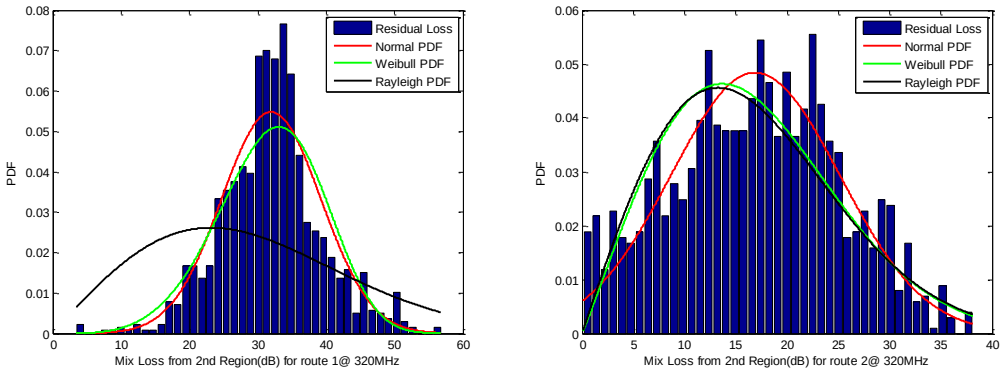

(a) (b)

Figure 24 Distribution of the Residual loss (dB) from 2nd region at 320 MHz measurement taken in Singapore, Orchard district. The red Gaussian curve suggests this loss ensemble is approximately log-normal (a) Residual loss distribution for route 1. (b) Residual loss distribution for route 2

We therefore express path loss model at 320 MHz as equation (4.4a) and (4.4b).

$$PL_1 = 10*(4.94)*\log_{10} d + \mathrm{N}(32.0, 7.3)(dB) \quad (4.4a)$$

$$PL_2 = 10*(4.80)*\log_{10} d + \mathrm{N}(16.6, 8.7)(dB) \quad (4.4b)$$

The analysis has been done across all the tested frequencies. Table VII presents the results of path-loss model parameters across the four selective frequencies in UHF band with MMSE linear curve fittings. It lists the path-loss exponents and Gaussian shadowing deviations. The aggregate data shows that path-loss decay rate is more significant at 320 MHz and 350MHz while all are within the range of 4.5 to 5.

Table VII: The path loss model parameters: *n*=path loss exponent, σ=standard Gaussian deviation

Frequency	**Route 1**		**Route 2**	
	n_1	**σ (dB)**	n_2	**σ (dB)**
250 MHz	4.57	7.4	4.10	8.5
320 MHz	4.94	7.3	4.80	8.7
350 MHz	4.94	7.7	4.86	9.3
370 MHz	4.60	8.7	4.62	9.9

Outdoor-to-indoor measurement results from other literature features slight smaller path loss exponents. In [106], path loss exponent of 4.3 was obtained for the case where receiver was placed at level B2 where surrounding urban environment was less dense compared to our case, yet the MRT tunnel located at the B2 also facilitated propagation as an analogous waveguide. Besides, [85] reported the *n*-factor range of 4-4.5 at 430MHz in the downtown areas. [93] showed a path loss exponent of 4.1 for NLOS links at 300MHz.

It is also observed that the shadowing standard deviations in our test cases have value range of 7.3dB to 9.9dB. The overall variation of route 1 is smaller than route 2, while the path-loss exponent of route 1 is slightly larger. The likely reason that

causes the trending is that route 2 covers larger area and has surrounding environment that contains more diverse settings include a large portion of foliage area and relative scattered residential areas which to some degree alleviate the path loss decay, while route 1 is more elongated with relative homogenous surrounding environment that features mainly high-rise buildings as shown in Figure 15. It is also noteworthy that the variance slightly increases with the increase of carrier frequencies, as also described in [54]. The shadowing is generally modeled by lognormal process and has been reported to have standard deviation range of 7.6-9.5 dB and mean path-loss exponent of 4.4 at 430MHz with typical 8dB for macro-cellular P2P channel in downtown Denver [14], [25] also reports an urban P2P path loss exponent of 4.9 and 7.7dB shadowing deviation, which matched closely to the results obtained in our measurement campaigns.

4.3.2. Hata Model Comparison

In the aforementioned path loss models proposed in the last 50 years, we found the Hata model satisfies our measurement condition regarding antenna heights, link distance, and carrier frequency range. Therefore, in this part, we make comparison between our path loss models with Hata model.

The Hata Model for big urban at less than 400MHz is considered. The formula is expressed as:

$$L_{median}(dB) = 69.55 + 26.16\log f_c - 13.82\log h_{te} - a(h_{re}) + \log d(44.9 - 6.55\log h_{te}),$$

$$a(h_{re}) = 8.29 * (\log 10(1.54 * h_{re}))^2 - 1.1 \quad (4.5)$$

Where $a(h_{re})$ is the mobile unit antenna correction factor, h_{te} is the height of the base station, it is within the range of 30 to 200 meters; h_{re} is the height of the mobile

station within the range of 1 to 10 meters. *d* is the path distance in kilometers within the range of 1 to 20 kilometers, and *f* is the carrier frequency in MHz within the range of 150 MHz to 1500 MHz.

We combined the path loss data from route 1 and route 2 to further perform log-distance path loss modeling. Figure 25 shows the log-distance path loss linear fitting for all selected frequencies. Since Hata model confined its range of link distance from 1km to 20km, we compared the obtained fitting model to the theoretical estimation of Hata Model from 1km.

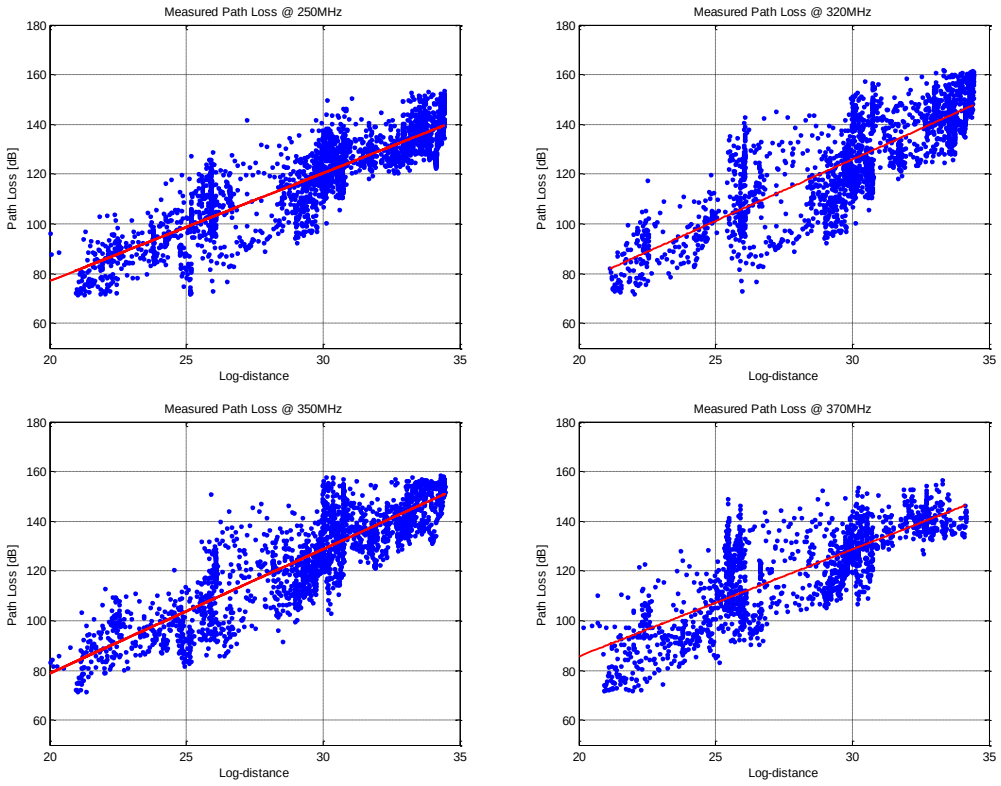

Figure 25 Log distance path loss linear fitting for total data, top left: 250MHz, top right: 320MHz, bottom left: 350MHz, bottom right: 370MHz

In Figure 26, it can be seen that the Hata model under-estimates the path loss for the outdoor-to-indoor propagation in the urban shopping district by mean value of 13-18dB. On the other hand, Hata assumed pass loss exponent affected by base station antenna height, which implies a flat rate of decay across all frequencies and

is impractical to our measured results. The Hata model path loss exponent de facto follows the 3.3 in our case, while we have path loss exponent of 4.32, 4.92, 4.78, and 4.58 for 250MHz, 320MHz, 350MHz and 370MHz respectively. The divergence between models is understandable, because the Hata Model is measured in 1980, Tokyo, Japan, the urbanization is less developed than what it is today. The average building height and infrastructure density is much lower and spectrum utilization was also low which led to 'cleaner' channel measurements and less severe path loss was expected.

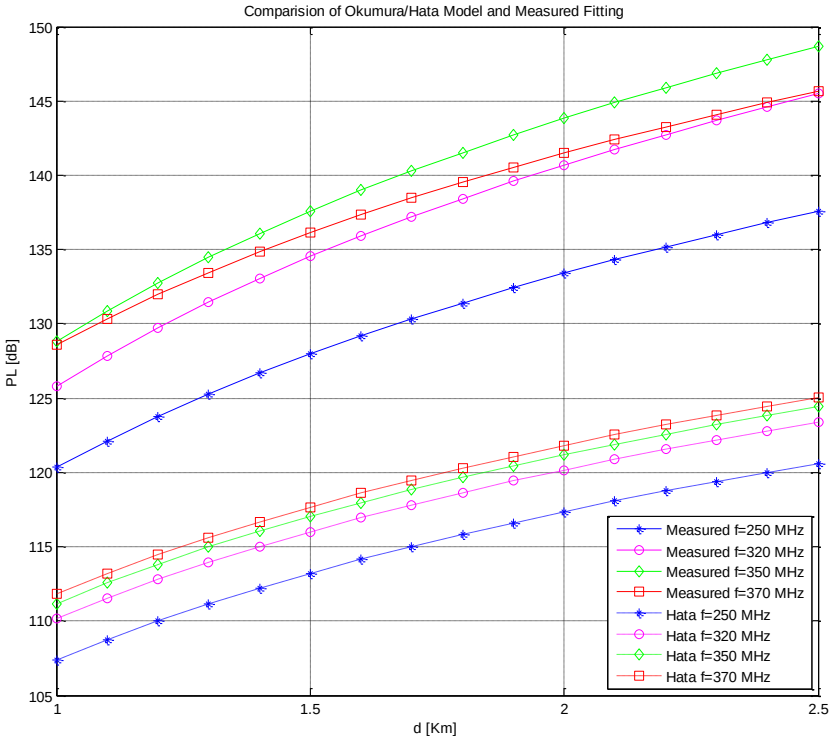

Figure 26 Comparison between Fitted path loss models with Hata Model for all frequencies. * for 250MHz, o for 320MHz, ◊ for 350MHz, □ for 370MHz. line for measured fitting, dashed line for Hata model.

4.4 Link Availability

We also performed the analysis on the link availability. For, reliable wireless communication links, a minimum power is required to ensure the quality of services (QoS), fade margin and proper SNR level are to be added to link budget [43]. In our

case, we define threshold x_0 as the sum of noise floor measured at each carrier frequency, 3dB SNR and also define minimum fade margin as 10dB. We have previously showed that lognormal distribution best present the shadowing in our test case. The probability that power exceeds the threshold is defined as:

$$\begin{aligned} P_0(d) &= P[x \geq x_0] = \int_{x_0}^{\infty} p(x)dx \\ \Rightarrow &= \frac{1}{2}(1 + erfc(\frac{m_d - x_0}{\sigma_A\sqrt{2}})) = Q(-\frac{FM}{\sigma_A}) \end{aligned} \tag{4.6}$$

Where $p(x)$ is the log normal distributed probability density function of shadowing defined as (4.9), and m_d is the mean signal strength at distance d.

$$p(x) = \frac{1}{\sigma_A\sqrt{2\pi}} \exp[\frac{-(x-m)^2}{2\sigma_A{}^2}] \tag{4.7}$$

We then evaluate the edge reliability theoretically by taking the case of 320MHz route 2 data covered previously. Where mean route 2 FM_2= 31.2dB, which led to final link reliability probability to be 99.97%, with larger mean FM_1 and smaller σ_A value, 100% link reliability for route 1 is achieved.

Alternatively, we compare data point by point to ensure collected signal exceed the defined minimum threshold we set by summing up receiver threshold, SNR and minimum Fade margin and calculate the percentage of valid data points. Table II summaries the link reliability percentage results from two methods mentioned above. From the results, we observed a decrement trending of link reliability versus frequency. The similar trend in the exact same selective frequencies has also been reported in another I2O scenario in [106]. As expected, route 1 has overall better link reliability than route 2. However, the theoretical approximation showed the overly optimistic link reliability estimation due to the reason that assumption of model is a regularly shaped cell assumption rather than the irregular routes' shape in our measurements campaigns.

Table VIII: Link reliability estimation from theoretical perspective and experiment data

Frequency	Route 1		Route 2	
	Theory Approx.	**Experimental Estimate**	**Theory Approx.**	**Experimental Estimate**
250 MHz	100%	94.57%	99.99%	94.41%
320 MHz	100%	97.22%	99.97%	94.86%
350 MHz	100%	97.81%	99.91%	84.05%
370 MHz	99.98%	89.25%	100%	75.92%

4.5 Conclusion

This chapter reports a channel measurement trial of Outdoor-to-Indoor link around the Orchard area in Singapore at Military UHF band (250-370MHz) through narrowband channel measurements and characterizations. The collected path loss data was modelled with classical log-distance model for two defined routes across four selected frequencies. A 3-D ray tracing simulation is performed and found to closely match the empirical results through correlation analysis and path loss fitting results comparison. Further investigation of qualitative propagation mechanism is performed based on the 3-D simulation results. The large path loss decay is deduced to result from indoor environment plus dense high rise, and residual path loss is found to follow the log-normal distributions. Path loss expressions for each route are derived. The new fitted models of combined data are then compared with Hata Models starting from 1km link distance. Mean discrepancies of 13- 18dB are found between two models. The Hata model's under estimation is then briefly explained

Subsequently, the link availability is analyzed from theoretical perspective and based on the empirical data by setting SNR and Fade Margin. Empirical data indicates a decreasing trend of link availability with the increase of the carrier frequency and Route 1 has general better link availability than route 2. On the other hand, theoretical approach is considered inapplicable in our case.

Chapter 5

Small Scale Multipath Fading in Urban Shopping District

The chapter presents the results from the identical measurement campaign of the last chapter. In this chapter, Small-scale multipath characteristics are investigated at military UHF band for selected frequencies (250-370MHz). Measurements deployed the spread spectrum sliding correlator system to perform wideband channel sounding covered in the chapter 3. The trials were also conducted around the Orchard area. The objective of the measurement is to investigate the outdoor-to-indoor link small scale multipath fading phenomena. To investigate the small-scale multipath fading effects in urban channel scenario, power delay profile of the channel impulse response is presented and modeled mathematically. System specification dependent threshold algorithm is introduced to find out the multipath components. Delay dispersion characteristics of urban channel are then presented. Distance dependency of time dispersion is explored in the chapter. The detailed results and discussion are illustrated in the subsequent sections.

5.1 Wideband sounder parameters and Doppler Effect

The description of Measurement campaign is covered in the chapter 4. The wideband channel measurement took place in the same predefined routes as presented previously to study the small scale fading effects in urban channel which covers multipath fading and Doppler Effect.

5.1.1 Doppler Effect consideration

In this measurement environment, the Pedestrian motion and automobile traffic are the main factors of Doppler Effect. Pedestrians are considered low speed objects who affect little to channel coherence time. Automobile traffic speed limit of Orchard district is 50km/h, using (5.1), we can evaluate the largest Doppler shift introduced at 370MHz.

$$f_d = vf / c = 14 \times (370 \times 10^6) / 3 \times 10^8 \cong 17Hz \quad (5.1)$$

This implies a minimum channel coherence time of 60ms – 90ms for the all the selected frequencies over UHF band which is much larger than our PXA typical sweep time of 1μs -10ms across the band. Therefore, the channels can be viewed as statistically wide-sense stationary. The focus of the wideband channel characterization is the multipath fading effects associated with frequency selective fading.

5.1.2 Wideband sounder parameters setup

Table IX summarizes the parameters of the wideband channel sounder. The components and wiring of the system are shown in Figure 11 of chapter 3. The measurement method involves transmitting a Binary Phase Shift Key (BPSK) signal modulated by an m-sequence (maximal-length PN sequence). We use 10MHz, 8091 bit long PN sequence which was phase-modulating the carrier at four frequencies

(250MHz, 320MHz, 350MHz, and 370MHz). This led to a temporal resolution of 0.1 μs, with an unambiguous delay span of 809.1 μs. the received signal was down converted and sampled at 100 MHz. Data collected were stamped with GPS time to synchronize the measured data with the transmitter location.

Table IX: Summary of wideband channel sounder parameters in Orchard Measurement Campaign

Centre frequency	250 MHz - 370MHz
Modulation	BPSK
PN length	8091-bits
Transmitting power	20dBm
PN Chip rate	10Msymbols/s
Data Logger Sampling Rate	100Msamples/sec

5.1.3 Data Collection & Signal Processing

The collected data would be demodulated with BPSK and cross-correlated with the same PN sequence to obtain the complex channel impulse response. The process is called “de-spreading”. Figure 27 shows an example of de-spreaded delay profiles from processing a collected data file at 250MHz. From the number of samples, we can estimate in Figure, there are three complete frames of PN sequences received (3x8091x10=2.43E5). We can also tell from the three distinct peaks, which contain power delay profile information.

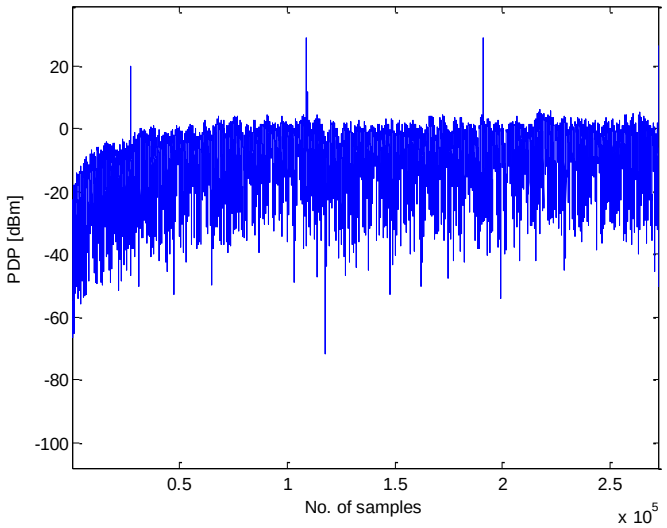

Figure 27 Example of de-correlated signal at the output of de-spreading at 250MHz

The multiple frames will be averaged to obtain the mean power delay profile that contained single data frame and mitigate the noise variation. In this study, for the ease of delay dispersion analysis, all the averaged power delay profile (PDP)'s noise floor are normalized to -20dBm and adjust the delay of first signal peak to 0 second. Figure 28 shows the averaged PDP from Figure 27.

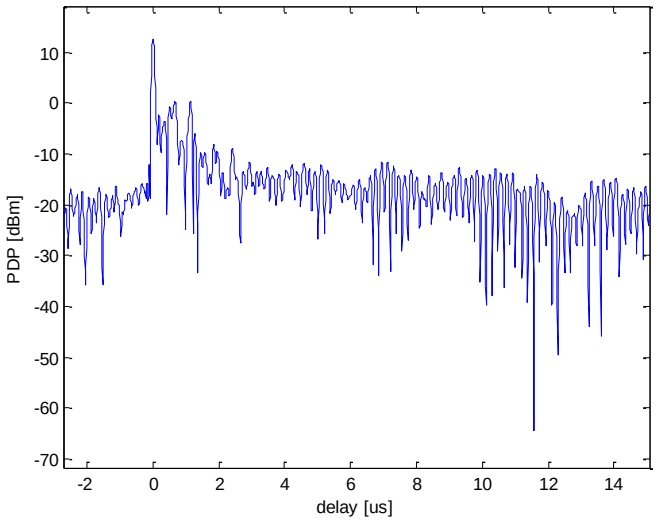

Figure 28 Power Delay Profile after averaging data from Figure 27 and normalize largest peak to 0 sec with normalized noise floor -20dBm

The PDP contains the information to describe delay dispersion characterization of channel. The PDP essentially describes the received energy envelope of channel impulse responses (CIRs). The CIRs, denoted as $h(\tau, t_i)$, is defined in (5.2):

$$h(\tau, t_i) = \sum_{k=1}^{80910} a_{ki}\, e^{j\varphi_i}\, \delta(\tau - \tau_{ki}) \tag{5.2}$$

where i indexes the i^{th} power delay profile (PDP), N is the number of multipath components (MPC) in the i^{th} PDP, α_{ki}, τ_{ki} and φ_{ki} represent amplitude, delay and phase of the k^{th} MPC, and δ is the delta function.

Based on (5.2), the each instantaneous power delay profile is expressed as (5.3):

$$P_i(\tau) = \sum_{k=1}^{80910} |a_{ki}|^2\, \delta(\tau - \tau_{ki}) \tag{5.3}$$

Subsequently, we investigate the multipath fading characteristics such as number of multipath components, delay spread and coherence bandwidth and so on based on the power delay profiles obtained.

5.2 Small scale multipath fading

Small scale multipath fading is studied from the two aspects: multipath components distribution and root-mean-square delay spread. In the following, PDP processing technique based on algorithm introduced in [5] is introduced; analysis of the number of multipath components and multipath components distribution is then studied. Lastly the time dispersion characteristics of channel are illustrated.

5.2.1 PDP thresholding procedure

As Figure 28 shows, the PDP has been further processed in order to separate multipath components from noise and extract the valid echo. The noise is normally assumed to be Gaussian and envelope of the noise is considered Rayleigh

distributed. One frame of data contains 89010 samples (10 times up sampling). Thus, there is a significant probability that some noise samples exceed significantly above the mean noise value because of the assumed Rayleigh distribution. Conventionally, a fixed high threshold is set based on the required value of signal-to-noise ratio to eliminate chance of miscounting noise as the valid received signal replicas. Sousa et al. [5] proposed a new threshold algorithm based on constant false alarm rate (CFAR). We generalize it to *N* and present it below.

The CFAR is a migrated method originated from Radar application and requires threshold value of (5.4)

$$\zeta = \eta\sigma_N \cong 0.85\eta\sigma_{median} \tag{5.4}$$

where ζ is intended threshold level, σ_N is the noise standard deviation

The noise exceeds threshold probability is thus expressed as:

$$P_f = \exp(-\eta^2 / 2), \tag{5.5}$$

Furthermore, improved algorithm is developed to judge miscounting noise sample across multiple frame samples based on the reasoning that noise samples at the output of sliding correlation process are highly uncorrelated so large noise presented in one bin will be unlikely emerge at the next at the same delay and very unlikely in all consecutive samples collected in one place. In [5], three frames of PDP are collected at every location, so authors developed a Markov chain to enumerate the possible sequential processes, and express the chain with Markov transition Matrix. We generalize the method for the case of *N* file samples to compose Markov transition Matrix as in (5.6):

$$A = \begin{bmatrix} 1-P & P & 0 & 0 \\ \vdots & 0 & \ddots & 0 \\ \vdots & 0 & 0 & P \\ 1-P & 0 & 0 & P \end{bmatrix} \tag{5.6}$$

where P is the probability that thresholds are crossed by noise in all N files. The probability to reach certain i^{th} steady state p_i (total N+1 states) is generalized in to N files and can be expressed as:

$$p_i = \begin{cases} P^{i-1}(1-P), & 1 \le i \le N \\ P^{i-1} & i = N+1 \end{cases} \tag{5.7}$$

Since the first two states correspond to no crossing or single crossing situation, in either of situations, no alarms will be activated. The rest states are accounted into the consideration of false alarm probability. Total P_{FA} can be expressed in following:

$$P_{FA} = \sum_{i=3}^{N+1} [N+1-(i-1)]p_i \tag{5.8}$$

For P<<1, P_{FA} is simplified as:

$$P_{FA} \approx (N-1)*P^2 = (N-1)*P_f{}^{2N} \tag{5.9}$$

where P_f is the probability that thresholds are crossed by noise in single files.

Substituting (5.5) to (5.9), the final equation between threshold level and predefined false alarm probability is expressed as following equation:

$$\zeta = \sigma_N * \sqrt{-2*\ln[\sqrt[2N]{\frac{P_{FA}}{(N-1)}}]} \tag{5.10}$$

where ζ is the threshold level derived from improved CFAR algorithm based on multiple frames data, σ_N is the estimated noise level.

In all our processed PDPs, we first normalized all PDPs' noise floor to -20dBm and arrival time of first multipath component to 0 sec. We conduct our thresholding evaluation based on 3 frames of data. We want to achieve false alarm probability of 1%, which for each data sample in PDP, which means less than one noise sample mistaken for MPC in 100 PDPs, as mentioned in previous part, each 8091 bit PN sequence with 10 Msym/s was sampled by 100MHz data logger, which results in 80910 signal samples per impulse response and delay profile. We can obtain that

true false alarm rate in terms of total samples collected is 1.23 x 10-7, thus the threshold should be set at η=2.35. Therefore, the threshold is set to be ζ=-12.6dBm. Any received signal samples below the threshold were not considered for MPCs.

The number of multipath components is able to be assessed with the above threshold algorithm. Figure 29 shows typical power delay profile example for links along route 1 and route 2 with the maximum RMS delay spread. The blue curve is the normalized the PDP, the red dashed line is the threshold determined from CFAR algorithm. The red markers demonstrate the multipath components, where peaks emerged within 10ns are considered as one MPC. We also compute the mean dynamic range as the difference in power between PDP peaks and CFAR threshold. Mean dynamic range of Route 1 is found to be 13 dB above while route 2 has only 5dB redundancy. Both routes are sufficient to provide voice communication.

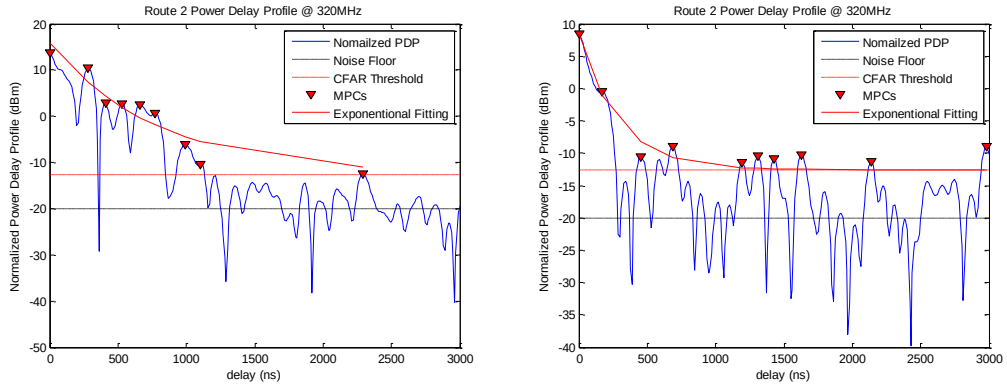

(a) (b)

Figure 29 Example power delay profiles (PDPs) from 320MHz (a) Route 1 with the maximum RMS delay spread. (b) Route 2 with the maximum RMS delay spread.

5.2.2 Multipath Component Distributions

With the above-mentioned algorithm, we conduct more in-depth analysis in multipath component distributions in the urban outdoor-to-indoor channels.

A. Number of multipath components

In the experiment, we have collected more than 12000 frames of PN sequence and generated 4056 copies of instantaneous PDPs from four selected frequencies and two routes as depicted in Figure 15. Each piece of averaged PDPs is processed based on the CFAR threshold algorithm. Table X lists summary of the mean and median number of multipath components obtained from all the available data.

Table X: The statistics for a number of multipath components *n*

Frequency	**Route 1 MPCs**			**Route 2 MPCs**		
	Λ(*μ*, *σ*)	Median	Mean	**Λ(*μ*, *σ*)**	Median	Mean
250 MHz	(1.8,0.67)	6	7.8	(2.1,0.84)	10	11.1
320 MHz	(2.0,1.00)	11	12.8	(2.4,0.70)	14	13.8
350 MHz	(2.8,0.65)	20	19.6	(3.0,0.49)	24	22.4
370 MHz	(2.9,0.57)	22	20.9	(3.0,0.47)	22	22.7

At 250MHz pertaining to our experiment environment, 8-11 multipath components sufficed, 11-14 MPCs sufficed for 320MHz, while 19-23 MPCs are recommended for 350 MHz and 370MHz. We also could observe an increasing trend of MPCs versus frequency and significant surge of MPCs required when frequency shifts from 320MHz to 350MHz. The difference between the numbers of MPCs from two routes is insignificant due to the similar small range distance fading source like concrete buildings walls and their highly dense urban settings. Thus, the number of MPCs depends more upon the frequency factor in our experiment. From our analysis, it is also noted that log-normal distribution found to be the best fit for the distribution of the number of multipath components by Maximum Likehood Estimation (MLE) method. The fitting parameters' values of lognormal distribution **Λ** (***μ***, ***σ***) are also listed in table X.

B. MPCs power distribution modeling

The area-wise MPC power distribution study is based on the averaged PDPs of all the instantaneous PDPs from the experiment at the given frequencies. Figure 30 shows the mean power delay profiles by averaging all power delay profiles from the experiment at the given frequencies, the analysis would be performed only for the data above the threshold bar set. We again observed mean PDPs of 350 MHz and 370MHz match closely in trending while 250MHz and 320MHz look similar. Although the NLOS links are mainly presented in our experiment, we observed no multiple distinctive clusters which is defined in [98] as a group of MPCs that have the similar delay and share the same long term evolution such that the group remains intact and could be visually inspected upon power delay azimuth profile to find out the number of uncorrelated clusters. Thus we use negatively exponential model, defined in (5.11) to fit mean PDPs presented, which is the common model for Power delay profile used by many literatures such as [45],[35].

$$P(\tau_k) = \alpha \sum_{n=0}^{N-1} \exp(-\tau_k / \gamma)\delta(t - \tau_k) \tag{5.11}$$

where γ is the exponential decay constant which indicates the decaying rate of power delay profiles, α is the received power at delay τ_0 (normalized to 0 second in our case). τ_k is the arrival time of the k^{th} signal.

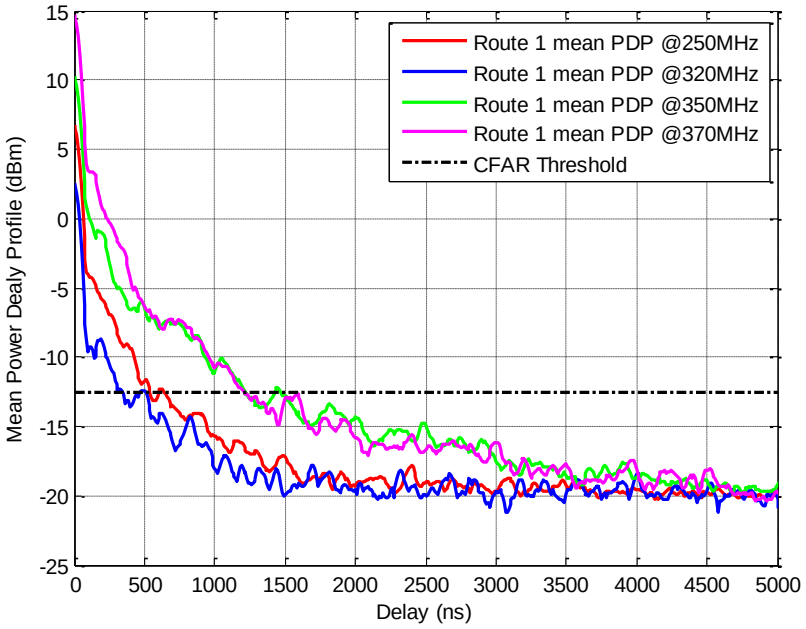

(a)

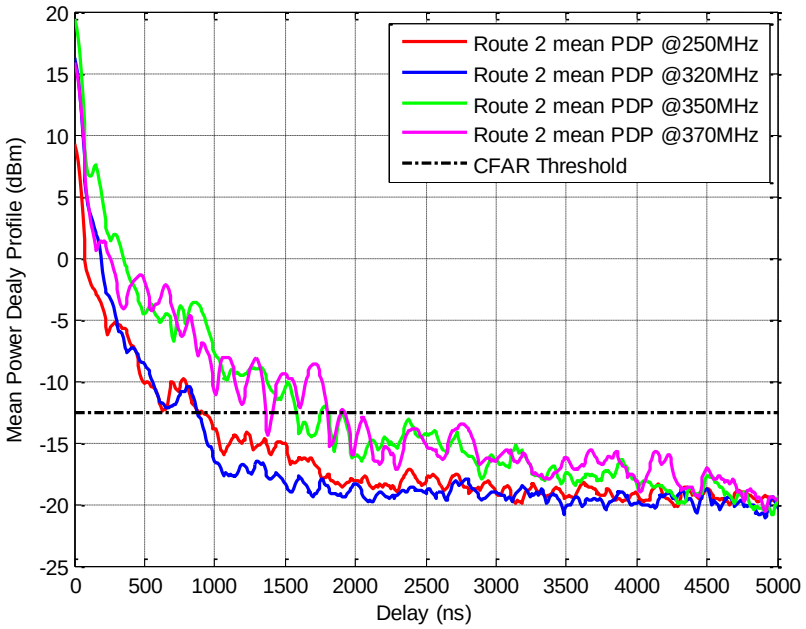

(b)

Figure 30 The average power delay profiles (PDPs) for all links at all tested frequencies with reference CFAR threshold reference bar (a) Route 1. (b) Route 2.

The measurement results of [97] showed the exponential decay of PDP with 40ns for the NLOS case. The likely reason was due to the reason that receiving antenna was placed at much higher elevation, which led to multiple MPCs from the surrounding environment were presented as one big cluster rather than several distinctive MPC groups. The use of clutters on urban macro-cell channel has been

presented in [98]. The verdict of clusters should be considered legitimate since there presented single cluster for 87% of the cases for 'Typical Urban' as documented in [98]. In addition, multiple exponential models can be used to model the multiple clusters at different delay for NLOS links as presented in [14], where three exponential terms were used to represent three major clusters found in the NLOS conditions.

Table XI: The power delay profile exponential fitting model parameters values

Frequency	**Route 1 Parameters**					**Route 2 Parameters**				
	α	γ	R^2	RMS-DS	I_{15}	α	γ	R^2	RMS-DS	I_{15}
250 MHz	0.004	64.5	0.96	117	330	0.007	64.1	0.93	166	380
320 MHz	0.002	61.7	0.92	96	520	0.035	62.9	0.93	89	180
350 MHz	0.009	66.7	0.93	247	340	0.074	62.9	0.94	179	210
370 MHz	0.025	64.5	0.93	171	280	0.032	64.9	0.93	268	250

The model parameters are given in Table XI, the fittings are considered highly reliable since the fitting *R*-squared values indicate that at least 92% of response variable variation is explained by the exponential model. From the table, we found that mean decay constant equals 64ns and could find out the decay rate for the specific route at given band. For example, the signal measured in route 1 at 320MHz, which features the fastest decay rate from the table, is decayed to e^{-1} (37%) for every 61.7 ns, or signal will experience 1.6% decay for every nanosecond. This gives us exponential decay rate of -0.07dB/ns, the decay rate is more intuitive by converting to natural units rather than decibel. Overall, the decay rates differentiate little across frequencies from -0.07dB/ns to -0.065dB/ns, thus we conclude that the exponential decay rate of PDP is around -0.07dB/ns in boisterous shopping district at the given band. We also find 320MHz is the frequency that decays fastest among four which

coincides with the analytical result from path loss exponent.

Finally, we note that equation (6) in [14] can also be applied to some of the mean PDP curves with uncorrelated clutters such as Route 2 mean PDP at 370MHz to find out the different decay rates for each clutters and lead to more accurate multipath power modeling. However, for the ease of comparison, we applied single exponential model consistently across all frequencies. Inquisitive readers could perform multi-exponential modeling for more accurate reflection on channel data to find out multiple decay values at different clusters.

5.2.3 RMS delay spread

The statistics of root mean square (RMS) delay spread values were analyzed in the section which illustrates the delay dispersion of MPCs of the channel. It is defined as the square-root of second central moment of the power delay profile covered in chapter 2. The reader can refer to (2.12) (2.13) and (2.14) for mathematical expression of RMS delay spread. We also performed our analysis on delay domain dispersion extensively on the delay interval I_{15} defined as delay duration from the first time amplitude of power fall off the threshold which is 15dB below the largest impulse level to the end which is the last time point which amplitude dropped below the threshold in International Telecommunication Union (ITU)-R P.1407 [6]. The delay spread statistics of mean PDP of given frequencies are listed in Table XI. It is deduced that the values of RMS-DS are highly related to the dynamic range value, as observed from Figure 30, 250MHz, 320 MHz have smaller peak dynamic range. For Route 1, mean dynamic range is 4.7 dB for 320MHz, followed by 8.7dB for 250MHz, 12.5dB for 350MHz, and 15.9dB for 370MHz, this leads to strength of MPCs taper off faster and fall off threshold at shorter range. As also reported in [29], RMS delay spreads generally increase with

the link distance and delay spread tapers off after 38m.

Table XII: The RMS-DS of instantaneous power delay profile summary

Frequency	**Route 1 Parameters [ns]**						
	min	max	mean	median	std	90%	CV%
250 MHz	15	842	120	118	64.3	271	53.6
320 MHz	53	408	108	88	47	214	43.5
350 MHz	9	1637	278	264	147	546	52.8
370 MHz	10	1343	243	216	163	567	67.1
	Route 2 Parameters [ns]						
250 MHz	32	848	126	132	49	232	38.9
320 MHz	16	1155	75	70	41	167	54.7
350 MHz	24	823	205	120	175	577	85.3
370 MHz	16	756	257	199	211	670	82.1

RMS delay spread analysis is also performed over all instantaneous power delay profiles collected at different locations along the given routes and four frequencies individually to qualify the variation of delay spread measures since the channel is the time-variant in nature.

The variability is assessed from 90% of the CDF as shown in Figure 31. The percentage route variability of channel parameter was quantified via the coefficient of variation as defined in (5.12), which is the percentage ratio of standard deviation to the mean,

$$CV = \sigma_{RMS-DS} / \mu_{RMS-DS} \tag{5.12}$$

It is noted that it is conventional to evaluate within the range of 90% cumulative distribution function data [14]. For the Route 1, CV values are listed in Table IV together with other relevant statistics on the instantaneous root-mean-square delay spread. The four variability of channel performance can thus be categorized in two frequency groups, 250MHz and 320MHz group has relative less dispersed and

relatively more stable channel due to the smaller mean value of RMS-DS and CV compared to 350MHz and 370MHz group. We can thus conclude the channel dispersion and variability is most likely frequency dependent. Still, the long range link distance could be an important factor that contributes to the route variability, since the overall variability about the mean is still too high compare to the short range NLOS link (5.5-80m) result in [14] which CV is found to be 0.27 in 700MHz. Our measured delay spread was smaller than those of macro-cell as suggested by Greenstein et al [48], which recommends 400ns for 'Typical Urban' and 1 μs for 'Bad Urban'. One of possible reasons is the elevated receiving antenna height (60m) in our experiments. The propagation is less governed by scatters in the vicinity and antenna is affected by fewer scatters at greater distance. Thus we expect milder small-scale path loss value and small RMS delay spread values. The decreasing trending of RMS-DS against antenna height was also verified in [99], where Mean RMS-DS gradually decreases from 61.4ns to 34.3 ns as antenna height varies from 5.5m to 10.5 meter.

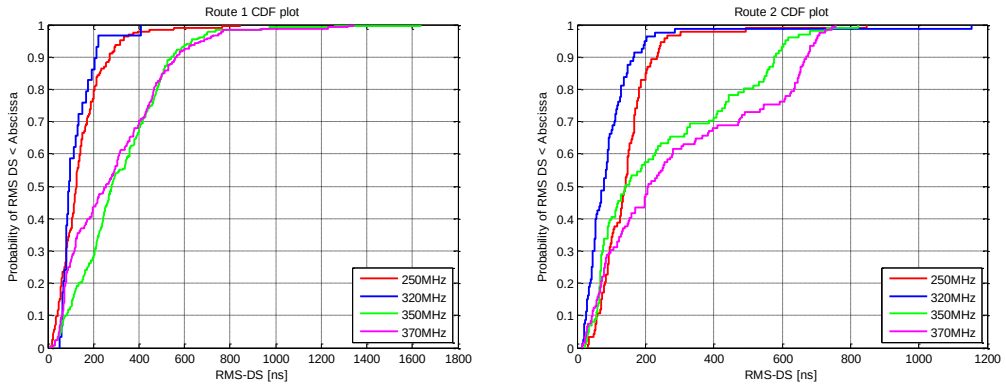

(a) (b)

Figure 31 The Cumulative Density Function (CDF) for root-mean-square delay spread (RMS-DS) for power delay profiles across all experiment frequencies (a) Route 1. (b) Route 2.

Furthermore, Coherence bandwidth values are derived to reveal the maximum usable bandwidth based on 50% frequency correlation in the urban shopping district.

Table XIII shows that the maximum usable bandwidth over the channel between a hotel room and streets in CBD areas is approximated to 1.2 MHz. Mean values of coherence bandwidth for two routes are similar. Since we use BPSK scheme, the recommended maximum usable data rate is 0.7Mbps for the communication around the Orchard area.

Table XIII: Summary of Coherence Bandwidth

Coherence Bandwidth(MHz)	250 MHz	320 MHz	350 MHz	370 MHz	**Mean**
Route 1	0.7	0.9	0.4	0.4	0.6
Route 2	0.9	1.2	0.4	0.3	0.7

5.2.4 Distance dependency of RMS delay spread

In [48], Greenstein attempted to find the correlation between delay spread, distance and path loss with assumption of lognormal distribution of delay spread for particular distance range, and an equation between median delay spread value and distance in urban areas and found delay spread is proportional to the square root value of maximum radius of the area. In this work, we attempted to relate RMS delay value to link distance in the range from 200m to 1km. The scatter plot of 10 based logarithmic value of RMS delay spread from two routes versus link distance for four frequencies represented by different marker shapes and colors is shown in Figure 32. The linear regression is found to the best fit relating the RMS delay spread to link distance.

As illustrated in Figure 32, we found brutally close increasing trend of logarithmic RMS delay spread with increase of link distance as indicated from (5.13a), (5.13b), (5.13c) and (5.13d), since the mean increasing rate across four frequencies is found to be 0.00036ns/m with only 0.15 percentage variability.

Therefore, regarding to our measurement environment and frequency bands, it is viable to conclude that logarithmic RMS delay spread increases linearly with link distance and follows mean gradient value of 0.00036ns/m and can be considered frequency-independent since it follows non general trending between frequencies. Still the value is for reference purpose for cell planning, since inconsistencies could be found between different set of measurements as the case in [40], in which reported RMS delay spread value occasionally slumps at the greater distance. Similar cases could be spotted in our data sets. For example, a small RMS delay spread of 30 ns is found from a 1km channel links.

$$\log_{10}(\tau_{rms\_250MHz})(ns) = 0.00035d(m) + 1.90 \quad (5.13a)$$

$$\log_{10}(\tau_{rms\_320MHz})(ns) = 0.00036d(m) + 1.88 \quad (5.13b)$$

$$\log_{10}(\tau_{rms\_350MHz})(ns) = 0.00030d(m) + 2.26 \quad (5.13c)$$

$$\log_{10}(\tau_{rms\_370MHz})(ns) = 0.00043d(m) + 2.10 \quad (5.13d)$$

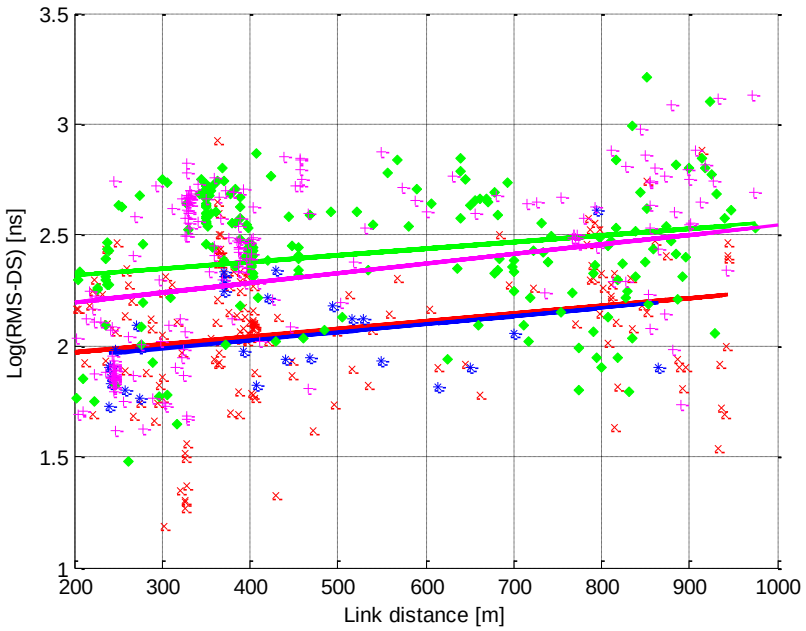

Figure 32 Scatter plot and linear regression line of Logarithmic value of RMS delay spread versus link distance. x is 250 MHz data, * is 320 MHz data, ◊ is 350 MHz data and + is 370 MHz data. Red line is 250 MHz data fitting, blue line is 320 MHz data fitting, green line is 350 MHz data fitting, magenta line is 370 MHz data fitting.

5.3 Conclusion

In this chapter, the continuation of the wide band channel characterization study for the identical measurement campaign from chapter 4 is presented. Brief wideband sounder parameters are introduced; the Doppler Effect is also analyzed and deemed to be negligible factor. Data collection and preliminary data processing are briefly touched. We deployed the improved CFAR threshing algorithm from [5] and further derive the general case results based on Markov chain analysis. With the new threshold algorithm, we investigate deeper to analyze the multipath component distribution and modeling. We found mean value range of 8-14 multipath components are sufficed for 250 & 320 MHz, mean value range of MPCs in 350 & 370 MHz was 19-23, distribution of number of multipath components is found to be best fitted with log-normal distribution with relevant parameters given for all frequencies and route cases. Almost all of the PDPs of outdoor-to-indoor links measurements are of “Single cluster” variety and mean PDPs for four frequencies are thus modeled by single exponential model and found to have very consistent exponential decay constant with mean value of 64ns and decay rate of -0.07dB/ns across all frequencies and given routes. Time dispersion exhibits similar traits between two routes, the 90 percentile values for root-mean-square delay spread for route 1 range from 214ns at 320MHz to 567ns at 370MHz, for route 2, it ranges from 167ns at 320MHz to 670ns at 370MHz. we have also found the channel variability is frequency dependent, since we have much unstable channel performance at 350MHz & 370 MHz judged from coefficient of variability analysis. Lastly, least-squared linear fits for the logarithmic root-mean-square delay spread versus link distance are computed and obtain a mean gradient value of 0.00036 with only 15% variability.

Chapter 6

Urban Indoor Wideband Channel Characterization in UHF Band

The chapter presents the indoor wideband channel characterization based on the measurement campaign conducted in high rise complex building: Fusionopolis. Small-scale multipath characterization is investigated at 5 selected frequencies (250, 320, 350, 410, 470MHz). Measurements deployed the spread spectrum sliding correlator system to perform wideband channel sounding covered in the chapter 3. The objective of the measurement is to investigate the indoor links' small scale multipath fading phenomena. Power delay profile of the channel impulse response is presented. Multipath decay rate is studied based on the linear model for links in enclosed environment. Delay dispersion characteristics of urban channel is then presented. 3-D ray tracing simulation based on the high fidelity building model is performed to study the propagation mechanism of same-level links and inter-level links and are visually illustrated with simulated ray paths. The detailed results and discussion are illustrated in the subsequent sections.

6.1 Measurement Campaign

The measurements were conducted within the Fusionopolis at One North of Singapore on September 4th and 11th, 2013. In the indoor measurement campaign, both narrowband and wideband measurement are carried out at five different levels: level B2, level 3, level 8, level 11 and level 21, As Figure shows, Fusionopolis complex (Figure 24) is a 20+ storey building with gross floor area totaling 120,000 m^2. It consists of three towers (Connexis South, Connexis North and Symbiosis). Our experiments are mainly conducted in Connexis North and Symbiosis.

Figure 33 Experiment site: Fusionopolis

6.1.1 Measurement Plan

We have set multiple fixed antenna positions at each floor. Level B2 is the basement level of the building; it mainly consists of a lobby of the MRT station, a supermarket and a few commercial shops which is confined by concrete walls. Three positions (as indicated in Figure 34) are chosen for the test. Position 1 is just

outside the lobby of the MRT station while Position 2 and 3 are in the spacious open space at the other end.

(a) (b) (c)

Figure 34 Antenna positions in B2. (a) Position 0, (b) Position 1(c), Position 2

Level 3 features several commercial shops and a kindergarten. Its interior decoration materials are mainly windows glass. The signal which impinges the glass will suffer less attenuation than walls as explained previously in chapter 4. As Figure 35 shows, Position 1 is placed near the elevator and Position 2 is placed near the lift lobby.

(a) (b)

Figure 35 Antenna positions in L3. (a) Position 1, (b) Position 2

Level 8 is an office environment. The antenna is placed inside two different offices of one of the institutes. As shown in Figure 36, position 1 was placed near the window, while position 2 is in the fully confined office.

(a) (b)

Figure 36 Antenna positions in L8. (a) Position 1, (b) Position 2

Level 11 features sky garden on the south tower of the building which is an outdoor environment. Only one antenna position is chosen as indicated in Figure 37.

Figure 37 Antenna positions in L11

Level 21 is a larger sky garden on the ceiling of the building. It consists of one open air viewing space and a small garden with roof which is connected through a bridge. Position 1 is located in the open space, Position 2 is near the connecting bridge, and Positions 3 and 4 are inside the small garden as indicated in Figure 38.

(a) (b)

(c) (d)

Figure 38 Antenna positions in L21. (a) Position 1, (b) Position 2, (c) Position 3, (d) Position 4.

Table XIV summaries all the indoor link slant distance estimation. All available tested links are listed in the table, the green shaded area are available links which

are not tested in our experiments.

Table XIV: Transmitter and receiver distances

Link (m)		B2 (-10m)			L3 (32.7m)		L8(65.2m)		L11(82m)	L21 (151m)			
		P0	P1	P2	P1	P2	P1(Stefan)	P2	P1	P1	P2	P3	P4
B2	P0		37.50	51.80	70.00	81.23	91.10	87.70	112.44	169.34	171.60		178.28
	P1				57.03	70.36	85.67	83.94	104.85	164.41	166.73		173.60
	P2												
L3	P1					25.00	76.34	74.40	68.90	121.77	124.88		133.92
	P2						94.34	92.78	79.89	128.55	131.51		140.12
L8	P1								78.50	108.84	112.32		122.29
	P2								78.25	107.49	111.00		121.09
L11	P1									78.63	82.66	87.19	99.71
L21	P1										45.50	68.00	54.00
	P2											33.00	35.00
	P3												
	P4												

6.1.2 Broad Band Sounding Setup

Table XV summarizes the parameters of the wideband channel sounder. The components and wiring of the system are shown in Figure 11 of chapter 3. The measurement method involves transmitting a Binary Phase Shift Key (BPSK) signal modulated by an m-sequence (maximal-length PN sequence). We use 25MHz, 8091 bit long PN sequence which was phase-modulating the carrier at four frequencies (250MHz, 320MHz, 350MHz, and 370MHz). This led to a temporal resolution of 40ns, with an unambiguous delay span of 323.6 μs. The received signal was down converted and sampled at 100 MHz. Data collected were stamped with GPS time to synchronize the measured data with the transmitter location.

Table XV: Summary of measurement parameters

Parameters	Value
Carrier frequency	250-410MHz
PN length	8091 bits
Modulation	BPSK
Symbol rate	25 Mchips/s
Delay resolution	40ns
Antenna type	Omni-directional
Antenna gain	2.4dbi

6.2 Wideband Measurement results

In this section, Small scale multipath fading for indoor environment is studied from the two aspects: multipath components distribution and root-mean-square delay spread. We follow PDP processing technique based on algorithm introduced in the previous chapter, analysis of the number of multipath components and multipath components distribution is then studied. Lastly the time dispersion characteristics of channel are illustrated.

6.2.1 Number of multipath components

Averaged instantaneous PDPs are processed using the processing method covered in chapter 5. We want to achieve false alarm probability of 1%, which for each data sample in PDP, which means less than one noise sample mistaken for MPC in 100 PDPs, as mentioned in previous part, each 8091 bit PN sequence with 25 Msym/s was sampled by 100MHz data logger, which results in 32364 signal samples per impulse response and delay profile. We can obtain that true false alarm

rate in terms of total samples collected is 3.08 x 10^{-7}, thus the threshold should be set at η=2.28. Therefore, the threshold is set to be ζ=-12.82dBm. Any received signal samples below the threshold were not considered for MPCs.

Table XVI lists summary of the number of mean multipath components obtained from all the available links and given frequency band and categorized in same level links and inter- level links.

Table XVI:

The statistics for a number of mean multipath components *n*

MPCs [n]	**Frequency**	250 MHz	320 MHz	350 MHz	370 MHz	410 MHz	470 MHz
Same Level	B2 to B2	14.5	10	4	6	4	3
	L3 to L3	18	30	21	25	16	13
	L21 to L21	6.5	6	7.3	8	8.7	6.7
Inter-Level	B2 to L3	14.5	11.8	6	8	7.3	6.8
	B2 to L11	8	21	8	22	34	17
	B2 to L21	4.5	5.5	5.5	9	12	5.5
	L3 to L8	21	17.5	15	16	17.5	9
	L3 to L11	40	83	65	77	60.5	24.5
	L3 to L21	17.8	51.8	32.5	33	21	16
	L8 to L11	11	12	12	12	13	13
	L8 to L21	9	15	10	12	13	13
	L11 to L21	13	18	17	36.7	21.7	22.7

For same level links, L3 exhibits much richer multipath than B2 and L21, for inter-level links that relate to L3 also illustrate the similar characteristics. The main

reason for the phenomena is due to the environment of L3. As mentioned, Level 3 is a commercial floor of the building, which is enclosed by glass windows not solid walls. The electromagnetic waves signal can get reflected and propagating out with much lower attenuation. On the other hand, as shown in Figure 35, antenna is placed near the lift shaft. As studied in [26], the life shaft can be modeled as a waveguide to facilitate the signal propagation and testifies that mechanism with the ray tracing modeling.

The other observations upon the number of multipath components is that the richness of MPC in the confined environment is better than open environment, because the worst counting of MPCs is presented at L21 to L21 where is a sky garden at elevation of 150m. Signals are easily deflected to the sky and never come back. The confined space, however, because of the ceiling, floor, walls, signals have better chance to be reflected, refracted and diffracted which again creates a class of new rays to further the richness of MPCs.

6.2.2 Decay rate of MPC distribution

In this section, we further investigate the decay rate of multipath component distribution with focus of propagation links related to enclosed space only. Thus, links relate to level 11, level 21 are not of interest, as we found that the decay multipath component strength decay linearly against delay in enclosed environments. PDP multipath components also followed the linear decay trend and were properly modeled with linear function in [29]. By deploying the CFAR threshold algorithm, we determined the linear decay rate for multipath in B2P0 to B2P1 link at 250MHz is 0.077dB/ns, while L3P1 to L3P2 at 250MHz is found to be 0.030dB/ns as shown in Figure 39. The higher decay rate is expected, because B2 is enclosed with concrete material lead to larger signal propagation attenuation, and fast degradation

of signal will lead to fast decay of multipath components. On the other hand, we can intuitively observe that L3 related links generally presents richer multipath components than B2 from comparison and thus testifies the reasoning from the previous section.

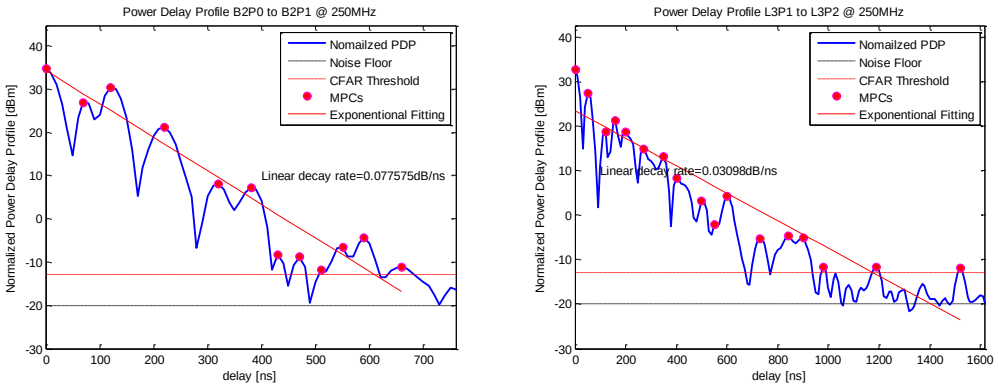

(a) (b)

Figure 39 Power Delay Profile for Same Level links linear decay fitting (a) B2P0 to B2P1 @ 250MHz, (b) L3P1 to L3P2 @ 250MHz

Besides the same level links in enclosed environment, the analysis is also applied to inter-level links where both transmitter and receiver are placed in the enclosed environments. Figure 40 shows the two example links: B2P0 to L3P1 and L3P1 to L8P1 at 250 MHz, the decay rates are found to be 0.045dB/ns and 0.010dB/ns respectively. From L3 to B2, there is big hollow atrium for signal to propagate to B2 (escalator is within the atrium and goes straight down to B2) as shown in Figure 35(a), this leads to big mean dynamic range of 23.4dB compare to the L3 to L8 link where there is only 9.5dB, since no explicit path that signal can traverse to the destination.

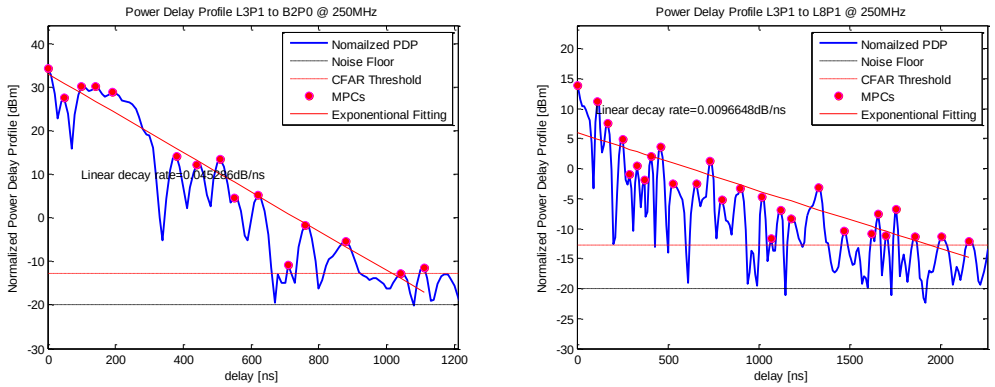

(a) (b)

Figure 40 Power Delay Profile for Inter-Level links linear decay fitting (a) B2P0 to L3P1 @ 250MHz, (b) L3P1 to L8P1 @ 250MHz

Table XVII: The statistics for mean MPC decay rate and mean dynamic range in indoor environment

Decay Rate (dB/ns)	**Freq**	250 MHz	320 MHz	350 MHz	370 MHz	410 MHz	470 MHz
Same Level	B2 to B2	0.08	0.05	0.08	0.06	0.07	0.08
	L3 to L3	0.03	0.03	0.04	0.05	0.05	0.05
Inter-Level	B2 to L3	0.05	0.05	0.06	0.06	0.06	0.05
	L3 to L8	0.010	0.012	0.012	0.011	0.010	0.007
Dynamic Range (dB)	B2 to B2	19.2	18.2	12.7	16.3	12.6	13.4
	L3 to L3	19.3	18.6	23.2	18.6	17.3	16.0
Dynamic Range (dB)	B2 to L3	23.4	20.6	13.6	18.2	16.2	14.8
	L3 to L8	9.5	9.1	9.3	8.3	8.0	4.8

Table XVII summaries the linear decay rate of multipath in all the links within the enclosed environments as well as the mean dynamic range values. Small variations can be observed for both same level link and inter-level links across the frequencies. The linear decay rate is probably frequency independent. The least

decay happens for L3 to L8, this is due to rich multipath nature for the propagation links as spotted from Table XVI compared to others listed in Table XVII. However, the low decay rate does not necessarily mean less attenuations, L3 to L8 is de facto the most heavily attenuated which can be seen from the mean dynamic range that is only around 8.2dB considering all frequencies. Therefore, there is no direct link between environment attenuation and multipath decay rate, but combinations of both provides indication of richness of multipath components in certain environments.

6.2.3 RMS Delay Spread

Table XVIII summaries the mean delay spread values obtained for indoor-to-indoor propagation within the building of Fusionpolis at different frequencies based on the post-processed PDPs. Level B2 and level 8 are not listed due to the wideband communication failure. Possible reason is the enclosed office environments of level 8 that led few multipath signals to reach the receiver with sufficient signal strength. From the table, it can be observed that the delay spread for same level propagation is within 100 ns due to the limited distance and few blockages between the transmitter and receiver. While the inter-level propagation is non-line-of-sight transmission mainly via multipath propagation, therefore a higher delay spread value is obtained. The larger value obtained from inter-level propagation in "Fusionopolis" is resulted from the complex structure.

Coherence bandwidth values are evaluated to find out the maximum usable bandwidth in such environment. For same level propagation, the maximum usable bandwidth is 2.2 MHz while that for inter-level propagation is 0.48 MHz if the worst case is taken for calculation (largest delay spread value).

Table XVIII: Indoor link RMS-DS for Fusionpolis trial

Delay Spread(ns)	Frequency	250 MHz	320 MHz	350 MHz	370 MHz	410 MHz	470 MHz
Same Level	B2 to B2	57.3	53.2	43.2	52.1	46.4	28.5
	L3 to L3	71.3	46.3	81.7	41.0	73.1	76.3
	L21 to L21	82.5	91.1	69.6	72.2	77.1	74.5
Inter-Level	B2 to L3	74.9	87.4	77.3	83.8	81.2	90.1
	B2 to L11	134.5	162.3	166.8	176.6	182.2	234.2
	B2 to L21	163.3	186.4	145.6	177.2	191.8	162.1
	L3 to L8	214.8	152.5	135.6	178.8	232.6	169.4
	L3 to L11	222.1	309.2	419.5	395.3	179.4	150.9
	L3 to L21	395.6	386.7	326.8	397.0	370.9	283.3
	L8 to L11	189.1	200.9	146.3	175.3	161.8	153.5
	L8 to L21	156.4	196.3	132.5	140.1	143.3	119.7
	L11 to L21	120.0	352.9	296.3	121.5	311.7	215.6

6.3 Fusionopolis 3D Ray Tracing and Verifications

In this section, 3-D ray tracing simulation is performed to further study the multipath propagation mechanism. The constructed 3-D model is illustrated; study of multipath propagation is then done from comparison of delay of multipath and corresponding signal amplitude with illustration of ray paths. The results serve as qualitative explanation rather than quantitative references.

6.3.1 3-D models of Fusionopolis

Based upon the master floor plan purchased from JTC, which is the owner of the Fusionoplis complex, we meticulously design the structure of each floor (example is shown Figure 41) and cascade them to construct our 3D model as shown in Figure 42.

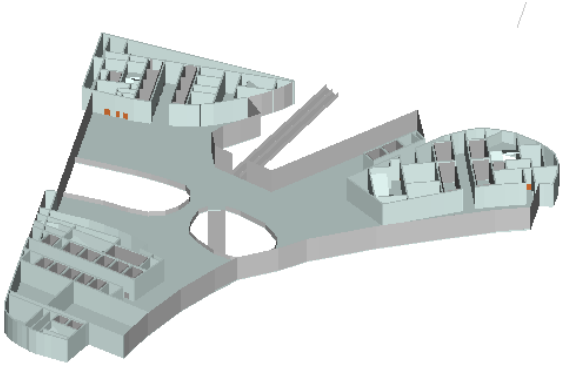

Figure 41 3D Design of Level 3

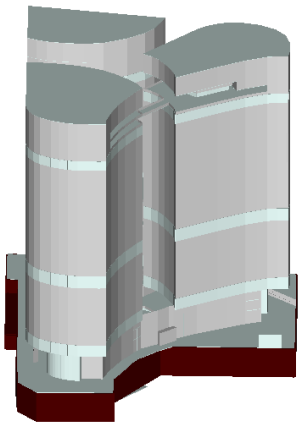

Figure 42 3D Model of Fusionoplis

6.3.2 Same level Link study

Figure 43 shows the measured time domain channel response when transmitter and receivers are both placed at level 3 of Fusionopolis complex. We divide it into two regions to identify the main sources of signals. Red dot steam plot depicts simulated PDP, red solid line curve represents the empirical PDP result. By

comparing two groups of data, the propagation mechanism can be analyzed with the help of 3*D* visualization shown in Figure 44 and Figure 45.

Through comparison, the information on time of arrival for first few distinct peaks from measured data and the simulated results is tabulated. It is observed that majority of peaks arrival time found in simulation can be closely matched to the measured results; the maximum deviation value is 28ns at the 7th peak.

Table XIX: Time of arrival of first 8 MPCs for LOS link

L3P1 to L3P2 (470MHz)	Simulated	Experimental
2nd Peak	45ns	40ns
3rd Peak	78ns	80ns
4th Peak	105ns	110ns
5th Peak	204ns	204ns
6th Peak	283ns	290ns
7th Peak	382ns	410ns
8th Peak	519ns	510ns

In the region 1 with delay ranging from 0 to 100ns, as observed from Figure 44 that the source of signals are direct signals from LOS link and those penetrate the walls, ceilings and floors, signals reflected by the surrounding objects such as glass wall, elevators and passenger life located at the left side of the receiver and signals reflected from the lower levels floors since the structure of level 3 are semi-open with big atrium at the escalator area. Figure 45 shows the propagation path range from 100 ns to 600ns, majority of signals within this region are mainly reflected by the three lift clusters. Some signals are bouncing back and forth between them before it reaches receiver.

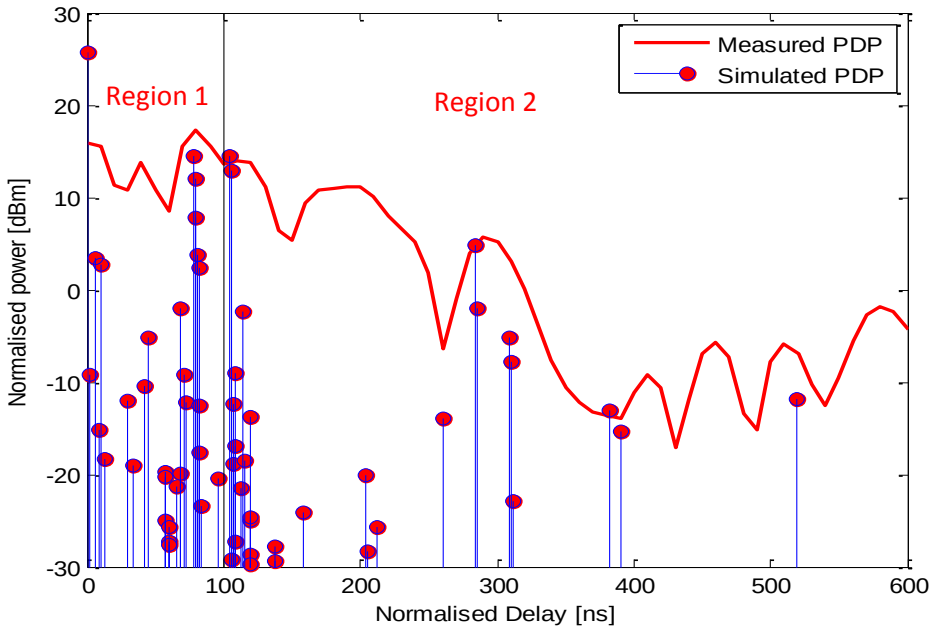

Figure 43 Measured PDP vs. Simulated ray tracing PDP for L3P1 to L3P2

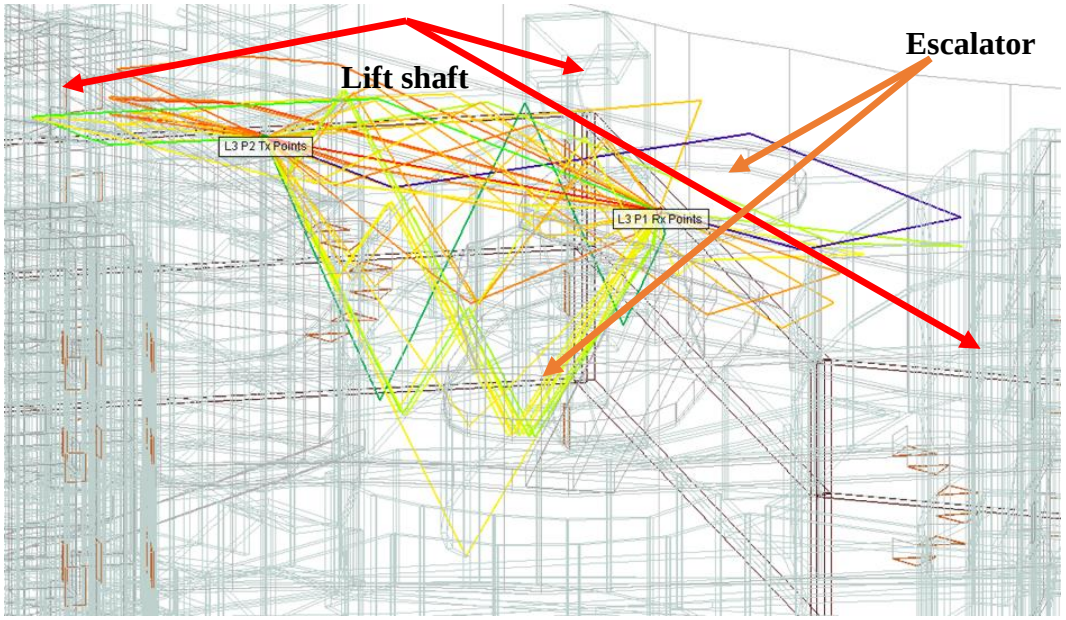

Figure 44 Propagation multipath delay range from 0 to 100ns

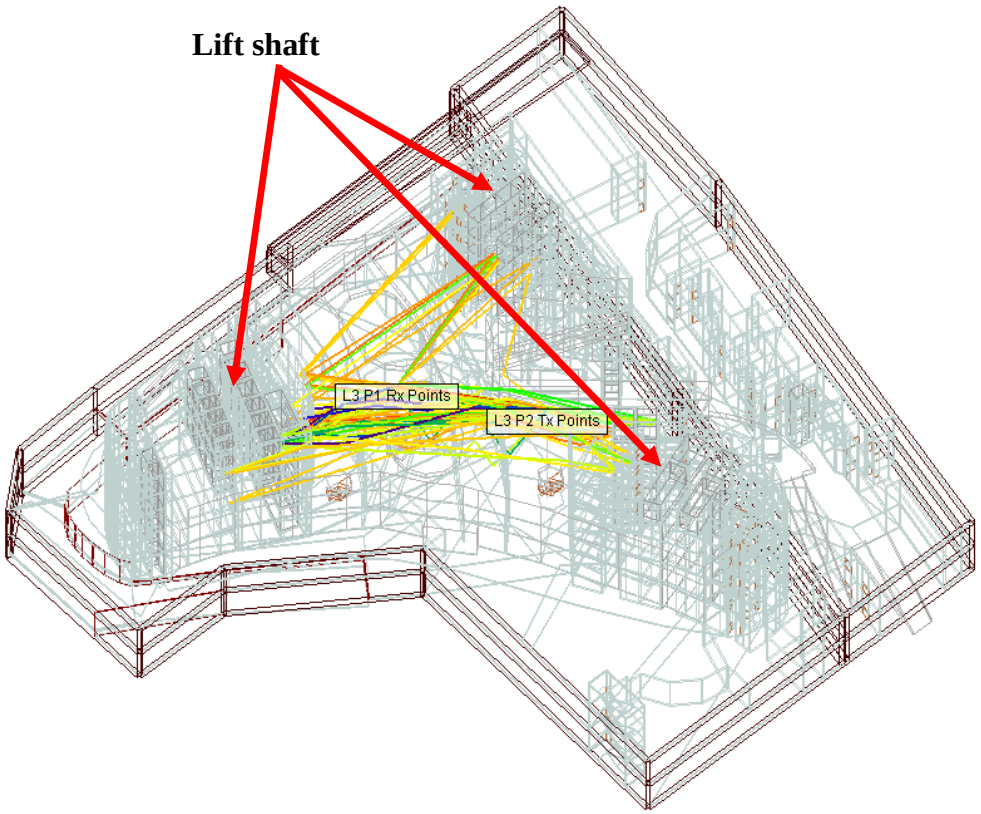

Figure 45 Propagation links range from 100 to 600ns

6.2.1 Inter-level link study

The measured power delay profile comparison for propagation link between L3 and B2 of Fusionopolis is shown in Figure 46, we divide it into two regions to identify the main sources of signals. Red dot steam plot depicts simulated PDP, red solid line curve represents the empirical PDP result. By comparing two groups of data, the propagation mechanism can be analyzed with the help of 3*D* visualization shown in Figure 47 and Figure 48.

Based on Figure 46, we can tabulate Table XX which contains information on time of arrival for first 6 distinctive peaks from measured data and the simulated results. It is observed that majority of peaks arrival time can be closely matched to the measured results; the maximum deviation value is 12ns at the third peak.

Table XX: Time of arrival of first 6 MPCs for NLOS link

B2P0 to L3P1 @ 470 MHz	Simulated	Experimental
2nd Peak	79ns	80ns
3rd Peak	138ns	150ns
4th Peak	204ns	210ns
5th Peak	254ns	250ns
6th Peak	339ns	330ns

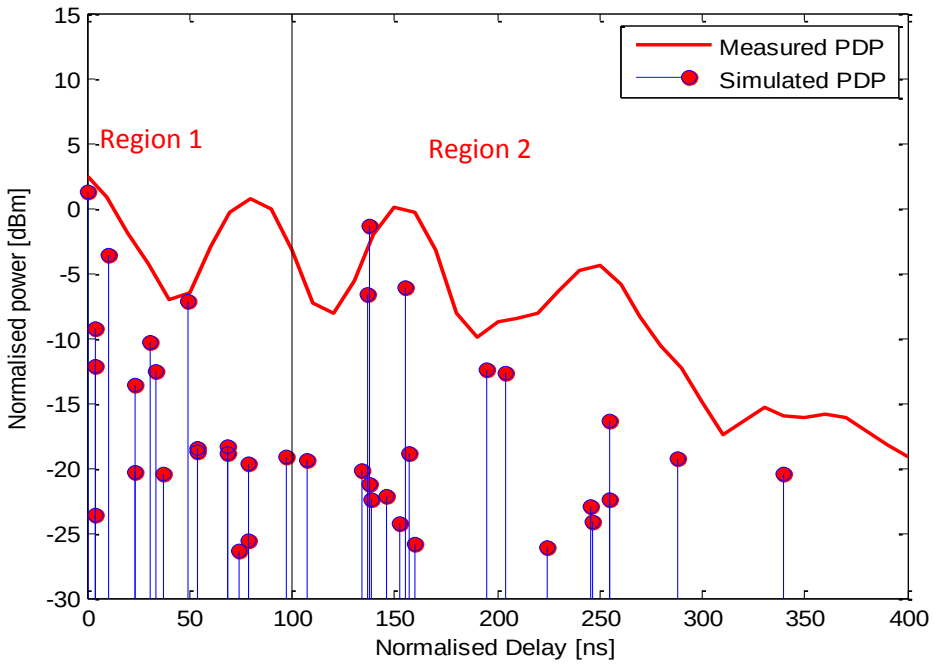

Figure 46 Measured PDP vs. Simulated ray tracing PDP for L3P1 to L3P2

Figure 47 shows all propagation paths spread in region 1, red dot is the position of L3P1, blue dot is the position of B2P0. In this region, signals mainly propagate through reflection and transmissions in the vertical direction through the hollow atrium, the main reflectors are ceilings and floors. However, region 2 exhibits more diverse propagation mechanism as shown in Figure 48. Besides a few paths that propagate through reflections and transmissions in the vertical direction, majority of propagation paths include reflection in the horizontal directions and impinges with surrounding medians. The main reflectors are identified to be walls and metallic lifts from Figure 48(b).

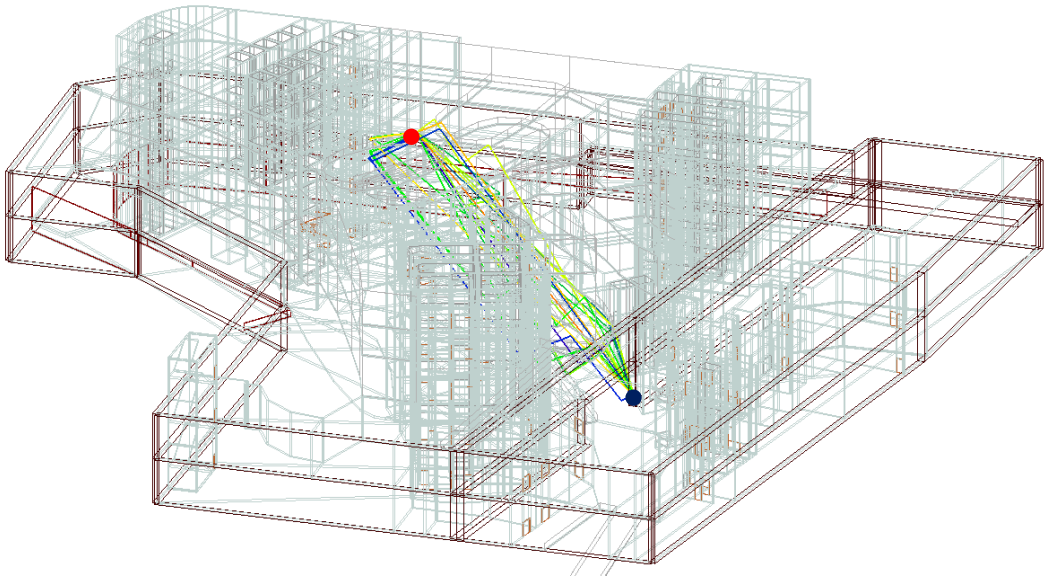

Figure 47 Propagation links range from 0 to 100ns for inter-level link

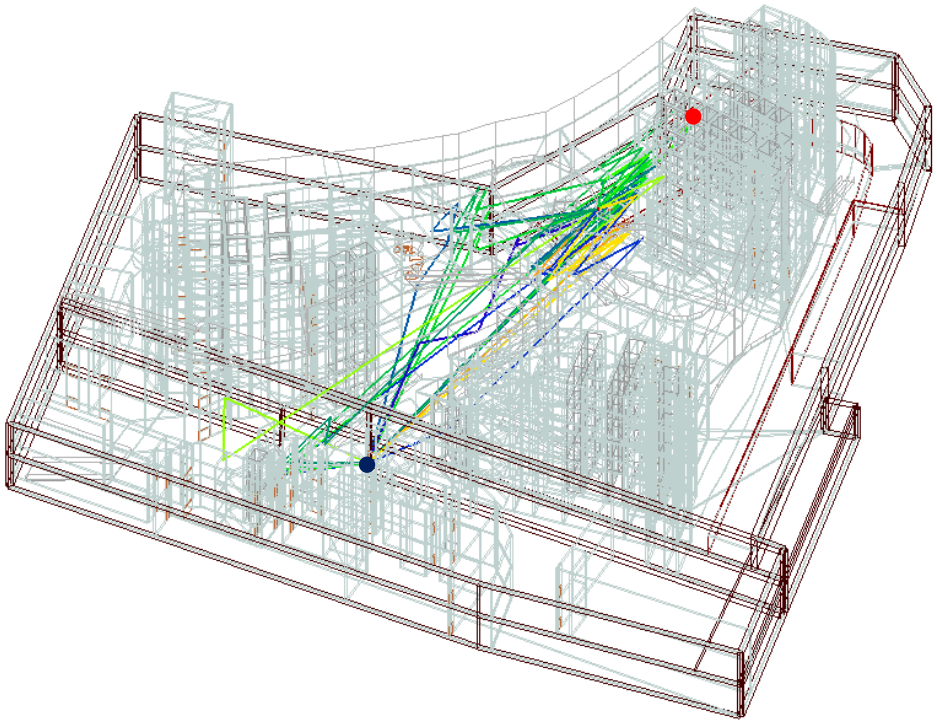

(a)

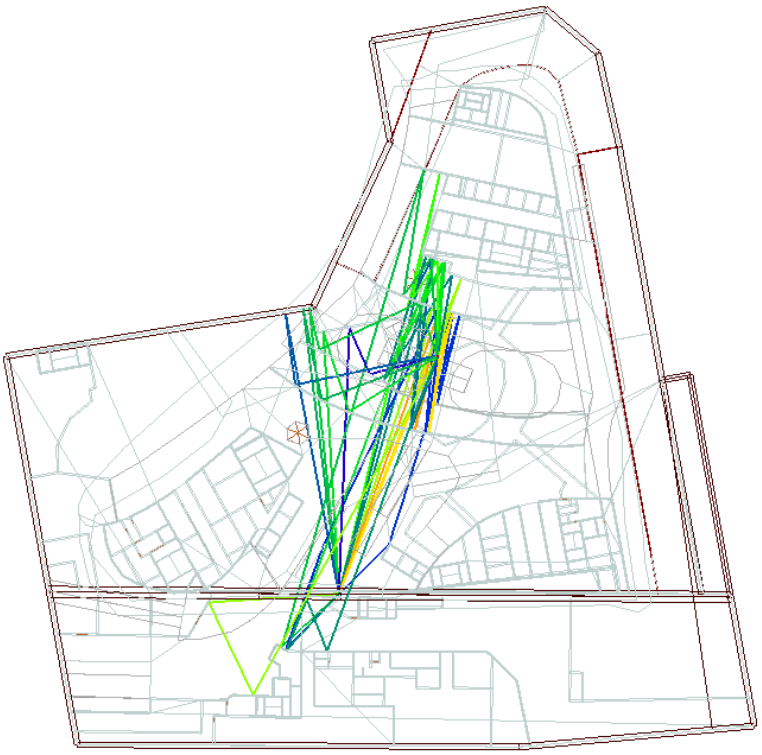

(b)

Figure 48 Propagation links range from 100 to 400ns for inter-level link (a) 3-D view Ray paths (b) 2-D view of ray paths

The 3-D ray tracing results shown here are exemplary examples from two typical link types conducted in our experiments. Only selective link analyses are demonstrated here. Overall, the 3D model created has reflected the original empirical experiment environment with good degree of details and simulated results show close match with the empirical data. Thus, it serves as reliable reference for radio signal propagation model to explain the propagation mechanisms.

6.4 Conclusion

The chapter presents the wideband channel characterization for Indoor environment based on the measurement campaign conducted in Fusionopolis, Singapore. Multiple indoor links have been studied and compared from the perspective of the small-scale fading characteristics. Based on the CFAR threshold algorithm, we list out all the multipath components statistics in Table XVI and found links related to L3 have higher multipath richness than other links due to the median that interacts with signal propagation is glass window. The distributions of multipath component of the indoor paths are studied with the focus of links features enclosed environments. The statistics of decay rate based on linear model is listed in Table XVII. The decay rate is highly correlated to the environment but is frequency independent. Combinations of decay rate and dynamic range can be used to predict multipath richness. Moreover, the RMS delay spread of the indoor channels has been studied and maximum usable bandwidths within such environment are recommended to use 2.2MHz for same level and 0.47MHz for inter-level links. Lastly, the 3-D ray tracing simulation is performed to detail the multipath propagation mechanism for both same-level links and inter-level links based on the created high fidelity 3-D models of Fusionopolis building.

Chapter 7

Conclusion and future work

In this thesis, the empirical channel characterization and modeling of the peer-to-peer urban environment have been conducted and reported. Special attention is given to outdoor-to-indoor channel characterization due to the little available channel statistics and models for the type of links at the military UHF frequency band (250-470MHz), yet it is important for the investigation of urban channel in this band due to the fast advancement of global urbanism and military tactical perspectives. In order to characterize the urban channels in the military UHF band, several measurement campaigns have been carried out in different areas of Singapore including endsville shopping district for outdoor-to-indoor channel study and high rise complex building for indoor channel characterization. Overall, results can be summarized into 3 major categories.

Firstly, path loss modeling is performed over the narrowband measurement data from outdoor-to-indoor measurement campaign across four frequencies in UHF band in two predefined routes around the Orchard area. The measured data was modeled with classical empirical model and path loss exponents for each route and frequencies are derived. To study the signal propagation, an urban 3-D ray tracing simulation is carried out and explained the main reasons that led to the huge decay rate and large signal variation. Lastly, the link availability analysis is performed and least value is found at 370MHz test cases with 76%.

Secondly, wideband channel characteristics are further investigated in the Orchard road in Singapore. With the focus of multipath fading effect, we deployed

the CFAR threshold algorithm to process instantaneous PDPs and studied the number of multipath components in different routes and frequencies and found to be best modeled by log-normal models. In addition, the overall averaged PDP are all found to be single clustered and thus power of multipath distribution is modeled with exponential functions. Little varied exponential decay constant with mean value of 64ns and decay rate of -0.07dB/ns across all frequencies and given routes is found and recommended for prediction. Lastly, the channel variability is studied with the 90% of RMS-DS cumulative distribution and linear relationships between logarithmic value of RMS-DS and link distance are found for the collected data, which could serve as good references for delay spread estimation for the local settings.

Lastly, urban indoor peer-to-peer links have been studied in Fusionoplis, with a focus of small scale multipath fading statistics. Multipath richness is found to be highly related to the surrounding environment types (enclosed, semi-open or open) and materials (glass, concrete). Further, inspired by [29], linear model of PDP strength distribution and corresponding decay rate study are carried out. The linear decay rates are found to be environment-selective but they are frequency independent in general. Combinations of decay rate and dynamic range can be used to predict multipath richness. RMS-DS for all links are derived and mean values are categorized in terms of link types (same level link and inter-level link). The values are within 100ns for same level links and higher for inter-level links (up to 500ns). The further studies of propagation mechanisms are performed with 3-D ray tracing simulations. Multipath components delay distributions between empirical data and simulated data are closely matched, the mechanisms for different types of links are thus identified with the 3-D ray paths from the simulation results.

There are still great potentials in extending the scope of the present work. Future work is recommended as below:

1. The credibility and accuracy of path loss model could be further improved by considering more factors such as the percentage of high rise buildings in area and gap/street ratio along the route that associated with the additional path loss. Path loss model can be further improved through segmenting the routes into smaller and more homogeneous segments so that more factors could be controlled and links can be better categorized such as LOS, "L-shape", and "U-shape".

2. Indoor-to-indoor link path loss modeling could be investigated for same level links and inter-level links to further look into the partition loss and floor attenuations by conducting additional series of strictly controlled trials within the Fusionoplis buildings.

3. Deployment of MIMO and OFDM or single carrier frequency diversion multiple access (SC-FDMA) waveform to our existing system will help to improve the channel stability and overcome multipath fading. The performance of the new system could be evaluated by comparing with existing system through putting them on trials in the identical environment with the same measurement plan.

Author's Publications

Portions of the work reported in this thesis have been published previously in the following papers.

Journal Papers To be submitted

1. X. Qian, Y. H. Lee, and X. H. Mao "Urban shopping district outdoor-to-indoor channel characteristics for military uhf band," to be submitted to *IEEE Transactions on Wireless Communications*

Conference Papers

2. X. H. Mao, Y. H. Lee, S. H. Ting, and X. Qian, "Propagation over the outdoor-to-indoor channel in military UHF band, " in *IEEE Ant. and Porpag. Society International Symposium*, 2013, pp. 1622-1623.

Bibliography

[1] J. X. Yeo, Y. H. Lee, and J. T. Ong, "Rain Attenuation Prediction Model for Satellite Communications in Tropical Regions," *IEEE Trans. Antennas Propag.*, vol. 62, no. 11, pp.625-635, Oct. 2014.

[2] J. D. Parsons, *The Mobile Radio Propagation Channel*, *Second Edition*, New York, John Wiley & Sons, 2000.

[3] A. H. Waynick, "The early history of ionospheric investigations in the United States," *Phil. Trans. R. Soc. Lond. A.*, vol. 280, no. 1293, pp. 11-25, 23 Oct. 1975.

[4] D. C. Cox, "Delay Doppler characteristics of multipath propagation at 910 MHz in a suburban mobile radio environment," *IEEE Trans. Antennas Propag.*, vol. 20, no. 5, pp. 625-635, Sep. 1972.

[5] E. S. Sousa, V. M. Jovanovic, and C. Daigneault, "Delay spread measurements for the digital cellular channel in Toronto," *IEEE Trans. Veh. Technol.*, vol. 43, no. 4, pp. 837-847, Nov. 1994.

[6] International Telecommunication Union (ITU), "Multipath Propagation and Parameterization of its Characteristics," Rec. ITU-R P.1407.

[7] H. Fruchtenicht, "Notes on duct influences on line-of-sight propagation," *IEEE Trans. Antennas Propag.,* vol. 22, pp. 295-302, 1974.

[8] T. Tamir, "Radio waves propagation along mixed paths in forest environments," *IEEE Trans. Antennas Propag.*, vol. AP-25, pp. 471–477, Jul. 1977.

[9] T. Chrysikos, G. Georgopoulos, and S. Kotsopoulos, "Wireless channel characterization for home indoor propagation topology at 2.4GHz," in *IEEE Wireless Telecommunications Symposiu*, pp. 1-10, 2011.

[10] P. F. M. Smulders, "Statistical Characterization of 60-GHz Indoor Radio Channels" *IEEE Transactions on Antennas Propag.*, vol. 57, no. 10, pp. 2820-2829, Oct. 2009.

[11] T. Chrysikos, G. Georgopoulos, and S. Kotsopoulos, "Impact of shadowing on wireless channel characterization for a public indoor commercial topology at 2.4 GHz", 2nd International Congress on Ultra Modern

Telecommunications (ICUMT 2010), Moscow, Russia, October 18-20, 2010.

[12] T. S. Rappaport, "Characterization of UHF multipath radio channels in factory buildings", *IEEE Trans. Antennas Propag.*, vol. 37, no. 8, pp. 1058-1069, Aug. 1989.

[13] G. Zzharia, G. E. Zein, and J. Citerne, "Analysis of the indoor propagation losses for the portable phone "pointel"," in *IEEE int. Symposium on Antennas and Propagation*, pp. 1069-1072, 1993.

[14] D. W. Matolak, Q. Zhang, and Q, Wu, "Path loss in an urban peer-to-peer channel for six public-safety frequency bands," *IEEE Wireless Communications Letters*, vol. 2, no. 3, pp. 263-266, Jun. 2013.

[15] Y. H. Lee, F. Dong, and Y S Meng, "Near sea-surface mobile radiowave propagation at 5GHz: measurement and modeling," *Radioengineering*, vol. 23, no. 3, pp. 824-830, Sep. 2014.

[16] Y. S. Meng, Y. H. Lee and B. C. Ng, "Empirical near ground path loss modeling in a forest at VHF and UHF bands," *IEEE Trans. Antennas Propag.*, vol. 57, no. 5, pp. 1461-1468, May 2009.

[17] R. J. C. Bultitude, Y. L. C. de Jong, J. A. Pugh, S. Salous, and K. Khokar, "Measurement and modeling of emergency vehicle-to-indoor 4.9 GHz radio channels and prediction of IEEE 802.16 performance for public safety applications," *Proc. IEEE Spring Veh. Tech. Conf.*, Dublin, Ireland, pp. 22-25 April 2007.

[18] M. Karam, W. Turney, K. Baum, P. Sartori, L. Malek, and I. Ould-Dellahy, "Outdoor-indoor propagation measurements and link performance in the VHF/UHF bands," *Proc. IEEE Spring Veh. Tech. Conf.*, Singapore, pp. 11-14, May 2008.

[19] A. F. Molisch, *Wireless Communications*, New York, John Wiley & Sons, 2005.

[20] Military Operations in Urban Terrain Focus Area Collaborative Team (MOUT FACT). [Online] https://www.moutfact.army.mil/research.asp.

[21] J. R. Hampton, N. M. Merheb, W. L. Latin, D. E. Paunil, R. M. Shuford, and W. T. Kasch, "Urban propagation measurements for ground based communication in the military UHF band," *IEEE Trans. Anten. Prop.*, vol. 54, no. 2, pp. 644-654, Feb. 2006.

[22] Y. Okumura, E. Ohmori, T. Kawano, and K. Fukuda, "Field strength and its variability in VHF and UHF land-mobile radio service," *Rev. Elect. Commun. Lab.*, vol. 16, no. 9–10, Oct. 1968.

[23] M. Hata, "Empirical formula for propagation loss in land mobile radio services," *IEEE Trans. Veh. Technol.*, vol. 29, no. 3, pp. 317-325, Aug. 1980.

[24] "Digital mobile radio toward future generation systems," European Commission: European Cooperation in Scientific and Technical Research (EURO-COST 231), Bruxelles, 1999.

[25] J. Turkka, and M. Renfors, "Path loss measurements for a non-line-of-sight mobile-to-mobile environment," in *Proc. International Conf. on ITS Telecommun.*, Oct. 2008, pp. 274-278.

[26] X. H. Mao, Y. H. Lee, and B. C. Ng, "Propagation modes and temporal variations along a lift shaft in UHF band," *IEEE Trans. Anten. Prop.*,vol. 58, pp. 2700-2709, Aug. 2010.

[27] A. M. Street, L. Lukama, and D. J. Edwards, "Use of VNAs for wideband propagation measurements," *IEE Proc. Commun.*, vol. 148, no.6, pp. 411-415, Dec. 2001.

[28] S. J. Howard and K. Pahlavan, "Autoregressive modeling of wide-band indoor radio propagation". *IEEE Trans. Commun.*, vol. 40, no. 91, pp. 1540-1552, Sep. 1992.

[29] X. H. Mao and Y. H. Lee, "UHF propagation along a cargo hold on board a merchant ship," *IEEE Trans. Wireless Commun.*, vol.12, no.1, pp. 22-30, Jan. 2013.

[30] B. Sklar, *Digital Communications: Fundamentals and Applications*, 2nd Edition, Upper Saddle River, NJ: Prentice Hall, Jan. 2011.

[31] R. C. Dixon, *Spread Spectrum Systems with Commercial Applications*. John Wiley and Sons, Inc., 1994.

[32] [Online]. Available: http://www.remcom.com/wirelessinsite.

[33] A. Papoulis and U. Pillai, *Probability Random Variables, and Stochastic Processes*, 4th ed. McGraw-Hill, 2001.

[34] P. E. R. Galloway and T. D. Welsh, "Extensions to the shooting bouncing ray algorithm for scattering from diffusive and grating structures," in *Proc. International Radar Symposium*, IRS. Berlin, pp. 747-754, Sep. 2005.

[35] A. F. Molisch, D.Cassioli, C. C. Chong, S. Emami, A. Fort, B. Kannan, J. Karedal, J. Kunisch, H. G. Schantz, K. Siwiak, and M. Z. Win, "A comprehensive standardized model for ultrawideband propagation channels," *IEEE Trans. Antennas Propagat.*, vol. 54, pp. 3151-3166, Nov. 2006.

[36] T. S. Rappaport, *Wireless communications principles and practice*: NJ: Prentice-Hall Inc, 2002.

[37] International Telecommunication Union (ITU), "GUIDELINES FOR EVALUATION OF RADIO TRANSMISSION TECHNOLOGIES FOR IMT-2000," Rec. ITU-R M.1225.

[38] A. Goldsmith, *Wireless Communications*, New York: Cambridge University Press, 2005.

[39] K. Pahlavan and A.H. Levesque, *Wireless Information Networks*, 2nd Ed., Wiley, 2005.

[40] F. Dong, C. W. Chan, and Y. H. Lee, "Channel modeling in maritime environment for USV," in *Defence Technology Asia 2011*, Singapore, Feb. 2011.

[41] F. Dong and Y. H. Lee, "Non-line-of-sight communication links over sea surface at 5.5GHz," in *Proc. 2011 Asia-Pacific Microw. Conf.*, Melbourne, VIC, Dec. 2011, pp. 1682–1685.

[42] A.G. Dimitriou, G.D. Seriadis, "Microcellular propagation prediction model based on a geometric progression approximation-process", *IEEE Trans. Antennas Propag.*, vol. 55, Mar. 2007, pp. 969-977.

[43] W. Jakes, *Microwave Mobile Communications*, (New York: IEEE, 1974, Reedited Piscataway: IEEE Press, 1993), pp. 125-127.

[44] Digital Mobile Radio Towards Future Generation Systems COST Action 231, European o-operation in Mobile Radio Research, European Commission, Brussels, Belgium, Final Tech. Rep. EUR 1857, 1999, E. Damosso, L. M. Correia (eds.).

[45] S. Chui, J. Chuang, and D. G. Michelson, "Characterization of UWB channel impulse responses within the passenger cabin of Boeing 737-200 aircraft," *IEEE Trans. Antennaas Propagat.* vol. 58, pp. 935-945, Mar. 2010.

[46] IEEE 802.16 Broadband Wireless Access Working Group, "Channel Models for Fixed Wireless Applications", contribution to 802.16a, 2003. [Online] http://wirelessman.org/tga/docs/80216a-03_01.pdf.

[47] C. Chrysanthou and H.L. Bertoni, "Variability of sector averaged signals for UHF propagation in cities", *IEEE Trans. Veh. Technol.*, Volume 39, no. 4, pp. 352–358, Nov. 1990.

[48] L. J. Greenstein, V. Erceg, Y. S. Yeh, and M. V. Clark, "A new path-gain/delay-spread propagation model for digital cellular channels", *IEEE Trans. Veh. Technol.*, Volume 46, Issue 2, pp. 477–485, May 1997.

[49] S. Y. Seidel, "Path loss, scattering and multipath delay statistics in four European cities for digital cellular and microcellular radiotelephone", *IEEE Trans. Veh. Technol.*, Volume 40, no. 4, pp. 721–730, Nov 1991.

[50] J. W. Porter, I. Lisica, and G. Buchwald, "Wideband mobile propagation measurements at 3.7 GHz in an urban environment", in *IEEE Antennas and Propagation Society International Symposium*, Volume 4, pp. 3645–3648, 20-25 Jun. 2004.

[51] C. Phillips, D. Sicker, and D. Grunwald. "A survey of wireless path loss prediction and coverage mapping methods," *IEEE Commun. Surv. Tuts.*, vol. 15, no. 1, pp. 225-270, Mar. 2013.

[52] Y. Okumura, E. Ohmori, T. Kawano, and K. Fukuda, "Field strength and its variability in VHF and UHF land mobile radio service," *Rev. Electr. Commun. Lab.*, 16:825–73, 1968.

[53] L. Barclay. *Propagation of radiowaves*. Institution of Electrical Engineers, 2003.

[54] M. Pätzold, *Mobile Radio Channels*, 2nd ed., WILEY, pp. 552-554, 2011.

[55] H. R. Anderson, *Fixed Broadband Wireless System Design*. John Wiley & Co., 2003.

[56] ECC. The analysis of the coexistence of FWA cells in the 3.4 - 3.8 GHz bands. Technical Report 33, European Conference of Postal and Telecommunications Administrations, 2003.

[57] NIST. http://w3.antd.nist.gov/wctg/manet/calcmodels r1.pdf.

[58] S. R. Saunders and F. R. Bonar. Explicit multiple building diffraction attenuation function for mobile radio wave propagation. *Electronics Letters*, vol. 27, no. 14, pp. 1276–1277, Jul. 1991.

[59] J. Waltisch and H. L. Bertoni, “A theoretical model of UHF propagation in urban environments,” *IEEE Trans. Antennas Propag.*, vol. 36, no. 12, pp. 1788-1796, Dec. 1988.

[60] F. Ikegami, T. Takeuchi, and S. Yoshida, “Theoretical prediction of mean field strength for urban mobile radio,” *IEEE Trans. Antennas Propag.*, vol. 39, no. 3, pp. 299–302, Mar. 1991.

[61] Y. S. Meng and Y. H. Lee, "Measurements and characterizations of air-to-ground channel over sea surface at C-band with low airborne altitudes," *IEEE Trans. Veh. Technol.*, vol. 60, no.4, pp. 1943-1948, May 2011.

[62] Y. H. Lee and Y. S. Meng, "Analysis of ducting effects on air-to-ground propagation channel over sea surface at C-band," in *Microwave Conference Proceedings (APMC), 2011 Asia-Pacific*, pp. 1678-1681, 2011.

[63] ITU-R. Attenuation in vegetation. Technical Report P.833, ITU, 2005.

[64] S. A. Torrico, H. L. Bertoni, and R. H. Lang. “Modeling tree effects on path loss in a residential environment,” *IEEE Trans. Antennas Propag.*, vol. 46, no. 6, pp. 872–880, Jun. 1998.

[65] G. Y. Delisle, J. Lef ́evre, M. Lecours, and J. Y. Chouinard, “Propagation loss prediction: A comparative study with application to the mobile radio channel,” *IEEE Trans. Veh. Technol.*, vol.34, no. 2, pp. 86–96, May 1985.

[66] Y. L. C. de Jong, M. H. J. L. Koelen, and M. H. A. J. Herben. “A building transmission model for improved propagation prediction in urban microcells. *IEEE Trans. Antennas Propag.*, vol. 53, no. 2, pp. 490-502, Mar. 2004.

[67] E. Anderson, C. Phillips, D. Sicker, and D. Grunwald, “Modeling environmental effects on directionality in wireless networks,” In *5th International Workshop on Wireless Network Measurements (WiNMee)*, pp. 1-7, 2009.

[68] K.T. Herring, J.W. Holloway, D.H. Staelin, and D.W. Bliss. “Pathloss characteristics of urban wireless channels,” *IEEE Trans. Antennas Propag.*, vol. 58, no. 1, pp. 171-177, Jan. 2010.

[69] J. R. Hampton, N. M. Merheb, W. L. Latin, D. E. Paunil, R. M. Shuford and W. T. Kasch, “Urban propagation measurements for ground based communication in the military UHF band,” *IEEE Trans. Antennas Propag.*, vol. 54, no. 2, pp. 644-654, Feb. 2006.

[70] M. J. Feuerstein, K. L Blackard, T. S. Rappaport, S. Y. Seidel, and H. H. Xia, "Path loss, delay spread, and outage models as functions of antenna height for macrocellular system design," *IEEE Trans. Veh. Technol.*, vol. 43, no. 3, pp. 487-498, Aug. 1994.

[71] J. Andrusenko, R. L. Miller, J. A. Abrahamson, N. M. M. Emanueli, R. S. Pattay, and R. M Shuford, "VHF general urban path loss models for short range ground-to-ground communication," *IEEE Trans. Antennas Propag.*, vol. 56, no. 10, pp. 3301-3310, Oct. 2008.

[72] M. Karam, W. Turney, K. Baum, P. Sartori, L. Malek, and I. Ould-Dellahy, "Outdoor-indoor propagation measurements and link performance in the VHF/UHF bands," *Proc. IEEE Spring Veh. Tech. Conf.*, Singapore, pp. 11-14 May 2008.

[73] J. Fischer, M. Grossmann, W. Felber M. Landmann, and A. Heuberger, "A measurement-based path loss model for wireless links in mobile ad-hoc networks (MANET) operating in the VHF and UHF band," in *IEEE-APS Topical Conference on Antennas and Propagation in Wireless Communications*, pp. 349-352, Sep. 2012.

[74] R. J. Luebbers, "Finite conductivity uniform GTD versus knife edge diffraction in prediction of propagation path loss," *IEEE Trans. Antennas Propag.*, vol. 32, no.1, pp. 70-76, Jan. 1984.

[75] W. Zhang, "Fast two-dimensional diffraction modeling for site-specific propagation prediction in urban microcellular environments," *IEEE Trans. Veh. Technol.*, vol. 49, no. 2, pp. 428-436, Mar. 2000.

[76] S. C. Kim, B. J. Guarino Jr., T. M. Willis, V. Erceg, S. J. Fortune, R. A. Valenzuela, L. W. Thomas, J. Ling, and J. D. Moore, "Radio propagation measurements and prediction using three-dimensional ray tracing in urban environments at 908 MHz and 1.9 GHz," *IEEE Trans. Veh. Technol.*, vol. 48, no. 3, pp. 931-944, May 1999.

[77] A. J. Rustako, Noach Amitay, G. J. Owens, and R. S. Roman, "Radio propagation at microwave frequencies for line-of-sight microcellular mobile and personal communications," *IEEE Trans. Veh. Technol.*, vol. 40, no.1, pp. 203–210, Feb. 1991.

[78] K. Rizk, J. F. Wagen, and F. Gardiol. “Two-dimensional ray-tracing modeling for propagation prediction in microcellular environments,” *IEEE Trans. Veh. Technol.*, vol. 46, no. 2, pp. 508 –518, May 1997.

[79] A. G. Kanatas, I. D. Kountouris, G. B. Kostaras, and P. Constantinou, “An UTD propagation model in urban microcellular environments,” *IEEE Trans. Veh. Technol.*, vol. 46, no. 1, pp. 185–193, Feb. 1997.

[80] G. Wolfe, R. Hoppe, and F. M. Landstorfer. “Radio network planning with ray optical propagation models for urban, indoor, and hybrid scenarios,” In *11th IEEE Wireless Conference*, 1999, pp. 159-162.

[81] G. Liang and H. L. Bertoni, “A new approach to 3-D ray tracing for propagation prediction in cities,” *IEEE Trans. Antennas Propag.*, vol. 46, no. 6, pp. 853-863, Jun. 1998.

[82] W. Ying, S. Safavi-Naeini, and S. K. Chaudhuri, “A hybrid technique based on combining ray tracing and FDTD methods for site-specific modeling of indoor radio wave propagation,” *IEEE Trans. Antennas Propag.*, vol. 48, no. 5, pp. 743-754, May 2000.

[83] Z. Sandor, L. Nagy, 2. Szabo, and T. Csaba, “3D ray launching and moment method for indoor propagation purposes,” *The 8th IEEE International Symposium on Personal, Indoor and MobileRadio Communications*, PIMRC ‘97, vol. 1, pp. 130-134, 1997.

[84] M. Iskander, and Z. Yun, “Propagation prediction models for wireless communication systems,” *IEEE Trans. Microw. Theory Tech.*, vol. 33, no. 3, pp. 662-673, Mar. 2002.

[85] P. Papazian, “Basic transmission loss and delay spread measurement for frequencies between 430MHz and 5750MHz,” *IEEE Trans. Ant. Propag.*, vol. 53, no. 2, pp. 694-701, Feb. 2005.

[86] K. Rizk, J. Wagen, and F. Gardiol, “Two-dimensional ray-tracing modeling for propagation prediction in microcellular environments,” *IEEE Trans. Veh. Technol.*, vol. 46, no. 2, pp. 508-518, May 1997.

[87] N. Blaunstein, “Average field attenuation in the street waveguide,” *IEEE Trans. Antennas Propag.*, vol. 46, no. 12, pp. 1782-1789, Dec. 1998.

[88] Y. P. Zhang, Y. Hwang, and J. D. Parsons, “UHF radio propagation characteristics in straight open-groove structures,’’ *IEEE Trans. Veh. Technol.*, Vol. 48, no. 1, pp. 249-254, Jan. 1999.

[89] H. W. Arnold, R. R. Murray, and D. C. Cox, "815 MHz radio attenuation measured within two commercial buildings," *IEEE Trans. Antennas Propag.*, vol. 37, no. 10, pp. 1335-1339, Oct. 1989.

[90] M. Polivka, M. Svanda, P. Hudec, and S. Zvanovec, "UHF RF identification of people in indoor and open areas," *IEEE Trans. Microw. Theory Tech.*, vol. 57, no. 5, pp. 1341-1347, May 2009.

[91] U. Dersch, J. Troger, and E. Zollinger, "Multiple reflections of radio waves in a corridor," *IEEE Trans. Antennas Propag.*, vol. 42, no. 11, pp. 1571-1574, Nov. 1994.

[92] Donald C. Cox, and Robert P. Leck, "Correlation bandwidth and delay spread multipath propagation statistics for 910-MHz urban mobile radio channels", *IEEE Trans. Comm.*, vol. 23, no. 11, pp. 1271-1280, Mar. 1975.

[93] G. Eriksson, S. Linder, K. Wiklundh, P. Holm, P. Johansson, F. Tufvesson, and A. Molisch,"Urban Peer-to-peer MIMO channel measurements and analysis at 300MHz," Mitsubishi Electic Labs Report TR 2008-076. Dec. 2008.

[94] T. S. Rappaport, S. Y. Seidel and R. Singh. "900-MHz multipath propagation measurements for U.S. digital cellular radiotelephone," *IEEE Trans. Veh. Techno.*, vol. 39, no. 2, pp. 132-139, May 1990.

[95] J. A. Wepman, J. R. Hoffman, L. H. Loew, and V. S. Lawrence, "Comparison of wideband propagation in the 902-938 and 1850-1990 MHz bands in various macrocellular environments", U. S. Department of Commerce, NTIA Report 93-299, Sep. 1993.

[96] J. A. Wepman, J. R. D Hoffman, and L. H. Loew, "Impulse response measurements in the 1850-1990 MHz bands in large outdoor cells", U. S. Department of Commerce, NTIA Report 94-309, Jun. 1994.

[97] D. Cassioli, M. Z. Win and A. F. Molisch, "A statistical model for the UWB indoor channel," in *Proc. 53rd IEEE Vehicular Technology Conference*, vol. 2, May 2001, pp. 1159-1163.

[98] H. Asplund, A. A. Glazunov, A. F. Molisch, K. I. Pedersen, and M. Steinbauer, "The COST 259 Directional Channel Model – part II: Macrocells," *IEEE Trans. Wireless Comm.*, vol. 12, no. 5, pp. 3434-3450, Dec. 2006.

[99] C. L. Hong, I. J. Wassell, G. E. Athanasiadou, S. Greaves, and M. Sellars, "Wideband channel measurements and characterization for broadband wireless access," in *Antennas and Propagation, 2003. (ICAP 2013) Twelfth International Conference on (Conf. Publ. No. 491),* vol. 1, Apr. 2003, pp.429-432.

[100] D. M. J. Devarivatham, "Radio propagation studies in a small city for universal portable communications," in *Proc. 38th IEEE veh. Technol. Conf.*, pp. 100-104, 1988.

[101] AWE Communications. Wave propagation and radio network planning. http://www.awe-communications.com/, Mar. 2015.

[102] EDX Wireless. Smart planning for smart networks. http://www.edx.com/, Mar. 2015.

[103] IDA Frequency Spectrum Allocation [Online]: Available:http://www-.ida.gov.sg/doc/Policies%20and%20Regulation/Policies_and_Regulation_Level2/20060421164253/SpectrumChart.pdf.

[104] Miscellaneous Dielectric Constants [Online]: http://www.microwaves101-.com/encyclopedias/miscellaneous-dielectric-constants.

[105] A. Valcarce, J. Zhang, "Empirical indoor-to-outdoor propagation model for residential areas at 0.9-3.5GHz," *IEEE Antenn. Wireless Propag. Lett.*, vol. 9. pp. 682-685, Jul. 2010.

[106] X. H. Mao, Y. H. Lee, S. H. Ting, and X. Qian, "Propagation over the outdoor-to-indoor channel in military UHF band, " in *IEEE Ant. and Porpag. Society International Symposium*, 2013, pp. 1622-1623.

[107] J. Lähteenamäki, "Radiowave propagation in office buildings and underground halls", in *Proc. 22nd Microw. Conf.*, Espoo, Finland, Aug. 1992, pp. 377-382.

[108] E. Tanghe, W, Joseph, L, Verlock, L. Martens, H. Capoen, K. Van Herwegen, and W. Vantomme, "The industrial indoor channel: large-scale and temporal fading at 900,2400 and 5200 mhz," *IEEE Trans. Wireless Commun.*, vol. 7, no. 7, pp. 2740-2750, Jul. 2008.